Hybrid Electric Vehicle Powertrain and Control System Modeling, Analysis and Design Optimization

by

Leon Yuliang Zhou
B. Eng, University of Science and Technology Beijing, 2005
M.A.Sc, University of Victoria, 2007

A Dissertation Submitted in Partial Fulfillment
of the Requirements for the Degree of

DOCTOR OF PHILOSOPHY

in the Department of Mechanical Engineering

Supervisory Committee

Hybrid Electric Vehicle Powertrain and Control System Modeling, Analysis and Design Optimization

by

Leon Yuliang Zhou
B. Eng, University of Science and Technology Beijing, 2005
M.A.Sc, University of Victoria, 2007

Supervisory Committee

Dr. Zuomin Dong, (Department of Mechanical Engineering)
Supervisor

Dr. Curran Crawford, (Department of Mechanical Engineering)
Departmental Member

Dr. Nikolai Dechev, (Department of Mechanical Engineering)
Departmental Member

Dr. Wu-Sheng Lu, (Department of Electrical and Computer Engineering)
Outside Member

Abstract

Supervisory Committee
Dr. Zuomin Dong, (Department of Mechanical Engineering)
Supervisor
Dr. Curran Crawford, (Department of Mechanical Engineering)
Departmental Member
Dr. Nikolai Dechev, (Department of Mechanical Engineering)
Departmental Member
Dr. Wu-Sheng Lu, (Department of Electrical and Computer Engineering)
Outside Member

Abstract:

Today uncertainties of petroleum supply and concerns over global warming call for further advancement of green vehicles with higher energy efficiency and lower green house gas (GHG) emissions. Development of advanced hybrid electric powertrain technology plays an important role in the green vehicle transformation with continuously improved energy efficiency and diversified energy sources. The added complexity of the multi-discipline based, advanced hybrid powertrain systems make traditional powertrain design method obsolete, inefficient, and ineffective. This research follows the industrial leading model-based design approach for hybrid electric vehicle powertrain development and introduces the optimization based methods to address several key design challenges in hybrid electric powertrain and its control system design. Several advanced optimization methods are applied to identify the proper hybrid powertrain architecture and design its control strategies for better energy efficiency. The newly introduced optimization based methods can considerably alleviate the design challenges, avoid unnecessary design iterations, and improve the quality and efficiency of the powertrain design. The proposed method is tested through the design and development of a prototype extended range electric vehicle (EREV), UVic EcoCAR. Developments of this advanced hybrid vehicle provide a valuable platform for verifying the new design method and obtaining feedbacks to guide the fundamental research on new hybrid powertrain design methodology.

Table of Contents

List of Tables

List of Figures

Acknowledgments

The experience for this dissertation research has been highly enjoyable. The contentment is largely a result of the good interactions that I had with my supervisor, colleagues, and industrial partners.

I would like to first acknowledge and express my sincere thanks to Professor Zuomin Dong, my supervisor who gave me the opportunity to work on this highly promising and exciting research area. Overall the years of graduate studies, he has provided important guidance at key moments in my work while also allowing me to work independently. Related researches carried out by fellow (and former) graduate students, Jeff Wishart, Adel Younis, Jeremy Wise, Jeff Waldner, Tiffany Jaster, and Jian Dong have contributed immensely to my work. Dr. Curran Crawford has also provided very important advice to my research and the UVic EcoCAR development.

Financial and technical supports from the Natural Science and Engineering Research Council of Canada, University of Victoria, U.S. Department of Energy, General Motors, Azure Dynamic, Auto21 and MITACS program are gratefully acknowledged.

Finally, a special thank you goes to my parents Zhou, Yong and Yu, Dongmei for their moral and financial supports during my study in Canada.

Acronyms

AER	All-electric Range
ANN	Artificial Neural Network
AWD	All Wheels Drive
BCM	Battery Control Module
CNG	Compressed Natural Gas
e-CVT	Electronically Controlled Continuously Variable Transmission
DOF	Degree of Freedom
DP	Dynamic Programming
EDS	Emergency Disconnect Switch
EECM	Energy Equivalent Consumption Measurement
EPA	Environment Protection Agency
E-REV	Extended Range Electric Vehicle
ESS	Energy Storage System
EV	Electric Vehicles
FDG	Front Differential Gear
FPM	Full Power Mode
FWD	Front Wheels Drive
GA	Generic Algorithm
GHG	Green House Gas Emissions
GREET	Greenhouse gases, Regulated Emissions, and Energy use in Transportation
HEV	Hybrid Electric Vehicle
HIL	Hardware In-the-Loop
HV	Hybrid Vehicle
HWFET	Highway Fuel Economy Driving Schedule
ICE	Internal Combustion Engines
Li-ion	Lithium-ion
LP	Linear Programming
LPM	Limited Power Mode

MIL	Model In-the-Loop
MDB	Model-based Design
M/G	Motor/Generator
MPG_{ge}	Mile per Gallon Gasoline-Equivalent
MTF	Maximum Traction Force
Ni-MH	Nickel-Metal Hydride
NLP	Nonlinear Programming
OEM	Original Equipment Manufacturers
PHEV	Plug-in Hybrid Electric Vehicle
PSAT	Powertrain System Analysis Toolkit
PSD	Power Split Device
PTW	Pump-To-Wheel
RESS	Rechargeable Energy Storage System
SIL	Software In-the-Loop
SOC	State of Charge
SP	Sub-Problem
SQP	Sequential Quadratic Programming
SSP	Sub-Sub-Problem
THS	Toyota Hybrid System
TPIM	Transmission Powertrain Interface Module
UDDS	Urban Dynamotor Driving Schedule
VDP	Vehicle Development Process
VTS	Vehicle Technical Specifications
WTW	Well-To-Wheel
WTP	Well-To-Pump

Chapter 1 Background and Research Objectives

1.1 Environmental Concerns for Future Transportations

In recent years, green house gas (GHG) emissions have raised concerns over climate change worldwide. The transportation sector accounts for a large portion (60% in US) of the GHG emissions, mostly owing to consumption of fossil fuels in internal combustion engines (ICE) [1]. Driven by the growing environmental concerns, uncertain petroleum fuel supply, and public expectations, upgrading vehicle powertrains to reduce fuel consumption and GHG emissions has become an urgent task for the automotive industry. Strict standards have been formulated worldwide; in the United States, the target is to lower GHG emissions of passenger cars and light-duty trucks to a combined level of 250 grams carbon dioxide (CO_2) per mile in model year 2016, and further to 162 grams per mile in model year 2025 [2], equivalent to 35.5 mpg and 54.5 mpg respectively, if the reduction of CO_2 level is all through fuel economy improvements. As of 2010, the North American vehicle powertrain mix is predominately occupied by the gasoline fuelled ICE powertrains, accounting for ninety-five percent of the overall transportation vehicles. The remaining five percent is made up of three percent of hybrid electric and two percent of diesel/ICE. With tougher GHG emissions standards in place, along with concerns over the oil price, the market share of gasoline fuelled vehicles is expected to continuously fall in the coming decade. The remaining market share is to be filled by vehicles with new powertrain technologies and alternative fuels capability.

1.2 The Need for Next Generation Advanced Hybrid Vehicles

To address the increasing energy and environmental needs, future vehicles are to be developed with improved energy efficiency, diversified energy sources, and satisfying performance and affordability.

The early renaissance of hybrid vehicles in the late 20th century is to bring in more fuel saving technologies to the conventional ICE based powertrain. The hybrid electric vehicle (HEV) technology plays an important role among various hybrid vehicle technologies, which utilize electric drives and innovative transmissions to improve overall energy efficiency, resulting lower fuel consumption than the conventional vehicle

counterparts[3]. By degree of hybridization which is essentially measuring the weighting of electric drive over mechanical drive, a HEV can be classified as micro-hybrid, mild hybrid, strong hybrid, to full electric; increasing of the hybridization generally allows better fuel efficiency improvement and stronger electric-only drive capability. The overall fuel efficiency improvement varies between ten to fifty percent [4], depending on hybrid configurations. This non-plug-in based hybrid technology is essentially comparable to other fuel saving technologies, such as highly efficient combustion technology, low loss transmissions, low aerodynamic loss vehicle body design, etc.

In addition to reducing fuel consumption, the introduction of electric drives and energy storage systems allow a vehicle to have multiple energy sources, such as regular petroleum based fuels, electricity, and hydrogen. These diversified energy sources allow a vehicle to selectively draw up different energy sources based on availability and efficiency. The recently introduced plug-in HEV (PHEV) concept is a fine example of such vehicles. These vehicles combine a hybrid powertrain with a sizable battery, allowing trips to be completed by partly using electricity collected from the power grid. The degree of hybridization in a PHEV also varies, and is largely decided by the powertrain architecture rather than the battery capacities. Most existing PHEVs have limited electric vehicle (EV) capability at certain vehicle speed and power demand. These limitations in driving electrically can heavily affect the overall energy diversity strategy, since the dual energy sources onboard a vehicle are not equally capable of providing propulsion power. The future PHEVs are to be developed with strong propulsion capability in EV mode and satisfying fuel efficiency in extended range running consumable fuels such as gasoline [5].

The electrically hybridized powertrain is a viable solution that can bridge the gap between conventional vehicles and electric vehicles. The concept of hybridization will continue to play an important role in vehicle development for the next decade; in the mean time, replacing ICE powered conventional vehicles with electric vehicles for different applications still have key issues unsolved, largely related to limited capacity and high cost of electric energy storage system and electric drives. Serving as an intermediate powertrain solution of the fully electric vehicles, HEV is a more complex powertrain system than the conventional ICE powertrain or the full electric powertrain,

due to the existence of dual energy storage and multiple power plants. Several design challenges in HEV development arise.

1.3 Challenge in HEV Powertrain Development

1.3.1 Complexity in Hybrid Powertrain Design

A hybrid powertrain is a complex mechatronics system involving not only conventional powertrain components, but also high power electric drives and high voltage energy storage systems. The flexible powertrain configurations and wide selections of powertrain components vastly enlarge the design space. Depending on vehicle sizes and applications, different hybrid powertrain designs are desirable in satisfying the requested propulsion power demand and delivering high energy efficiency. Performing design using the traditional trial-and-error based approach is increasingly difficult as the system complexity increases; the multi-disciplinary system involving mechanical, electrical and control knowledge makes the design process demanding on human experience.

1.3.2 Control Strategy Development and Optimal Energy Management

The flexible configurations, multiple power plants, and energy storage of a hybrid powertrain expend the control flexibilities by allowing different propulsion combinations among the power plants. The main design target for control development is to achieve optimal energy efficiency.

Consuming both fuel and electricity, the overall energy efficiency of a hybrid vehicle includes both electrical and ICE efficiency. Traditional control strategies developed using engineering rules frequently fail to yield the best overall efficiency. For instance, to achieve low fuel consumption in a HEV, most control strategies are developed on rules that can prioritize engine operation efficiency, compromising the less significant electric drive efficiency. The optimal control strategy that maximizes the overall powertrain system efficiency should not only consider the ICE efficiency but also include the electric drive efficiency as well as other powertrain components. Developing such optimal strategies demands intensive modeling and calculations. To facilitate this design need and shorten the vehicle development process, the model-based design (MBD) method and optimization based design tools are needed.

1.3.3 Selecting Fuels to Lower Life Cycle Environmental Impacts

The hybrid powertrain technologies and electric drive capabilities can reduce fuel consumption and utilize electricity in vehicle propulsion. There are however other alternative fuel options that have different energy pathways in the energy cycle. Some of the most considered alternative fuels include ethanol, biodiesel, hydrogen, natural gas, and electricity. To have powertrain designs that can best address the crucial environmental concerns including reducing GHG emissions and petroleum consumptions, the overall impacts of alternative fuels must be well understood on the life cycle basis and compared with the conventional fuels. Carrying out fuel cycle related analysis demands extensive knowledge that is usually beyond the powertrain technology itself. Knowing the alternative fuels with lower environmental impact will have a significant impact on the national energy strategy and will gradually guide the development of future vehicle powertrain.

1.4 Research Objectives

The objective of this study is to apply MBD approach and advanced optimization methods to the design and development of a next generation hybrid vehicle powertrain. A number of key issues are targeted, which covers the complete powertrain design process from architecture selection to vehicle calibrations.

1.4.1 Next Generation Fuel and Powertrain Selection

Selection of fuel and powertrain for future transportation is fundamental to powertrain design and development. Due to the large number of fuel options and powertrain selections, knowing the best fuel and powertrain combination for the targeted environmental and energy supply issues is difficult. The Well-to-Wheel (WTW) [35] analysis method studies the complete life cycle of each fuel from upstream fuel production to downstream vehicle energy consumption. A wide range of fuel and powertrain configurations are investigated, covering most existing technological solutions for transportations. This predictive study also takes into account developments and changes in near future and therefore can guide the current and future vehicle design.

1.4.2 Model Development for HEV Powertrain and Control System

The model-based design approach for hybrid powertrains can significantly transform the vehicle design process and enable better design of complex powertrain systems. To carry out studies on designs of powertrain and control systems, high fidelity models of powertrain components are developed in this work, using either first principle based mathematic models or data driven empirical models. These models are calibrated with experimental data and can well represent the performance of real-world systems.

1.4.3 Applications of Optimization in Model-based Design Solution for Powertrain and Control System

With models developed for powertrain components, powertrain system design are performed using the MBD approach. Due to the large number of design variables and flexible design configurations, determining optimal design using the trial and error method is time consuming and impractical for complex systems. This work applies optimization based methods in searching for the optimal design solutions in the MBD process. Established research problems include powertrain design and control system design. The optimization based solution is compared with solutions obtained using the traditional design approach.

1.4.4 Design and Development of a Extended Range Electric Vehicle

In addition to carrying out theoretical studies for powertrain modeling and design, the gained knowledge and experience is applied to develop a real-world hybrid vehicle which has plug-in capability and full EV performance running on battery. The MDB process is implemented though out the project, from architecture selection to vehicle testing.

1.5 Outline of the Dissertation

The dissertation is organized in eight chapters. After the initial introduction and definition of research problems in Chapter 1, a more detailed review on hybrid vehicle powertrain and the MDB method is included in Chapter 2. Chapter 3 presents a Well-To-Wheel based design method in determining the fuel and powertrain selection for future vehicles. Chapter 4 introduces developed models for the studied powertrain design and control system problems. Chapter 5 applies a global optimization based approach to

determining the best performance of the electronically controlled continuously variable transmission (e-CVT) based HEV powertrains. Chapter 6 applies optimization tools to identify the optimal control strategy of a HEV for the best system efficiency. Chapter 7 implements the gained knowledge to the design of a hybrid powertrain with full electric vehicle capability. At the end, the research work is summarized in Chapter 8.

Chapter 2 Review of Hybrid Powertrain Design and Control Problems

2.1 Hybrid Electric Vehicle Development

2.1.1 Hybrid Electric Vehicle Powertrain Architectures

A hybrid vehicle (HV) has more than one power source, making numerous possible combinations. This study mainly focuses on the HEV powertrain architecture, while other hybrid technologies such as hydraulic or mechanical technologies are also documented previously in separate reports [6-8]. The three most representative HEV architectures are the series hybrid, parallel hybrid, and e-CVT hybrid.

In the series HEV architecture, energy from the ICE generates electricity and an electric motor drives the vehicle [9]. This configuration allows improved engine efficiency with the engine de-coupled from direct propulsion. A main disadvantage is the significant electric losses caused by the energy conversions between mechanical and electrical energies. In addition, the series configuration demands two electric motors (a generator and a motor) of high capacity which potentially increase the cost and add challenges to packaging in the engine bay area. Figure 1 below depicts a schematic of a generic series HEV powertrain. Note that in this and all subsequent figures that a solid line denotes a mechanical connection while a dashed line denotes an electrical connection. Several automotive OEMs examined the possibility of development programs for series HEV. Some of the most notable are the Mitsubishi ESR, Volvo ECC, and BMW 3 Series [10].

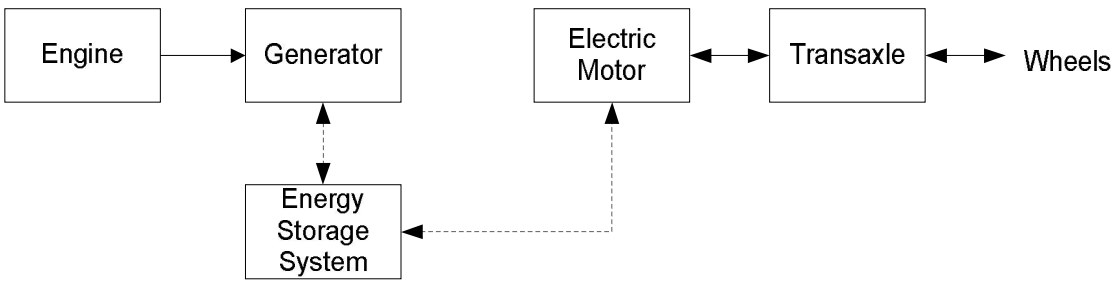

Figure 1 Generic Series Hybrid Vehicle Architecture

In the parallel HEV architecture, an electric motor and an ICE are connected to the drivetrain and provide propulsion power [9]. With the electric motor, this configuration can reduce the ICE size compared with a conventional vehicle, without compromising the vehicle performance[11]. The energy efficiency of the ICE can also be improved with assistance from the electric motor. Some early developed parallel HEVs include the BMW 518, Citröen Xzara Dyn-active and Saxo Dynavolt, Daimler-Chrysler ESX 3, Fiat Multipla, and the Ford Multiplia and P2000 Prodigy [10]. A generic parallel architecture is depicted in Figure 2.

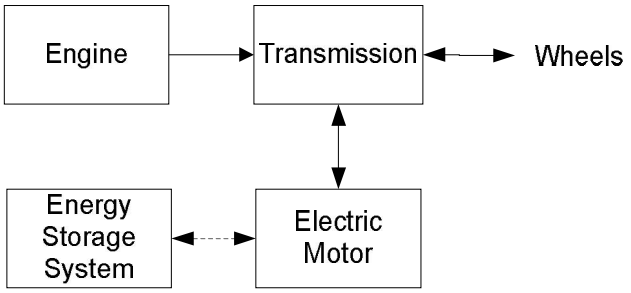

Figure 2 Generic Parallel Hybrid Vehicle Architecture

In an e-CVT HEV powertrain, the vehicle can operate as a series hybrid, a parallel hybrid, or a combination of the two. The keys to this configuration are the presence of two motor/generators and the mechanical and electrical connections between the two. The mechanical connection between the engine and electric machines is usually accomplished by planetary gear sets known as power-splitting device (PSD). Toyota and Ford utilized the one-mode power split configuration with a single e-CVT configuration; it has a single planetary gear and the input split configuration is relatively simple with only one pure mechanical path [12]. GM, Renault and others have introduced the two-mode power split configuration with two e-CVT configurations, which has multiple planetary-gears and an input/compound split function that is more complex. It however offers different possible transmission configurations which increases energy efficiency and improves performance under different driving conditions [12].

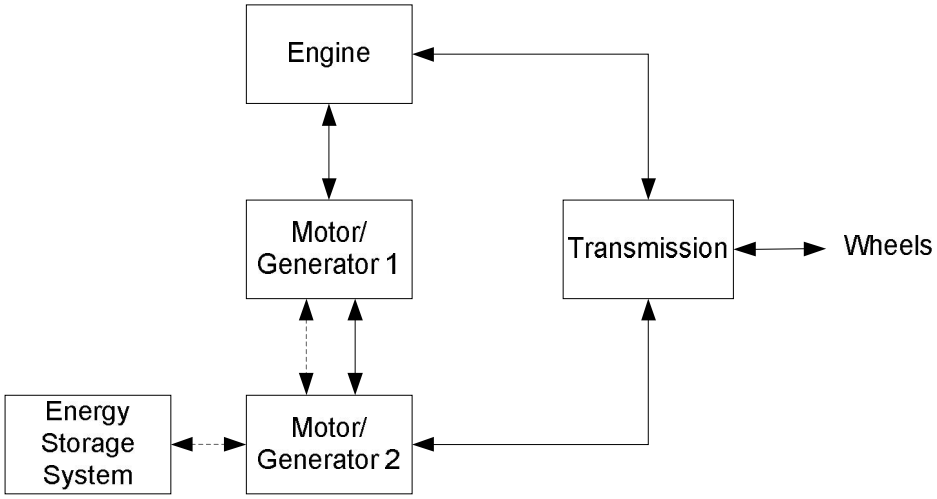

Figure 3 Generic Series-parallel Combination Architecture

Each of the three introduced hybrid architectures can be designed with different electric drives and electric energy storage systems. The increased vehicle powertrain electrification enable vehicles to run as strong hybrid or PHEV utilizing energy from both consumable liquid fuels and electricity from the grid.

2.1.2 Electric Drive Systems and Energy Storage System

The electric drive system is a key component to a HEV. The characteristics of an electric drive system include fast response, ease of control, low mechanical noise, and relatively high energy efficiency over a set of wide operation conditions, in comparison with an ICE. With the space and weight limits in a HEV, developing smaller and higher power electric drive systems at reasonable cost is essential for future HEVs. The selection of electric drives depends on HEV configurations. For light-duty vehicles, direct-drive-wheel motors can reduce system complexity and save space for packing [13]. For a parallel HEV, the induction machine is often used which is low in cost and still have respectable energy efficiency [14]. In a power-split HEV, permanent magnet (PM) motors are most often selected which provide high energy efficiency[15].

The need for electric energy storage system (ESS) also depends on vehicle applications. Important requirements for an ESS include: high energy density, high charging/discharging capability, long battery life, high robustness and reliability, and low cost. Batteries such as Nickel-metal Hydride (Ni-MH) and Lithium-ion (Li-ion) batteries

often serve as energy storage systems. In addition, ultracapacitors have emerged recently as a beneficial supplement to the batteries. Ni-MH batteries are widely used in most earlier and many current HEVs [16]. It has proven a significantly higher life than most lead-acid batteries during shallow cycles [17]. Li-ion batteries are experiencing a rapid improvement. They have been demonstrated as a technology that can provide higher specific power than the Ni-MH batteries. Li-ion batteries are increasingly used in newer HEVs to replace Ni-MH batteries, as many OEMs are shifting from Ni-MH to Li-ion batteries [18, 19].

With significantly inferior energy density compared to batteries, ultracapacitors are not considered as a substitute to batteries [20]. Instead, they can be used in combination with batteries and improve the dynamic response of the ESS, as well as protect batteries from harmful operations (e.g. rapid charging during regenerative braking). Ultracapacitors have extremely long lifetimes, especially during shallow-cycles. The current use of ultracapacitors is still limited to R&D phase [20-25].

2.2 Traditional Design Method for a Powertrain of Conventional and Early Hybrid Vehicles

While developing a conventional vehicle powertrain, the ICE design and transmission design are usually in parallel and relatively independent. This conventional vehicle powertrain architecture can flexibly accommodate different ICEs and transmissions combinations, while the remaining work for calibration is moderate. The main design task at system level is to choose an ICE based on the power demand specifications and select a mating transmission with similar power capability. Completion this design task is a relatively straightforward process that are preceded based on engineering experiences using the trial and error based approach. Satisfying designs can usually be achieved using the approach, due to the simple nature of the powertrain at system level, and limited possible propulsion combinations.

The early HEVs based on the parallel or series hybrid architectures add moderate system complexity to the conventional vehicle powertrain. The design process of these HEVs also follows the similar traditional design approach. However, to further optimize powertrain design and improve the energy efficiency, the design challenging increases

and the traditional experience based approach can no longer fulfill the design task. A more advanced design method is needed which should dynamically computes the powertrain performance and accelerate the whole design process.

2.3 Model-based Design Method for Recent Advanced Hybrid Vehicles

Model-Based Design (MBD) is a new design methodology that utilizes high fidelity, multidisciplinary, mathematical and computer models of the system under design to predict design performance and to guide design improvements for designing complex controls, signal processing and communication systems to meet given design requirements [26]. In applications to automotive powertrains, MBD is significantly different from traditional design methodologies and it can efficiently accelerate the design process from architecture selections to near-production calibrations. A complete MBD process includes four main steps: plant modeling and design, controller modeling and design, performance simulation and design improvements, and design deployment.

2.3.1 Plant Modeling

Plant modeling in a vehicle powertrain includes modeling of an ICE, electric motors, transmission, batteries, vehicle dynamics, and sometimes a human driver. These models can be first principle or data-driven based. The first principle models are created using algebraic-differential equations governing plant dynamics. Models generated using this approach can well represent the transient and steady state responses of the system. Model calibrations are necessary to ensure model accuracy. The computation load using this approach can be significant as model complexity increases. The data-driven models use processed results from the raw data of a real-world system and sometime mathematical models are derived according to the data. The data-driven nature can ensure high model accuracy without high demand of computational power.

2.3.2 Controller Modeling

There are a number of controllers in a vehicle powertrain that perform at either component level or system level. Functions for the controllers at component level are usually less complex, which involve communications with system controls and implementation of direct control commands. For studies of a complete vehicle

powertrain, these controllers at component level are frequently combined with the respective powertrain component and considered as part of plant modeling. The controller at system level, also called supervisory controller, plays at a superior role in a vehicle system and usually requires significant engineering efforts.

Modeling of a supervisory controller is critical to the performance of the overall vehicle, especially for complex powertrain systems like a HEV. The flexible hybrid powertrain configurations and multiple power plants create numerous different propulsion possibilities, making developing the optimal controller strategy a challenging task. Control strategies are traditionally rule-based, heavily relying on engineering experiences. More recent trend is to apply advanced engineering approaches such optimization techniques in the MBD to assist the design process.

2.3.3 Simulation

With modeled plants and controllers, simulations are carried out in software environment as well as with real world devices. Hybrid vehicle powertrain simulations can be performed at three different stages: model-in-the-loop simulation (MIL), software-in-the-loop simulation (SIL), and hardware-in-the-loop simulation (HIL).

The MIL simulations are applied throughout the whole develop process from architecture selections to vehicle calibrations. Models at MIL can sometime be simplified in order to quickly generate the performance model and accelerate the simulation speed.

The SIL simulations performed at the second stage involves more detailed modeling of powertrain components and controllers. The powertrain communication networks such as CAN network are defined and code for controller are generated. No hardware is required at SIL phase which makes SIL a flexible and less expensive testing approach. However, the simulation time may be completed differently from a real-time system.

The HIL is to connect the computer plant model to real world controllers. The virtual vehicle is used to verify and validate the developed controller, since in vehicle tests are often time-consuming and expensive. A variant of HIL is rapid control prototyping which implements control algorithm on a real-time computer and connect it to devices with real input/output.

2.3.4 Deployment

HIL and control rapid prototyping greatly reduce the gap between software modeling and real-world deployment. The developed controller uses automatic code generation while iterative debugging process is still needed. The vehicle testing and calibrations are performed after satisfying HIL and control prototyping models are generated. This is an iterative process between debugging in the software environment and validating in the testing environment.

2.4 Next Generation Hybrid Vehicle Design

The use of MBD has greatly accelerated design process of advance vehicle powertrains, and made low-cost and less time consuming testing possible in the simulation environments. Consequently, performing design improvements and design optimization of the complex powertrain system become possible while different design scenarios can be easily evaluated. Two important applications of optimizations in MBD powertrain are components parameterization in architecture selection and optimal controller/control strategy development.

2.4.1 Architecture Selection and Parameter Determinations

Selecting powertrain architecture and component is a more challenging task in a HEV powertrain than in a conventional powertrain. The flexible hybrid configurations, wide selections of drive components, and multiple energy sources, have significantly widened the design space and created numerous design combinations. HEV design in early days follows the traditional empirical based approach; the developed powertrain are evolved from conventional powertrains with incremental improvements. This design approach is heavily empirically dependent and the slow human involved process only allows few design iterations to be performed. To further improve the current designs and to identify innovative new designs, an advanced design approach which can automatically search among different design variations and identify optimal designs is in need. Optimization based searching algorithms can play an important role in identifying optimal design, while the function evaluation is carried out using MDB simulations. Even with supports of advanced optimization algorithms, this multi-disciplinary MDB is usually demanding on computational power which makes number of possible design variables limited. The

multi-optima nature of most powertrain problems often leads to using of global optimization searching approaches.

2.4.2 Control System and Strategy Design

Developing control strategies for the supervisory control of a HEV powertrain generally follows two approaches: rule-based or optimization based. The rule-based approach is a elementary method that was adopted in many early HEV powertrain developments [27]. A widely adopted rule-based control strategy for power split hybrid vehicles is basically: a) Increase/decrease engine power when the state of charge (SOC) is low/high; b) the engine power request is based on the most efficient engine operation. These rule-based controls are generally straightforward to implement and requires modest computation power [28]; however, most rules cannot fully ensure best performance of a powertrain, and defining rules that can generate near optimal results is a time consuming task that requires extensive engineering experiences.

Combining optimization and MBD provides a unique tool that makes developing the optimal control strategy possible. Depending on when the optimizations are performed, the optimization based control strategies are divided into static/offline optimization strategies and real-time/online optimization strategies.

The static optimization method runs the design optimizations through performance simulation off-line, and data obtained from the optimizations are used later to produce specific control strategies for real-time operations. This approach is widely applied to complex control problems which require intensive computation time. Some previous studies applied this method to powertrain control, and several optimization algorithms were used, including dynamic programming (DP) [29-31], sequential quadratic programming (SQP) [32], and DIRECT [33]. Many of the control problems are highly non-linear and non-continuous with many local optimums. Therefore, local optimization methods frequently failed to converge to a global solution [34].

The real-time optimization based strategies run optimizations in real-time. This control approach generally uses the real-time and real-world data as computation inputs, such as traffic conditions, route selections, charging/refuelling availabilities, and current vehicle status. Due to the considerable computations needed to carry out vehicle

performance simulation and performance optimization using built in model, and the limited computation power of the vehicle's ECU, solving an optimization in real time is a challenge task and computation hardware dependent. As a result, most problems are simplified problems and advanced vehicle controllers with high computation capabilities are needed. Using the real-time optimization based control strategies is an emerging research field, in which little work has been previously carried out. The needs for adaptive controls using optimization strategies have grown quickly with arise of the much increased control complexity in advanced hybrid vehicles.

2.4.3 Limitations and Room for Improvement

Even with advanced optimization algorithm, performing design optimization on powertrain architectures and control strategies is highly challenging due to the system complexity and high computation load. As a result, applications of optimization in MBD have been limited in the development of previous hybrid vehicle powertrains. This work investigates the applications of optimization to both architecture design and control strategies developments.

Chapter 3 Next Generation Vehicle Powertrain and Fuel Selection

3.1 GHG Emission Standards for Future Vehicles

Strict standards are formulated in the United States to lower GHG emissions from passenger cars and light-duty trucks to a combined level of 250 grams carbon dioxide (CO_2) per mile in model year 2016, and further to 162 grams per mile in model year 2025, equivalent to 35.5 mile per gasoline-equivalent gallon ($MPG_{ge.}$), and 54.5 MPG_{ge} respectively, if the reduction of CO_2 level is all through fuel economy improvements. The currently posted standards narrowly measure GHG emissions from only the tailpipe end instead of the complete fuel cycle on the WTW basis. Therefore, variations of considerable GHG emissions generated at the upstream stages are not differentiated. Considerations for future powertrain and fuel should include the complete WTW fuel cycle which includes the Well-To Pump (WTP) process of fuel generation and distribution at upstream stages, as well as the Pump-To-Wheels (PTW) side during the vehicle operation.

Previous works applying the WTW based analysis approach tend to have different focuses; but few included a comprehensive selection of different fuels and powertrains, especially for the U.S market [35], compared the WTW energy efficiency of hybrid electric and fuel cell powertrain on a medium size SUV [36], performed a life cycle analysis of four powertrain configurations based on small family cars in Belgium [37], studied energy fuel pathways using batteries and fuel cells powered vehicles in Italy [38], examined efficiency, cost, and GHG emissions of electric cars based on demand in Netherlands [39], and studied the WTW energy use and GHG emission of plug-in hybrid vehicles at different all-electric range (AER).

This work investigates different fuels and powertrains combinations, not only in satisfying the tougher government standards for automotive manufacturers, but also the WTW based complete fuel cycle. The vehicle category is focused on the passenger cars and light-duty trucks for the time frame up-to year 2025. In section 3.2, this paper starts introducing the WTW based study approach for the fuel and powertrain pathway

selections. In section 3.3, results from the fuel cycle analysis and vehicle powertrain simulations are presented; a comprehensive review on fuel and powertrain state-of-the-art is performed; a cost effectiveness study in GHG emissions is carried out. Finally, section 3.4 summarizes the work by pointing out promising fuel and powertrain options for both the near term and longer term future.

3.2 Integrated Fuel and Powertrain Selection Approach

The study for fuel and powertrain selection includes three closely connected modules: a WTW based analysis, a review on powertrain technology, and a review on fuel supply, as outlined by the block diagrams in Figure 4. The WTW based analysis calculates GHG emissions, fossil and petroleum energy consumption of every fuel and powertrain pathway. This two-step approach first analyzes life cycles of different fuels on the same energy basis; and then modeling and simulation of different powertrain technologies are performed the compute fuel consumption and GHG emissions in vehicles. In additional to the WTW based analyses, the state-of-the-art powertrain technologies and fuel supplies are reviewed to assess the technology feasibility, economic practicality, and other aspects.

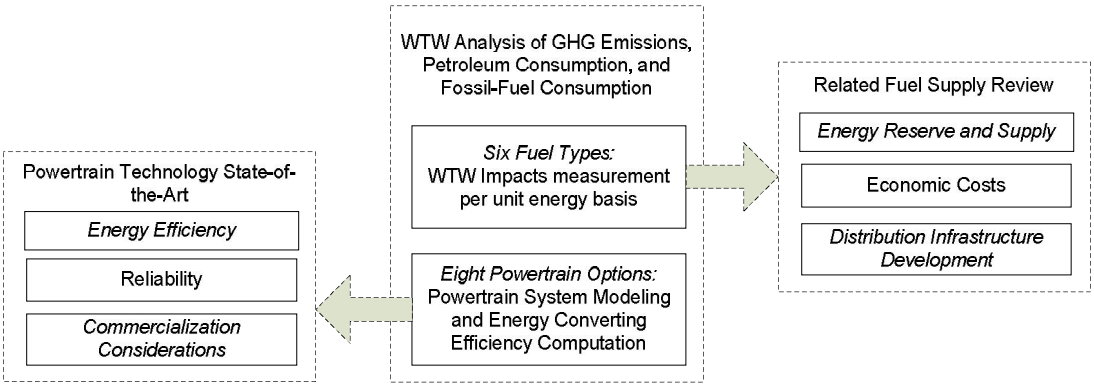

Figure 4 Outline of the Future Fuel and Powertrain Selection Process, including the WTW based analysis, a Powertrain Technology Review, and a Fuel Supply Review

3.2.1 Fuel Cycle Well-To-Wheels Analysis

The seven representative fuels selected in this study include gasoline, diesel, ethanol (EtOH), biodiesel, compressed natural gas (CNG), electricity, and hydrogen. Additional fuels blended using these base fuels are also considered, such as E10 (mixture of 10% ethanol and 90% gasoline by volume), E85 (mixture of 85% ethanol and 15% gasoline by

volume), and B20 (mixture of 20% biodiesel and 80% diesel); results of these additional fuels can be interpolated from results of the base fuels. The WTW is further divided in to WTP and PTW. The WTP examines the energy use and GHG emission effects of energy feedstock recovery and transportation fuel production, transportation, and distribution. The PTW calculates the energy use and GHG emissions when a fuel consumed in vehicles. Calculations of the fuel cycle analysis use the GREET program, which is an analytical tool to model Greenhouse gases, Regulated Emissions, and Energy use in Transportation [40]. Some modeling considerations in the GREET program are highlighted and presented in Table 1[41]. Calculations for the downstream stages of PTW in the fuel cycle analysis are based on fuels with the same energy content of one mega-joule, independent of powertrain technologies. Table 1 summarizes assumptions and considerations for every fuel type. The calculated results are presented in Section 3.3.1 Fuel WTW Analysis.

Even though the powertrain related models are also available from the GREET program, these models are relatively constrained to limited powertrain options, and lack of vehicle size variations. Therefore, the powertrain based analysis in this work is carried out separately in the next step, independent of models from GREET, as discussed in the following section 3.2.2.

Table 1 Assumptions and Considerations for the Well-To-Pump Calculations for Seven Fuel Types

Fuels	**Feedstock**	**Calculation Assumptions and Considerations**
Gasoline	Petroleum	50% of gasoline are reformulated (RFG), and the remaining 50% are conventional (CG). Both RFG and CG has low sulfur level of 25.5 ppm; RFG contains 2.3% of ethanol as oxygenate.
Diesel	Petroleum	100% diesel is Low-sulfur diesel (LSD) with sulfur ratio at 11 ppm. 98% crude recovery efficiency and 89.6% refining efficiency are used.
Biodiesel	Bio-mass	Most biodiesel in U.S is produced from soybean oil. Other oils such as canola oil and sunflower seed oil can also be used.
Ethanol	Corn	Corn is the main feedstock for ethanol production. Shares of ethanol plants are 88.6% Dry Milling Plants (DMP), and 11.4%WMP of Wet Milling Plants (WMP). Domestic and foreign CO_2 emissions from potential land use change of farming are included.
CNG	Natural Gas	NG recovery and recovery efficiency is 97.2%; NG compression efficiency is 93.1% and electric compressor efficiency is 97.3%.
H2	Natural Gas	Most gaseous hydrogen is produced from distributed station using natural gas. 70% production efficiency is assumed.
Electricity	U.S. Mix	U.S. Mix for generation use is made up of 47% from coal, 21% from nuclear, 20% from NG.

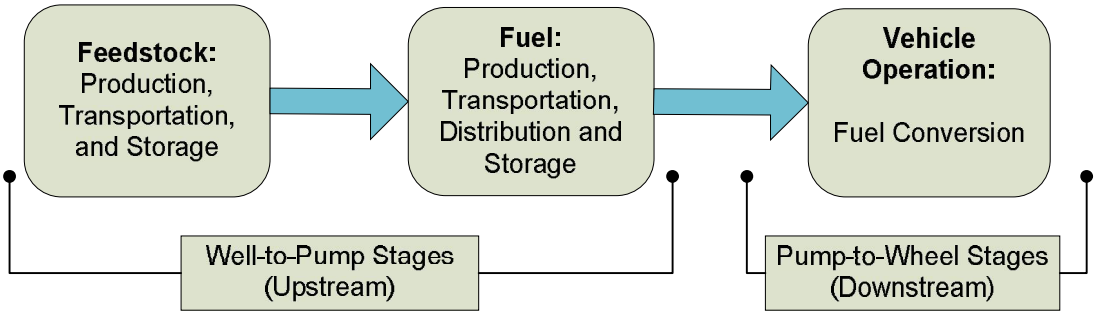

Figure 5 A Fuel Cycle Well-to-Wheels Analysis

3.2.2 Powertrain Modeling and Simulation

Vehicle powertrains are modeled and simulated to evaluate the vehicle performance, energy consumptions and GHG emissions going through each fuel pathway. Figure 6 shows the different fuel and powertrain combinations. Two considered vehicle platforms are a passenger car and a light-duty truck. Overall, there are nine fuel pathways for each of the two vehicle platforms. Six of the nine fuel pathways go through the ICE based energy conversion. Hydrogen and ethanol are the two fuels with two potential powertrain pathways: ICE or fuel cells (FC).

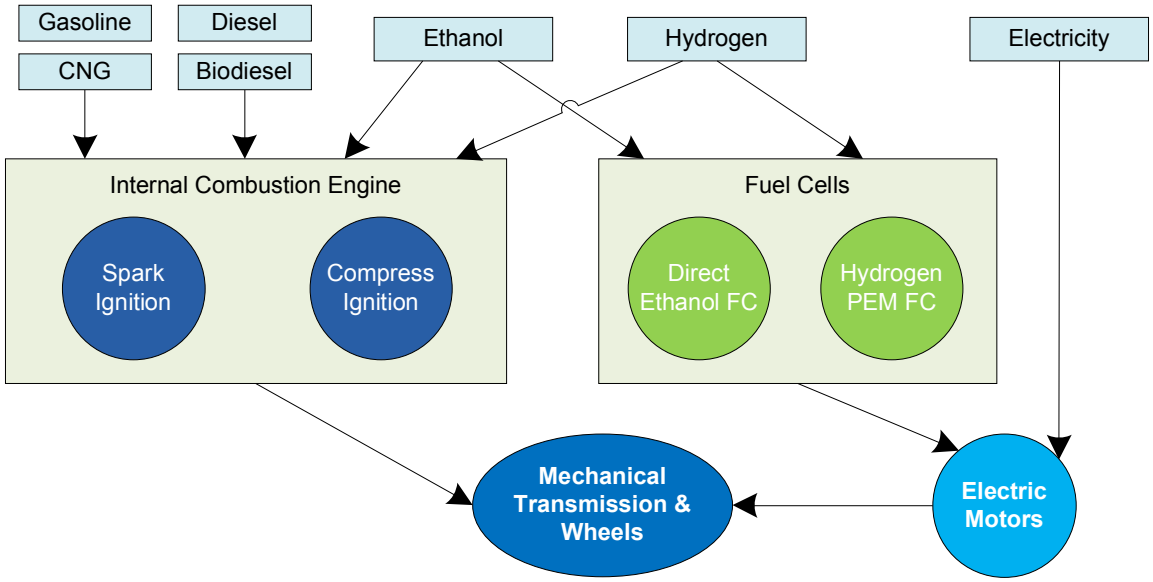

Figure 6 Nine Fuel Pathways with Different Powertrain Technologies

The modeling and simulations are performed using the Powertrain System Analysis Toolkit (PSAT), developed by Argonne National Lab [42, 43]. At this time, some

powertrain technologies such as hydrogen ICE and fuel cells are not yet commercially available and well tested. Therefore, data are insufficient for modeling of these powertrains; assumptions are made for three fuel-powertrain pathways to have consistent energy efficiency as the conventional fuel counterparts, ethanol ICE, ethanol FC, and biodiesel ICE. The modeling parameters for the two vehicle platforms and different powertrain configurations are listed in Table 2 and Table 3. The modelled battery capacity for EV is 40 kWh; the modelled hydrogen tank capacity is 83 kg at 2 kWh/kg.

Two driving cycles are selected for evaluations of fuel economy: the Urban Dynamotor Driving Schedule (UDDS) and the Highway Fuel Economy Driving Schedule (HWFET). These two driving cycles were previously used by EPA for new cars fuel consumption measurement until year 2011; the recently updated method by EPA adds more testing procedures such as the cold and warm starts to better approximate the real world driving condition[44]. This new measuring technique is however not reflected in this work, due to the lack of knowledge to model and simulate the additional cold temperature operations, air conditioning, and etc.

Table 2 Main Powertrain Energy Converter of Studied Vehicles

Energy Converter	**Passenger Car**	**Light-duty Truck**
Gasoline/Ethanol ICE	Honda 3.0 V6 147 kW	4.8L Silverado 201 kW
Diesel/Biodiesel ICE	Audi 2.5L 88 kW	Catepillar 3126E 7.2 L 205 kW
CNG ICE	John Deere CNG engine 186 kW (scaled to 90 kW)	John Deere CNG engine 186 kW
Hydrogen ICE	H2_67 ICE engine model by ANL	H2_67 ICE engine model by ANL, Scaled to 180 kW
H2/Ethanol Fuel Cells	80 kW Direct H2 by ANL (scaled)	180 kW Direct H2 by ANL (scaled)
Electric Drives	UQM Powerphase 75	UQM Powerphase 145

Table 3 Specifications of Representative Passenger Car and Light-duty Truck

Vehicles	**Passenger car**	**Light-duty truck**
Curb weight(Gasoline ICE)	1700 kg (Gasoline ICE Config.)	2200 kg (Gasoline ICE Config.)
Rolling resistance	Crr1=0.009; Crr2=0.00012	Crr1=0.12; Crr2=0.00012
Wheel radius	205/65 R16	275/65 R18
Aerodynamics	f0= 112.85; f1=4.6; f2=0.542	f0=107.7; f1=10.66; f2=0.9042

The measurement of fuel consumption among different fuels is converted to $MPG_{ge.}$, where a gasoline-equivalent gallon is the amount of alternative fuel it takes to

equal the energy content of one liquid gallon of gasoline, calculated using the lower heating values of 34.8 MJ/L. The calculations of MPG_{ge} use Eq.(1), where L is the travelled distance in miles, E_{fuel} is energy of consumed fuel in joules, e_g is energy of a gallon of gasoline in joules. The PTW efficiency is calculated as the propulsion energy divided by the energy in the fuel. Due to the vehicle weight differences of different powertrain components, the MPG_{ge} and PTW efficiency are not lineally correlated. The weighted PTW efficiency $\eta_{weighted}$ is the average of the highway and city fuel measurements, calculated using to Eq. (2). A weighting factor of 50% is applied to passenger cars and light duty trucks, according to the close number of car and pickup truck sales in recent years[45]. For either passenger cars and or light-duty trucks, MPG_{ge} is measured for both city and highway driving cycles.

$$MPG_{gasoline\ equivilent} = \frac{L}{E_{fuel} / e_g} \tag{1}$$

$$\eta_{PTW\_Weighted} = \frac{\eta_{car\_city} + \eta_{car\_hiway}}{2} \times 50\% + \frac{\eta_{truck\_city} + \eta_{truck\_hiway}}{2} \times 50\% \tag{2}$$

3.2.3 Review of Fuel and Powertrain

In addition to identifying the energy pathways with low GHG emissions and high energy efficiency, the availability and cost of these fuels and powertrain technologies also play a very important role in market penetrations of these vehicles. In this work, a comprehensive review of powertrain technologies and transportation fuels is performed. The fuel supply, price, and distribution infrastructure is discussed. The technology state-of-the-art and key remaining issues of each powertrain technology are reviewed. A cost effectiveness sensitivity analysis for each fuel pathway in reducing GHG emissions is performed.

3.3 Results

3.3.1 Fuel WTW Analysis

Calculations of the fuel cycle analysis are performed on each two-year intervals between years 2010 and 2020, during which time period data is available in the GREET program.

Most calculated results only show slight changes from year to year and no significant trend of changing is identified. Therefore, only results for years 2010 and year 2020 are presented, as shown in Table 4. The WTW based results for GHG emission, petroleum consumption, and total fossil fuel consumption are compared. The following conclusions from the results are highlighted for GHG emissions and petroleum consumption of each fuel.

Table 4 Energy and GHG Emission Facts for a Megajoule (10^6) of the Seven Base Fuels (Year 2010~2020 U.S Mixture)

		Gasoline	**Diesel**	**Bio-diesel**	**Ethanol**	**Elec.**	**CNG**	**H_2**
Well-To-Pump	GHG	85~75 g	99~97g	-30~--30	-2~-5 g	133~134g	112~111g	153~158g
	Petroleum (MJ)	0.39~0.34	0.45~0.42	0.04~0.04	0.05~0.05	0.02~0.02	0.04~0.04	0.01~0.02
	Fossil Fuels (Excluding Petroleum) (MJ)	0.51~0.52	0.53~0.56	0.11~0.10	0.37~0.38	0.83~0.80	0.89~0.87	0.94~0.93
Pump-To-Wheels (Tailpipe)	GHG	74~74 g	76~76 g	77~77 g	72~72 g	0	57~57 g	0
	Petroleum (MJ)	1	1	0	0	0	0	0
	Fossil Fuels (Excluding Petroleum)(MJ)	0	0	0	0	0	1	0
Well-To-Wheels (Total)	GHG	159~149g	175~173g	47 ~47g	70 ~67 g	133~134g	169~168g	153~158g
	Petroleum (MJ)	1.39~1.34	1.45~1.42	0.04~0.04	0.05~0.05	0.02~0.02	0.04~ 0.04	0.02~0.02
	Fossil Fuels (Including Petroleum)(MJ)	1.9~1.86	1.98~1.98	0.15~0.14	0.42~0.43	0.85~0.82	1.93~1.91	0.95~0.95

According to the relatively close results for both year 2010 and 2020, biodiesel and ethanol are among the lowest in WTW GHG emissions on unit energy of fuel basis. Compared with the gasoline counterpart, the significant WTW GHG emissions reduction for these two biofuels takes contributions from the low upstream GHG emissions, while the tailpipe GHG emissions only show little improvements. Both electricity and hydrogen have no GHG emissions at tailpipe, but the upstream GHG emissions remain high. The least favourable fuels for GHG emission reductions are gasoline, diesel, and CNG; both upstream and tailpipe GHG emissions for these fuels are high. CNG has slight advantage in tailpipe GHG emissions, roughly at 20% less than gasoline and diesel.

In terms of petroleum energy usage, diesel and gasoline unavoidably carried the most petroleum footprints, averaging 1.4 MJ of petroleum energy consumption for one

mega-joule of fuel. All remaining five fuels have significantly lower petroleum usage, varying between 0.02 MJ and 0.05 MJ for one mega-joule of fuel. In terms of total fossil fuels consumptions including petroleum, coal and natural gas, biodiesel is the lowest by a big margin, followed by ethanol, electricity and hydrogen. Gasoline, diesel, and CNG consume nearly two times of fossil fuel energy for one mega-joule of fuel.

Figure 7 compares GHG emission, petroleum and fossil fuel consumption of eleven fuel types, including four additional fuels which are blended from the seven base fuels. Diesel has the highest rating in all three compared categories and consequently serves as baseline for the comparison; results for all other fuels are scaled in relative to diesel. Biodiesel and ethanol has the lowest rating in all three categories. E10, E15, B20 follow the decreasing order, largely benefited from the increased weighting of biofuels contents.

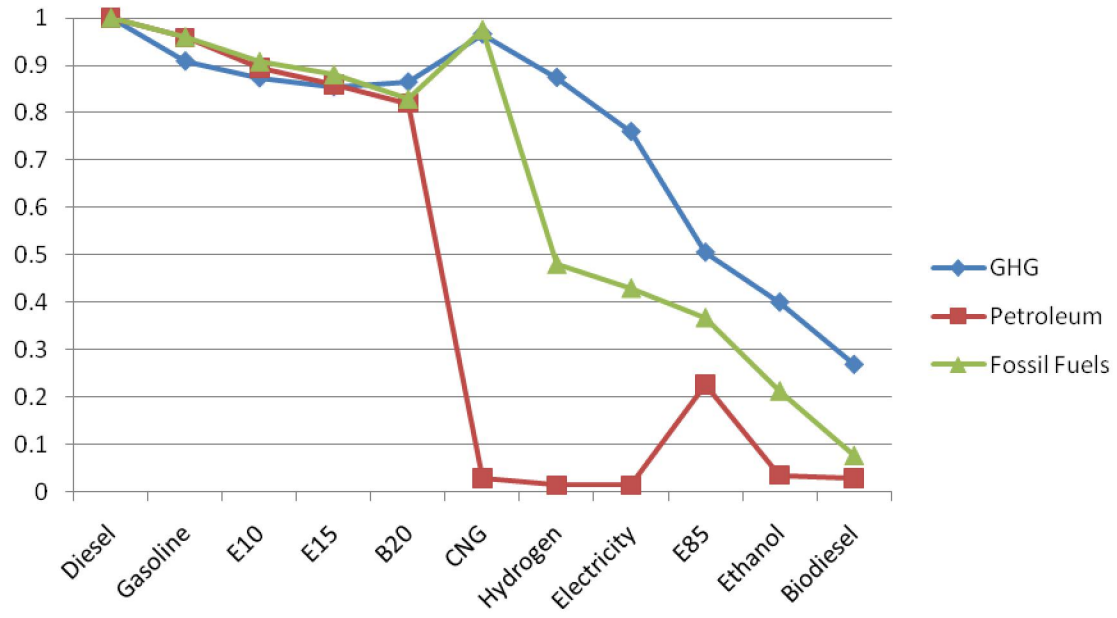

Figure 7 Relative Comparison of GHG, Petroleum and Fossil Energy Consumption per unit Energy of Seven Base Fuels and Four Blended Fuels (Year 2010)

3.3.2 Powertrain System Modeling and Simulations

The simulated results of different vehicle powertrain configurations are summarized and shown in Table 5. The powertrains under internal combustion engine are conventional powertrain without hybridization. For easy comparison, all results of fuel consumptions are converted to mile per gallon gasoline equivalent (MPG_{ge}). Results for powertrain

efficiency are also calculated, which are not linearly associated with fuel consumption due to the weight difference of powertrain components. Results from both the previous fuel based WTW analysis in Table 4 and the powertrain based WTW analysis in Table 5 are incorporated and an intuitive chart is generated as shown in Figure 8. The horizontal axis represents the petroleum consumption (in thousand joules per kilometre travelled) and the vertical axis represents the GHG emissions (grams per kilometre travelled). The seven dashed lines represent the seven fuels, where the slope is determined by results from Table 4. Specific results for each simulated vehicles are addressed in the chart.

Table 5 Fuel Economy and Pump-To-Wheels Efficiency of Selected Fuels and Powertrain Configurations

		Internal Combustion Engine				Fuel Cells	Electricity
		Gasoline /Ethanol	Diesel/ Biodiesel	H2	CNG	H2/ Ethanol	Electricity
Pass. Car	MPG_{ge} City/Highway	26/41	25/43	29/47	28/39	66/68	84/81
	PTW Eff. City/Highway	17.4%/ 24.4%	19.8%/ 26.8%	20.1%/ 27.1%	19.7%/ 22.9%	38.9%/ 28%	77.9% /51%
Light Truck	MPG_{ge} City/Highway	13/20	15/21	15/25*	15/20*	33/34	46/42
	PTW Eff. City/Highway	14.4%/ 23.8%	17.5%/ 24.9%	20.1%/ 27.1%	19.7%/ 22.9%	38.9%/ 28%	77.9% /51%
Weighted PTW Efficiency		20%	22%	24%	21.3%	33%	65%

The following points are addressed according to results presented in Figure 8.

- Diesel and gasoline with the ICE based powertrains are the energy pathways consume highest petroleum (over 4,000 kJ/km) and emit most WTW GHG emissions (~=500 g/km). All remaining fuel pathways can reduce at least 95% of petroleum consumption.
- To satisfy the U.S government's tailpipe GHG emission standard of 155 g/km by 2016 and 101 g/km by 2025, all fuel pathways except hydrogen/ethanol fuel cells and electric vehicle need powertrain improvement.
- The biodiesel-ICE pathway yields the lowest WTW GHG emissions among all powertrain competitions with an ICE, including the hydrogen ICE powertrain. The

tailpipe GHG emission for biodiesel is however closely comparable to gasoline, diesel, and ethanol with no significant reduction.

- The electricity and hydrogen based fuel pathways have no tailpipe GHG emissions (except for minor NOx during hydrogen combustion). The upstream WTP GHG emissions during hydrogen production are however very high, due to the natural gas reformation based hydrogen production process.
- The CNG and ICE based fuel pathway has no advantage in WTW GHG emissions reduction over the petroleum fuels; the tailpipe/PTW GHG emission however is lower than diesel and gasoline, since a higher percentage of the WTW GHG emission is contributed by the WTP phase of fuel production.

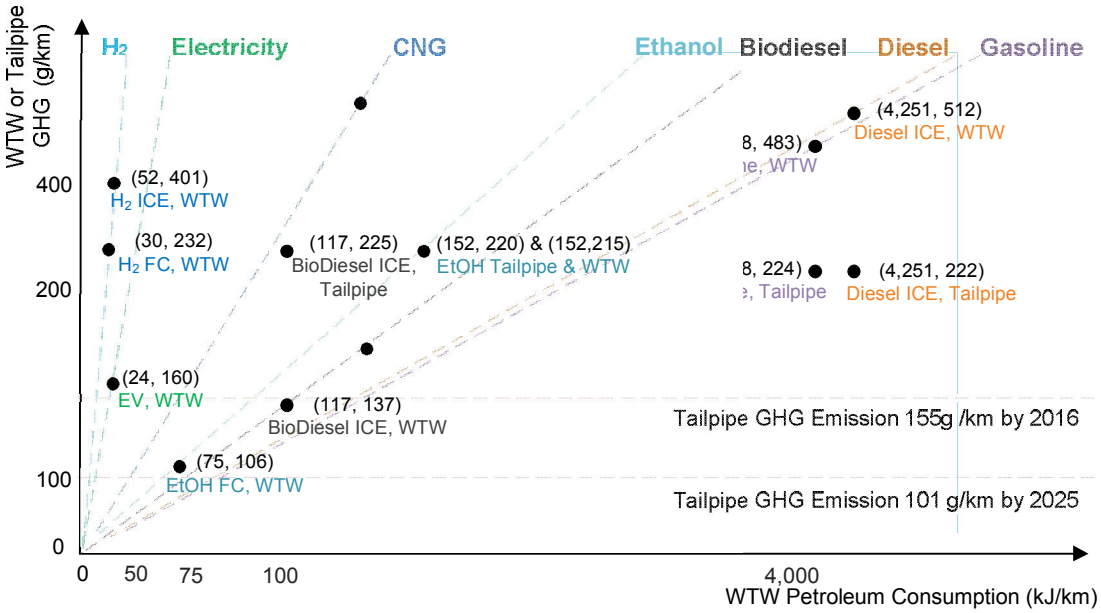

Figure 8: Passenger Car and Light Truck WTW Analysis Based on Year 2010 U.S. Mix Data

The modeled powertrains are based on each of the seven base fuels and associated powertrain pathways. There is however additional energy pathways involving more than one fuel consumption, such as vehicles running blended petroleum fuels, biofuels, or electricity stored in grid chargeable batteries. The GHG emissions and energy usage for these vehicles can be calculated by interpolating results of the simulated fuel and powertrain pathways. Two most representative multiple-fuel powered vehicles are

discussed, which consume electricity, biofuels, and petroleum fuels; the results are shown in Figure 9. The two shaded area represents consumption of three fuels of at different mixes. Results for two popular blended fuels, E85, and B20 are identified in the chart. It should be noted that simple linear interpolation assumes no efficiency changes when blended fuels are consumed; some vehicles running blended fuels such as the plug-in hybrid vehicles can achieve 20-40% efficiency improvements due to the powertrain hybridizations[46].

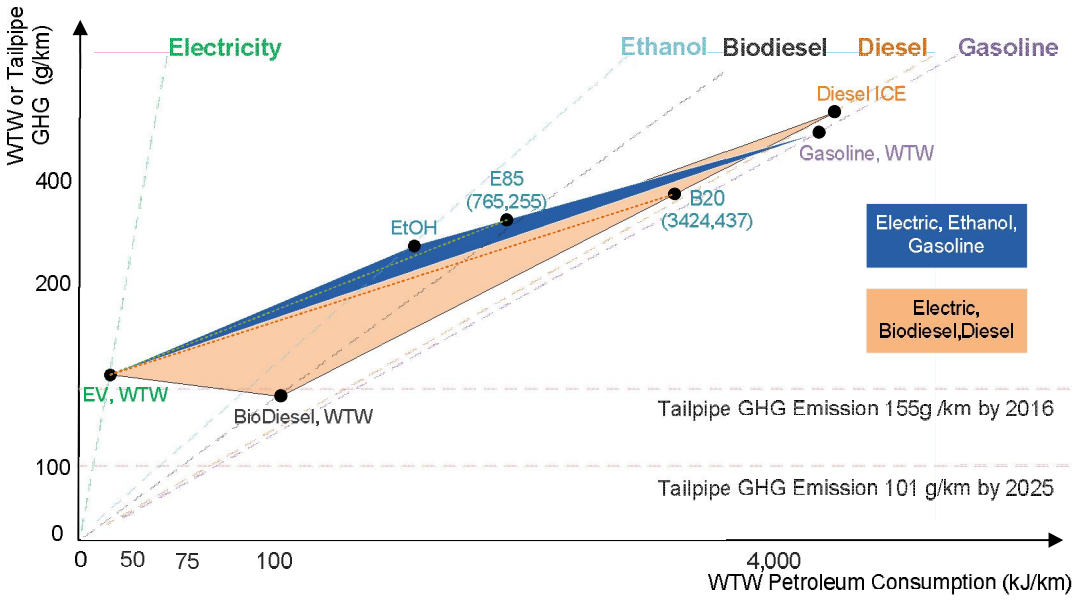

Figure 9 Interpolated Results for Hybrid Vehicle Powertrain Including Multiple Fuel Pathways

3.3.3 Fuel Cost and Availability

The price and availability of each fuel are important factors that form people's perception of powertrains selection. The price and availability of each fuel option across the United States is studied. As differences in fuel measurement create difficulties for price comparison, conversions to gasoline-equivalent gallon (gge) are made, which is the amount of alternative fuel it takes to equal the energy content of one liquid gallon of gasoline. The obtained fuel price is summarized and shown in Table 6. On the gasoline equivalent gallon basis, the price for CNG is the lowest at $2.1/gge. Biodiesel and ethanol are most expensive, driven by the continuously raising price of the feedstock,

such as corn and soybean. The final fuel cost for end consumers is calculated using studied fuel prices and simulated fuel consumption, based on 100 km of travelled distance. The results are shown in Figure 10. According to the results, electricity is the least costly fuel option which is over 70% lower than conventional gasoline. Among fuels consumed by ICEs, CNG is the least expensive, taking advantage of its lowest price on the equivalent energy basis.

Table 6 Comparison of Fuel Price at Retails in U.S (mixed data of 2010~2011)

	Price	**Availability**
Gasoline	$3.70	Conveniently accessible for most drivers. 121,446 retail gasoline outlets in the USA in 2002, according to U.S. Energy Information Administration.
Diesel	$3.95/gal $3.48/gge	
Ethanol	$2.60/gal $3.95/gge	Ethanol blended with gasoline is available at many fuel stations across north American. Concerns for ethanol price increase due to the sharply increased feed stock price. Corn price increased from $3.5/bushel in the summer of 2010 to $7.5/bushel as of April 2011 [47].
Biodiesel	4.64/gal 4.58/gge	The most common source of biodiesel in the U.S. is soybean oil and yellow grease. Using yellow grease can produce biodiesel more cost competitive with petroleum diesel, but the yellow grease supply is limited to 100 million gallon per year [48].
CNG	$2.1/gge	Many fuel stations in U.S to support 120,000 CNG vehicles operated in fleet basis in the United States. The price of CNG price varies from $1.7/gge in remote areas, to 2.3 gge in some bigger cities.
Electricity	11.2 ¢/kWh $3.74/gge	11.2 ¢/kWh is the average electricity price in the U.S as of February 2011, according to U.S. EIA. Electric grid upgrade is needed for the electricity drive transportation transition.
Hydrogen	$4.00/kg $3.99/gge	Very few fuel stations constructed for demonstration projects, predicated cost varies from $4-12/kg using different techniques [49].

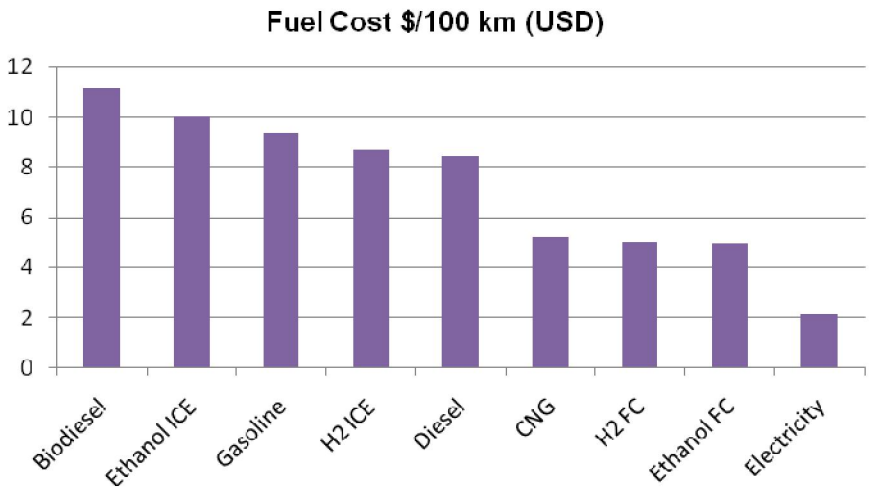

Figure 10 Comparison of Final Fuel Cost on 100 kilometres Traveled Distance

3.3.4 Key Powertrain Components State-of-the-ART

- Internal Combustion Engines and Fuel Economy Boosting Technologies

A conventional vehicle powertrain with an internal combustion engine and mechanical transmission has been the popular vehicle powertrain option. With high production volume, low initial cost and predictable fuel cost, the ICE based vehicles are likely to continuously dominate a large market share in the next coupe decades. Two main design challenges for the ICE technology are energy efficiency improvement and adaption for alternative fuels.

The current ICE running gasoline or diesel fuels can achieve up-to 40% of net energy efficiency in principle, if operated at the most efficient speed and torque combinations. The actual efficiency in real-world use is however significantly lower, due to the transmission frictions and load cycle changes because of the road conditions. The advancement of energy efficiency in ICE based powertrains is pursued along two pathways, either by improving the combustion efficiency, or by reducing losses of the remaining powertrain, such as transmissions. The gain in engine efficiency can largely be pursued through the lean burn effect and reduced heat loss, using several new techniques such as PISI, SISI, and etc [50]. These new technologies have gradually been adopted by car manufacturers and increased fuel efficiency is achieved in some newer vehicles. For

overall energy efficiency improvement, an estimate suggested 6-15% fuel efficiency gain by year 2020 and additional 21-28% fuel reduction if hybrid with electric motors [46].

Using ethanol, biodiesel, CNG, and hydrogen requires modifications of the conventional ICE at different levels, even though lightly blended gasoline with ethanol (E10, E15) or diesel with biodiesel (B20) can be consumed by most existing vehicles with no modifications. Highly blended or pure ethanol or biodiesel can be used on many newer engines with minor modifications and requires little cost increase [51]. The energy efficiency of running ethanol and biodiesel is expected to be similar to petroleum based fuels. Despite of the benefits in reducing petroleum consumption and GHG emissions, the feedstock supply for the biofuels rises concerns over air pollution, risk to biodiversity, and groundwater contaminations [52].

The hydrogen ICE powertrain solution is considered as a low-cost and near-term solution bridging the transition to hydrogen fuel-cells powered cars[53]. The efficiency of hydrogen in combustion generally suffers from high heat loss due to the higher burning velocity and shorter quenching distance of hydrogen compared with hydrocarbons [54]. Hydrogen can solely fuel the ICE or mixed with other fuels such as CNG and diesel[55]. Adaptation of hydrogen from the traditional gasoline engines requires hardened combustion components, higher voltage ignition coil, stronger crankshafts, and etc.; the overall cost increase is estimated at 1.5 times of an gasoline engine [56], excluding increased cost for hydrogen storage. The CNG engine operates on the same basic principal as gasoline or diesel powered engines. Both spark ignition engines and compression ignition engines can be converted to run CNG with little efforts[57].

- Fuel Cells Stack Technologies and Hydrogen Fuel Distribution Infrastructure

The PEM fuel cell is the most suitable fuel cells type for automotive applications. Both hydrogen and ethanol fuelled fuel cells technology are yet struggling in commercialization with a number of technical and social economical issues unresolved [58]. The current targets for hydrogen fuel cells technology is as following: life of 6000-8000 hours (~100,000 miles), cost of $45 US/kW, peak net efficiency of 62%, and cold-start capability at -40^{o}C [59]. The primary issues of the hydrogen fuel cells pathway studied in this work are performance, durability, cost, and hydrogen fuel distribution. Compared with hydrogen PEM fuel cells, direct ethanol fuel cell is in premature phase

and the detailed testing results of a full stack is not yet available. Due to lack of knowledge in literature and industrial applications, the ethanol fuel cell fuel pathway is not further explored in this study and the possibility for near term commercialization is highly limited. However, studies show that direct ethanol fuel cells can achieve no less efficiency compared with direct hydrogen fuel cells [60].

The durability of PEM fuel cells for commercialization is partially tested and presented in the literature. Under conditioned and stable lab environments, the current fuel cells can well exceed the basic lifetime requirement which varies from 4000 hours for car and up-to 20,000 hours for bus applications [61]. The Ford Focus fuel cells vehicle fleets were sent for yearly road test and demonstrated durability for 36,000 miles or higher [62]. The low temperature capability is however only tested up to 5 ^{o}C [59], while lower temperatures operations lower than 5 ^{o}C remains challenging. The degradation mechanism is yet to be fully understood before further performance improvement is achieved [63].

PEM fuel cell powered vehicles are already in services in a number of pilot programs [64]. However, the large scale commercialization of this technology still requires further technical improvements and cost reduction [22]. A study estimated potential cost for an 80 kW fuel cell system cost at a range of $60/kW to $80/kW, based on 2008 technology, extrapolated to a volume of 500,000 system per year [65]. In addition, the added cost of fuel cells accessory, electric drive, and batteries is also significant. As a result, commercialization of hydrogen fuel cell vehicle in near term is highly challenging, and some have predicted that no meaningful percentage of fuel cell vehicle in the total industrial volume is likely until 2030 [59].

- Electric Drive System and Energy Storage System

Energy storage system and electric drive are two key powertrain components in many vehicle powertrains including electric vehicle, fuel cell vehicle, and many hybrid gasoline powered vehicles. Recent technology advances brought highly efficient lithium based batteries closer to large volume production for EV, HEV and plug-in hybrid electric vehicle (PHEV) [66]. The advancement of motor technology such as permanent magnet motors has considerably improved energy conversion efficiency [58]. The cost of

battery has also come down fast, fallen to $450/kWh in 2010 and expected to further lowering to $250/kWh in 2020[67].

3.3.5 Cost Sensitivity Analysis for GHG Emission Reduction

Combining studies of fuel cost, powertrain components cost and GHG emissions, a cost effectiveness sensitivity study in GHG emissions among different powertrain fuel pathways is performed. The gasoline-ICE pathway which dominates the market share is selected as the baseline for comparison. Five alternative fuels which show significant WTW GHG emission reduction potential are compared, including diesel, ethanol, bio-diesel, hydrogen, and electricity. A 25% efficiency gain from the conventional powertrain to the hybrid electric powertrain is assumed, according to reviewed literature[46]. Calculation of the combined consumer cost is includes fuel cost and main powertrain component cost, while the cost for the remaining common components (such as metal cost, wheels, etc) in the vehicle is excluded. The fuel cost and GHG is calculated based on 100,000 km travelled distance for an average of five years driving. The detailed results are shown in Table 7.

Table 7 Consumer Cost Comparison of Different Powertrain Technologies and Fuel Selection on 100,000 km (five years) driving Scenarios

Fuel & Powertrain	Main Powertrain Component	Fuel Cost (USD)	Consumer Cost	WTW GHG (Tonnes)	Tailpipe GHG (Tonnes)
ICE-Diesel	100 kW ICE, Transmission, $2000	8,480	10,480	51.2	22.2
ICE-Gasoline	100 kW ICE, Transmission, $2000	9,380	11,380	48.3	22.4
ICE-Ethanol	100 kW ICE, Transmission, $2000	10,010	12,010	215	22.0
ICE-H2	100 kW ICE, Transmission, $2000	8,720	11,720	40.1	0
ICE-Biodiesel	100 kW ICE, Transmission, $2000	11,160	13,160	13.7	22.5
H_2 FC	Fuel Cells 80 kW $6,400 Battery 4 kWh $1,000 Electric Drive 100 kW $2,000	5,030	13,430	23.2	0
Electric Vehicle	Electric Drive 100 kW $2,000 Battery 20 kWh $5,000	2,100	9,100	16.0	0
ICE Hybrid-Gasoline	Electric Drive 100 kW $2,000 Battery 4 kWh $1,000 ICE, Transmission, 2000	7035	12,035	36.2	16.8

The sensitivity analysis is performed by defining a carbon cost function which compares the economic cost of different powertrain technologies in reducing the GHG emissions. The consumer's cost for the GHG reduction is compared and shown in Figure 11. All vehicles require a net capital cost increase from a consumer in order to reduce GHG emissions. The cost increase in hybrid, full electric, and fuel cells vehicles are largely associated with higher vehicle price, while the future fuel cost is reduced. Cost increase associated with choosing ethanol or biodiesel based pathway are due to higher fuel cost driven by the rising price for the feedstock. The calculation uses Eq.(3) and the results are shown in Figure 11. The calculated results using this function are also consistence with carbon tax, which has been gradually adopted by six provinces and states across North America. For instance, British Columbia as the first North America jurisdiction to implement such a tax has reached a high rate of $25/tonne carbon dioxide beginning July 2011.

$$carbon\_reduction\_\cos t = \frac{\cos t\_increase}{emission\_reduction} = \frac{Cost_{powertrain\sim fuel} - Cost_{ICE\sim gasoline}}{GHG_{ICE\sim gasoline} - GHG_{powertrain\sim fuel}} \quad (3)$$

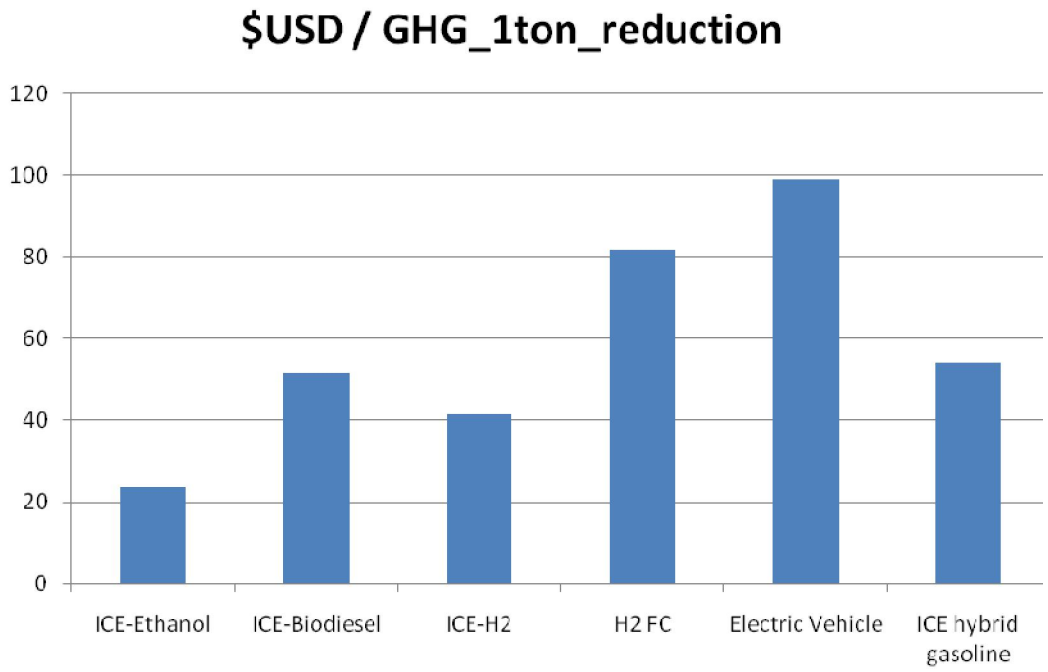

Figure 11 A Cost Sensitivity Analysis for GHG Emission Reductions

3.4 Summary

Based on the WTW analyses of different fuel and powertrain pathways, ethanol-FC, biodiesel-ICE, and EV are superior candidates for future transportation, in terms of reducing GHG emissions and conserving petroleum. However, adding factors of economic cost, availability, and technology availability into considerations, four pathways that are most promising in the upcoming decade are EV, ICE-ethanol, ICE-biodiesel, and ICE-hybrid. A number of vehicle powertrain variations are be derived from these four pathways, either from an individual pathway, or combing multiple pathways.

- If issues with supply volume can be resolved, running biofuels or blended fuel with high biofuels content is an effective and low cost solution for reducing WTW GHG emissions. Lightly blended fuels such as E10, E15, and B20 which can be operated in most existing vehicle engines is an immediately release of the high WTW GHG emission and petroleum consumption; pure or highly blended biofuels can further reduce WTW GHG emissions by over fifty percent. The tailpipe GHG emissions running these biofuels is however unlikely to differentiate from the petroleum fuels.

- The electric vehicle pathway is a promising solution in GHG reduction. The technology is at near-mature stage and the production cost is gradually coming down as production volume grows. Two main issues with the pure electric driven vehicles are higher initial cost and limited range, due to the long battery charging time. These issues will considerably limit the market share of electric vehicles in the near future.

- The hybrid electric technology consuming gasoline or alternative fuels can improve fuel efficiency at a price of higher powertrain cost. The GHG emission is reduced as the fuel consumption reduces. The increased consumer capital cost is however unlikely to be fully recoverable in five years of driving. Enhancing electric vehicle capability (plug-in hybrid) can partial leverage the higher powertrain cost by reducing fuel cost; adaption of biofuels instead of petroleum fuels can further reduce the GHG emissions on WTW basis.

In additional to the four identified fuel and powertrain pathways in the near future, hydrogen fuel cells vehicle can still emerge as a appealing option in longer future. The estimate powertrain if mass produced has come near to a reasonable range and the durability for moderate driving conditions have been proved. The main issues for the hydrogen and fuel cells pathway is the natural gas reformation based hydrogen production resulting significant GHG emission, and the lacking hydrogen fuelling infrastructure.

Chapter 4 Modeling of Hybrid Vehicle System

4.1 Vehicle Dynamics Modeling

The vehicle dynamics model is generated to calculate the kinetic energy of a vehicle when traveling on the road. Four primary loads considered are forces for acceleration/deceleration (F_a), rolling resistance (F_r), aerodynamic losses (F_a), and inclination (F_I). The free body diagram of a vehicle glider is shown in Figure 12. The modeling parameters for a representative compact SUV is provided as shown in Table 8. The modeling the vehicle dynamics and calculation for power demand serves important foundation for defining the powertrain system design target and it is an important component of the complete powertrain system model.

$$F(t) = F_I(t) + F_a(t) + F_r(t) + F_g(t) + F_b(t)$$

$$F_a(t) = \frac{1}{2}\rho_a A_f c_d v^2 = f_0 + f_1 v + f_2 v^2$$

$$F_r(t) = c_{rr} mg\cos(a)$$

$$F_g(t) = mg\sin(a)$$

$$F_I(t) = (mg + nI_{wheel} / R_{wheel}{}^2)\frac{dv}{dt}$$

$F_b(t)$ is braking force

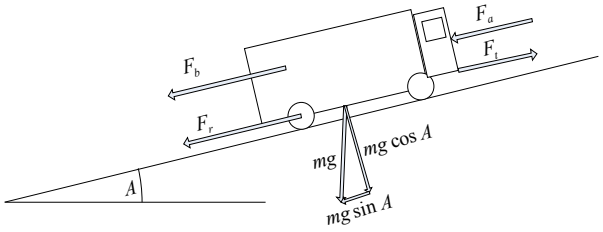

Figure 12 Free Body Diagram of a glider

Table 8 Dynamic Modeling Characteristics of a Compact SUV

Vehicle Mass	1800 kg
Rolling resistance	C_{rr1}=0.009; C_{rr2}=0.00012
Wheel radius	0.367 m
Wheel inertia	1 kg/m^2 (each)
Aerodynamics	f_0= 112.85; f_1=4.6; f_2=0.542

4.1.1 Power Demand in Driving Cycles

The defined vehicle dynamic model above is programmed in Simulink and power demand at the wheels for four driving cycles are computed: UDDS, HWFET, US06 cycle (aggressive driving) and LA92 (high-speed, high-acceleration) drive cycles. The average and peak propulsive/braking power is calculated as shown in Table 9, and histograms of the power demand are found in Figure 13.

Table 9 Characteristics of Power Demand

	Average / Peak Propulsion Power	Average / Peak Braking Power
City (UDDS)	10.02 kW / 45.2 kW	8.1 kW / 28.5 kW
Highway (HWFET)	19.1 kW / 38.3 kW	9.9 kW / 38.6 kW
Aggressive (US06)	33.3 kW / 118.2 kW	19.6 kW / 67.1 kW
LA92	16.1 kW / 63.2 kW	12.2 kW / 119.2 kW

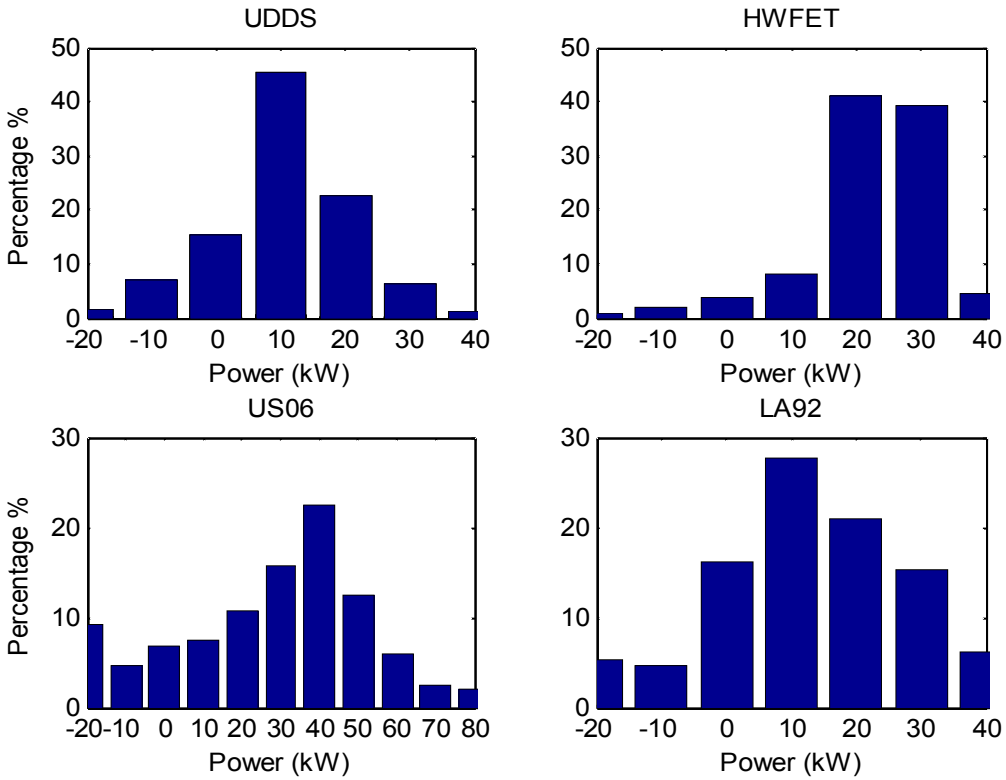

Figure 13 Wheel Power Demand Distribution for Four Speed Cycles

4.1.2 Energy Demand

The propulsion energy demand measures the mechanical energy demand at the wheels, regardless of powertrain configurations. If no braking energy is recovered, the propulsive energy demand includes three components: aerodynamics, rolling resistance and braking. The distribution of the three components running the UDDS and HWFET driving cycles is calculated. According to results shown in Figure 14, the highway driving cycle consumes more kinetic energy per kilometre travelled than the city driving cycle. As regard to weighting among the three components, more braking energy is consumed in the city driving cycle than the highway driving cycle; while the highway cycle demand more aerodynamic energy. The braking energy is transferred to heat loss in conventional vehicles. With electric powertrain, the braking energy can potentially be recovered by regenerative braking.

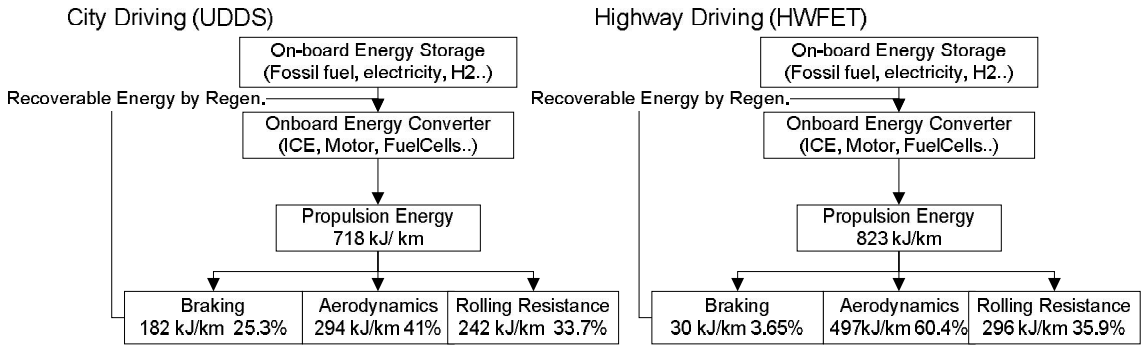

Figure 14 UDDS and HWFET Energy Consumption

Using the vehicle dynamics model, a weight sensitivity analysis is performed to evaluate the increase of propulsion energy demand as the vehicle weight increases. Three vehicle weights are selected, including the 1800 kg base weight, and 2250 kg which is 25% increase from 1800 kg, and 2520 kg which is 40% increase from 1800 kg. The results in Figure 15 show that the overall propulsion energy increase 13.6% with 25% of weight increase, and 21.8% with 40% weight increase.

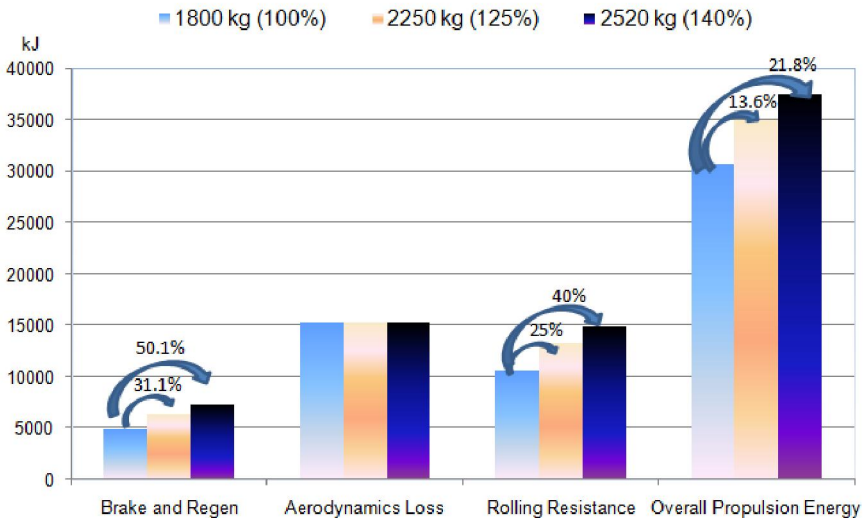

Figure 15 Energy Consumption with Increased Vehicle Weight

(Combined City-Highway cycle)

4.2 Modeling of e-CVT Hybrid Powertrain

The e-CVT initially introduced for strong HEV presents promising powertrain architecture for vehicle electrification. With design changes, an e-CVT can also be applied to a PHEV or Extended Range Electric Vehicle (E-REV) which requires increased electrical propulsion capability beyond a conventional HEV. Due to the system complexity and widely open design possibilities, identifying the optimal e-CVT design for different HEV/PHEV performance requirements is a challenging task.

4.2.1 Speed, Torque and Power of the Planetary Gears

In an e-CVT, the mechanical transmission that blends power from multiple power plants is commonly based on single or multiple planetary gears. Single planetary gear includes three parts, a sun gear, a ring gear and several planet gears connected by a gear carrier; the section view of it is shown in Figure 16. Understanding the dynamics of a single planetary gear lays foundation for modeling of the more complex e-CVT system. The kinematics among the three outputs in a planetary gears can be described using Eq.(1), where ω_c ω_s ω_r is the angular velocity of gear carrier, sun gear and ring gear respectively; k is the basic gear ratio which equals to the radius of ring gear divided by the radius of sun gear; and i_{sr}^c is the relative drive ratio between sun and ring gear.

$$\frac{\omega_s - \omega_c}{\omega_r - \omega_c} = -k = i_{sr}^c \tag{1}$$

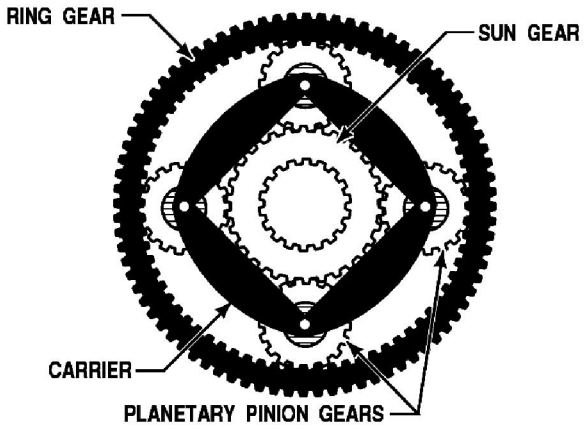

Figure 16 Cross Section View of a Planetary Gear

The kinematics relations described in Eq. (1) can be further expanded to Eq. (2). The drive ratio R is the speed ratio between each two of the three outputs. The kinetic relations is expressed by Eq. (3) [68], T_R, T_S, T_C represent torques at ring, sun and gear carrier respectively. To simplify the problem, gear friction is not included. In equilibrium state with gear friction neglected, the external torques is balanced, according to Eq.(3). The power in and out the planetary gear is also balanced, P_s, P_r, P_c are inputs or output power on sun, ring and gear carrier, according to Eq. (4).

$$\left.\begin{aligned} R_{sr} &= \frac{\omega_s}{\omega_r} = (1+k)R_{cr} - k \\ R_{rc} &= \frac{\omega_r}{\omega_c} = (1+k-R_{sc})/k \\ R_{cs} &= \frac{\omega_c}{\omega_s} = (1+kR_{rs})/(1+k) \end{aligned}\right\} \tag{2}$$

$$T_s + T_r + T_c = 0 \tag{3}$$

$$P_s + P_r + P_c = T_s\omega_s + T_r\omega_r + T_c\omega_c = 0 \tag{4}$$

From Eqs. (3) and (4), the torque relations is derived and represented in Eq. (5)

$$\left.\begin{aligned} T_s &= -\frac{1}{k+1}T_c \\ T_r &= -\frac{k}{k+1}T_c \\ T_s &= \frac{1}{k}T_r \end{aligned}\right\} \quad (5)$$

θ is defined as a power flow factor (PF) represented by Eq(6). They are used to study directions of the power flow in and out of the planetary gear. If θ=1, the two nodes either both provide or withdraw power to the planetary gears. There is no power flows from one to the other. If θ=-1, the power flows from one node to the other. If θ=0, there is no flow of power on the node.

$$\left.\begin{aligned} \theta_{rs} &= \frac{R_{rs}}{|R_{rs}|} \\ \theta_{rc} &= -\frac{R_{rc}}{|R_{rc}|} \\ \theta_{cs} &= -\frac{R_{cs}}{|R_{cs}|} \end{aligned}\right\} \quad (6)$$

Using Eq. (6), the power flow can be determined by the direction of rotation of each gear. When θ_{rc}=-1, θ_{rs}=-1, θ_{cs}=1, the power flow chart is represented by Figure 17, where the arrows point out directions of power flow.

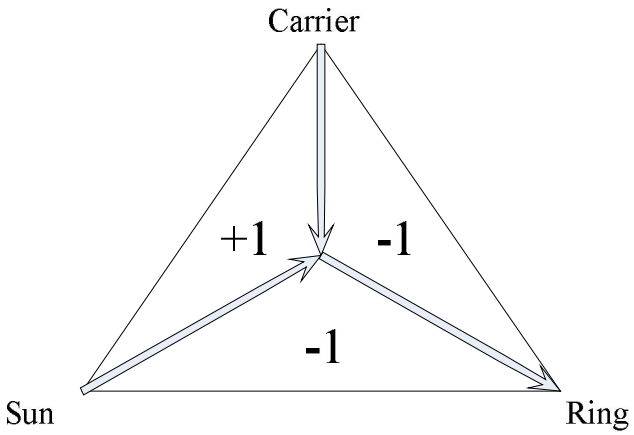

Figure 17 Power Flow Chart of Planetary Gear

4.2.2 Four Representative Hybrid Vehicle Powertrain Architectures

Several representative HEV/PHEV powertrains are used for case studies in the thesis. For e-CVT powertrains, four configurations are selected, representing two mainstream PHEV/HEV hybrid platforms in different configurations: the General Motors's FWD 2-mode and "Voltec" using the GM 2MT70 and 4ET50 platform, and the Lexus RX450h and Toyota Prius based on the Toyota Hybrid System (THS) platform.

The GM 2-mode 2MT70 and 4ET50 hybrid transaxles are designed for the midsize vehicle chassis, and previously installed on the Saturn VUE and well known Chevy Volt [69]. The front wheel drive (FWD) Saturn VUE 2mode hybrid's powertrain has a 3.6 L engine connected to the 2MT70 transaxle. The Volt's powertrain is developed from the 4ET50 transaxle coupled with a 1.4L engine. Simplified configurations of the two powertrains are shown in Figure 18 and Figure 19. R, C, and S represent the ring, carrier and sun gears in a planetary gear; C1, C2, C3 represents three clutches; M/G A and M/G B are motor generator A and B; and ICE represents the internal combustion engine. These two transaxles from GM share design similarities. The 2MT70 transaxle has two variable speed modes and four fixed gear ratio modes. The 4ET50 transaxle re-uses the second planetary gear of the 2MT70 system [70], enabling four modes of gear configurations, including two EV modes and two Extended Range (ER) modes.

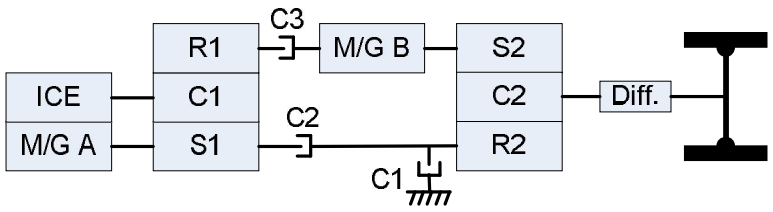

Figure 18 GM FWD 2- mode Hybrid Powertrain with the 2MT70 Transaxle (Saturn VUE)

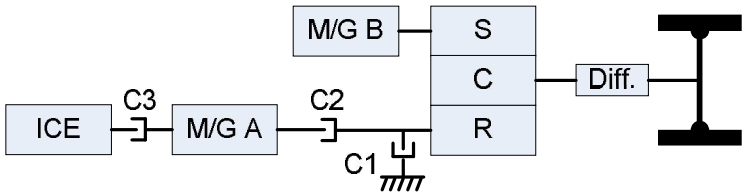

Figure 19 GM E-REV Hybrid Powertrain with the 4ET50 Transaxle (Chevrolet Volt)

The first generation Toyota Synergy Drive and Toyota Hybrid System (THS) was developed in the late 1990s [3, 71, 72]. Despite of improvements made on the high voltage electric drive and energy storage side [72, 73], the mechanical configurations remain largely unchanged in later THS generations. The e-CVT transaxle is developed using a single planetary gear set and two electric machines, as in the configuration shown in Figure 20. The Lexus 400/450h hybrid added a second planetary gear set to increase the speed of M/G B [74], and the ring gear on the added planetary gear is fixed, as shown in Figure 21. The latest third generation model with AWD capability added an additional electric drive to the rear wheels, while the powertrain configuration on the front wheels remain unchanged [75] .

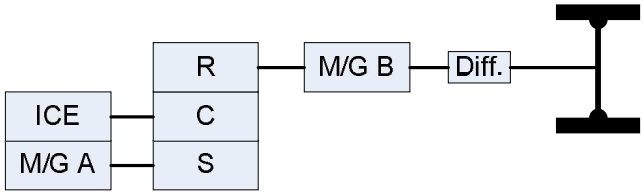

Figure 20 First and Second Generation THS Powertrain Configuration (Toyota Prius)

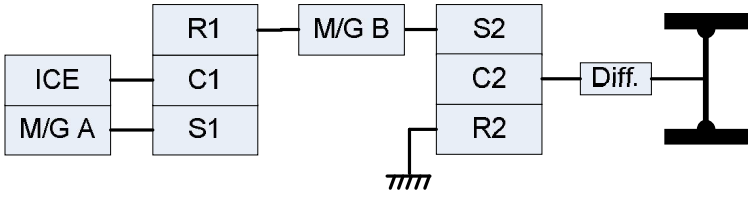

Figure 21 Third Generation THS Powertrain (Lexus RX450h)

4.2.3 Mechanical Gear-train Modeling

Modeling of an e-CVT based hybrid powertrain mechanics covers the planetary-gear sets and clutches. Parameters for each hybrid system are listed in Table 10 [76-78] [70, 79]. The final drive ratios and wheels radius are also included.

Table 10 Mechanical Powertrain Parameters of the Four Vehicle Powertrain Systems

Vehicle Type	**No. of Planetary Gears**	**No. of Clutches**	**Gear Ratios**	**Final Drive Ratio**	**Wheel Radius**
2MT70	2	3	k_1=60/44; k_2=97/43	3.22	350.77 mm
4ET50	1	3	k_1=60/44; k_2=97/43	2.16	328.42 mm
THS 1st Gen	1	0	k=78/30	4.113	310.64 mm
THS 3rd Gen FWD	2	0	k_1=72/28; k_2=1.478	3.542	369.57 mm

There are two variable speed modes in a 2MT70 hybrid powertrain, namely Mode 1 and Mode 2. Based on the parameters in Table 10, the kinematic and kinetic relations for the two modes are derived in Equations (7) and (8), where T_{MGA}, T_{MGB} , T_{ICE}, and T_{out} are the torque output at M/G A, M/GB, ICE and output shaft; w_{MGA}, w_{MGB}, w_{ICE}, and w_{output} are the speed variables of respective components. The remaining three hybrid architectures including the 4ET50 and THS are also modeled using the same approach.

$$\begin{cases} T_{MGA} = -\dfrac{1}{1+k_1} \times T_{ICE} \\ T_{MGB} = \dfrac{1}{k_2+1} \times T_{Out} - \dfrac{k_1}{1+k_1} \times T_{ICE} \\ \omega_{MGA} = (1+k_1) \times \omega_{ICE} - k_1(1+k_2) \times \omega_{Out} \\ \omega_{MGB} = (1+k_2) \times \omega_{Out} \end{cases} \tag{7}$$

$$\begin{cases} T_{MGA} = \dfrac{k_2}{1+k_2} \times T_{Out} - \dfrac{1}{1+k_1} \times T_{ICE} \\ k_2 T_{MGB} = \dfrac{k_2}{1+k_2} \times T_{Out} - \dfrac{k_1 k_2}{1+k_1} \times T_{ICE} \\ T_{MGA} = \dfrac{k_1 k_2}{1+k_1} \times T_{ICE} - \dfrac{1}{1+k_1} \times T_{ICE} + k_2 T_{MGB} \end{cases} \quad (8)$$

4.2.4 Electric Drive Modeling

The peak torque and energy efficiency of an electric motor is modeled. The energy efficiency characteristic of motors, which is not related to the peak torque capability, has not been considered in this work. Experimental data from the electric motors are summarized in Table 11 [80, 81]. As shown in Figure 22, the performance characteristics of an electric motor is modeled as three operational phases: start-up, steady torque, and peak power. The period from zero to 3% of maximum motor speed is defined as start-up phase; in this phase, the peak torque linearly increases from 80% to 100% of the motor's highest torque. The second phase has near steady torque for a wide speed range; the slightly reduced peak torque as speed increases reflects increased electric losses. In the third phase the motor can output near peak power, the torque curve is modeled as a quasi-iso-power curve with slightly reduced power at high speed, in order to account for the increased resisting loss at higher speed. The model characteristics of the three phases for the M/G A of the 2MT70 system is shown in Figure 22. Figure 23 is the energy efficiency contour map for a representative electric motor similar to the 2MT70 electric motor.

Table 11 Performance Characteristics of the Electric Motors on the Four Selected Hybrid Powertrains

		Speed range (RPM)	Peak Torque (N m)	Power Range (kW)
2MT70 (EcoCAR)	M/G A	7,600	201	60
	M/G B	9,100	234	50
04 Toyota Prius	M/G A	10,000	153	25
	M/G B	6,200	400	50
4ET50 (Volt)	M/G A	6,000	200	55
	M/G B	9,500	370	110
Lexus RX450h	M/G A	13,000	130	116
	M/G B	13,500	335	123

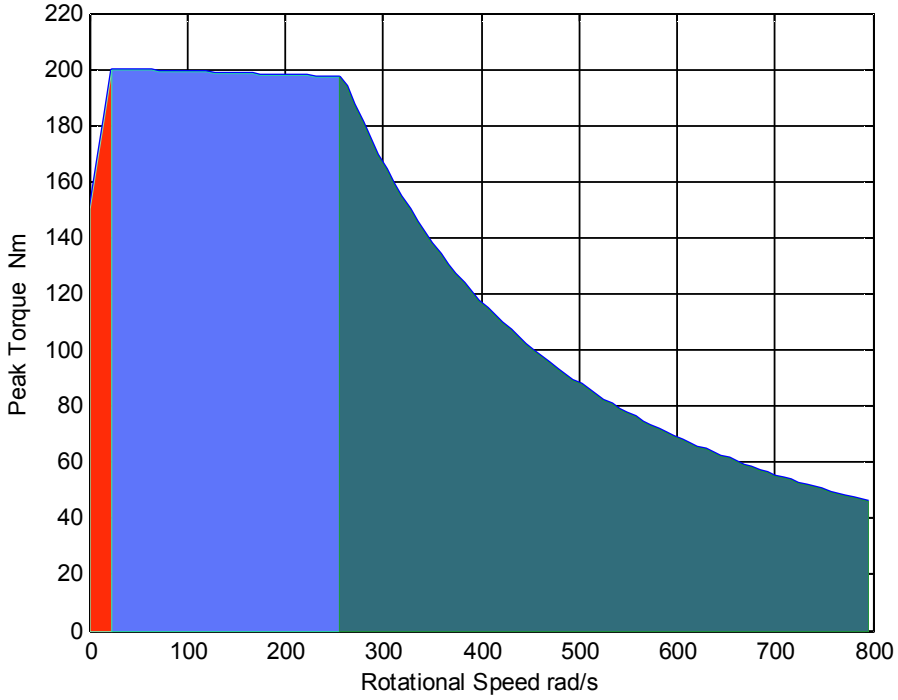

Figure 22 Performance Modeling of an Electric Motor

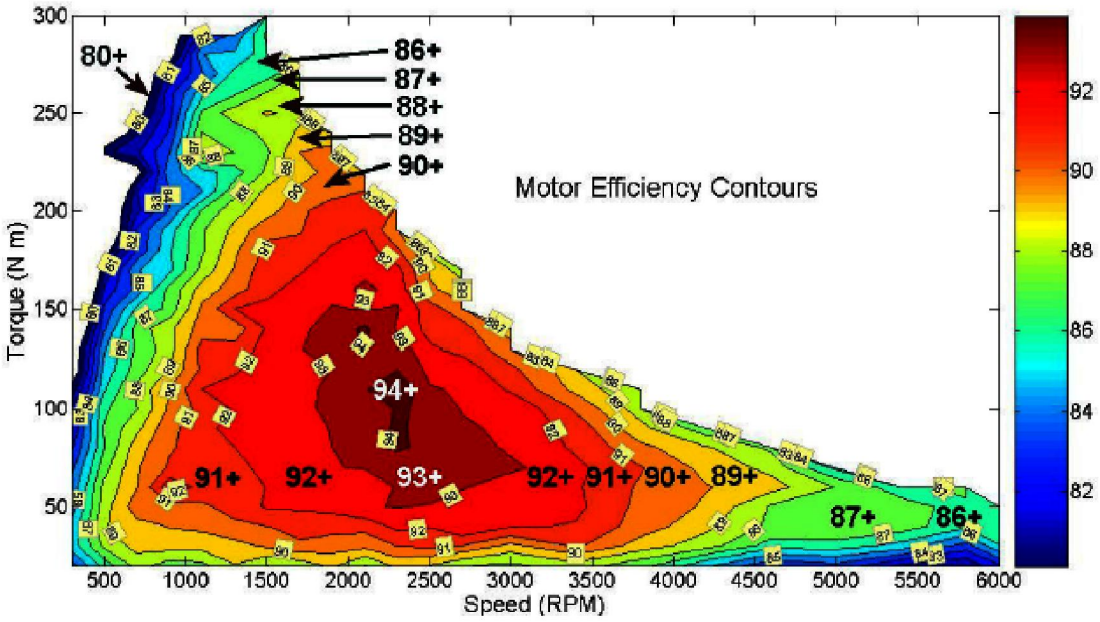

Figure 23 Electric Motor Efficiency Contour Map

4.2.5 Internal Combustion Engine Modeling

Four ICEs for the four hybrid system are also modeled by the speed input and maximum torque output relations, according to the experimental performance characteristics listed in Table 12. The fuel consumption aspects, is not considered. Limited information on the ICE is obtained from the Chevy Volt and Lexus RX450h, and the estimated parameters are used, as shown in Table 12. These empirical and hypothetical models are fitted using 4th or higher order polynomials so that models are scalable to support design optimization. Figure 25 is an energy efficiency map of a representative ICE.

Table 12 Performance Characteristics of Four ICEs on the Selected Powertrains

	Speed range	**Peak Torque**	**Power Range**
Chevy EcoCAR LE9	6750 rpm	230 Nm @4700 rpm	130 kW @6300 rpm
Toyota Prius- 1NZ-FXE	4500 rpm	122 Nm @4000 rpm	42.7 kW @4500 rpm
Chevy Volt	6000* rpm	200 Nm @4000*rpm	104 kW@5500* rpm
Lexus RX450h	6000* rpm	317 Nm @4800 rpm	183 kW @6000 rpm
*estimated values			

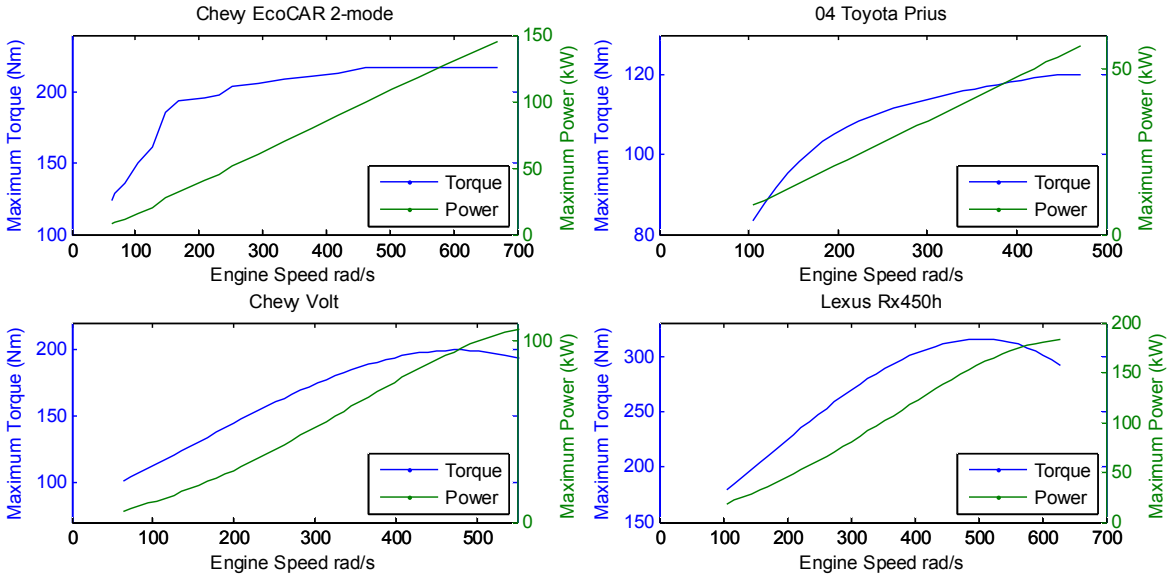

Figure 24 Modeled ICE Performance Characteristics

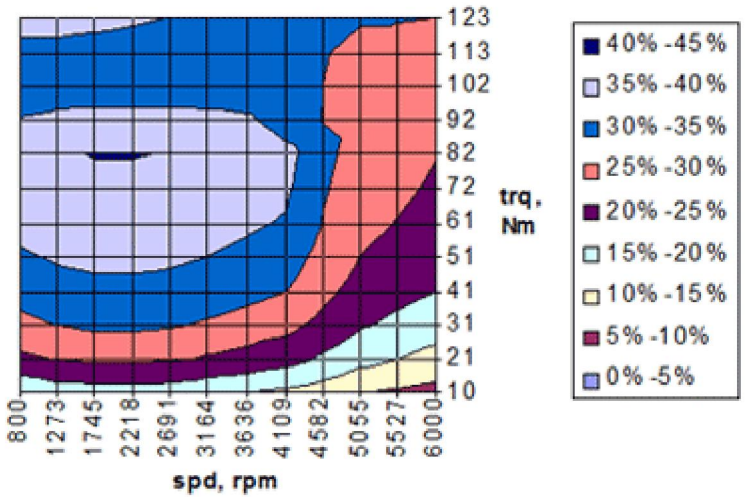

Figure 25 An ICE Engine Efficiency Contour Map

Chapter 5 Model-based Optimization for e-CVT Based HEV Powertrain Design

5.1 Advanced Hybrid Powertrain and e-CVT System

The e-CVT initially introduced for strong HEV presents promising powertrain architecture for vehicle electrification. With design changes, an e-CVT can also be applied to a PHEV or E-REV which require increased electrical propulsion capability beyond a conventional HEV. Due to the system complexity and widely open design possibilities, identifying the optimal e-CVT design for different HEV/PHEV performance requirements is a challenging task.

Design of hybrid vehicle powertrain with e-CVT can potentially achieve substantial improvement in fuel economy over the benchmark [82]. In the meantime, satisfying road performance of available torque should also be guaranteed. The peak torque that a powertrain can provide directly determines the vehicle's capability for acceleration, towing, and handling grade. With an electrified powertrain, the capability for regenerative braking and EV mode performance is also affected. In this work, a performance optimization based approach is introduced to facilitate the design and architecture selection of hybrid vehicle powertrains. This new approach can be applied to the design of various e-CVT and powertrain architectures. The method automatically identifies the peak powertrain performance capability and the system constraints imposed by key powertrain components for improvement. Compared with the conventional trial and error based design approach, the new design method can considerably improve the efficiency and accuracy of the powertrain architecture selection process, making it feasible to perform rigorous design alternative evaluations over a boarder design space to identify the optimal design solution, as illustrated in Figure 26.

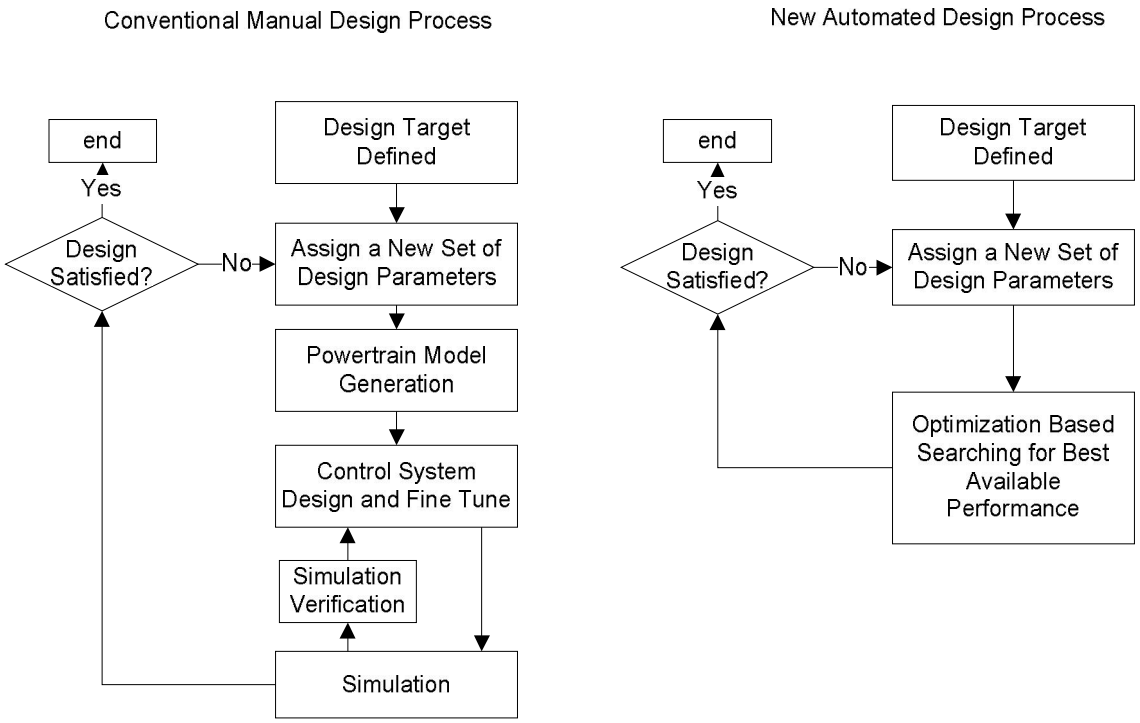

Figure 26 Powertrain Design Processes of Conventional and Optimization Based Approaches

To present this new powertrain performance modeling and optimization based e-CVT design method, Section 5.2 introduces the modeling of major powertrain components, and Section 5.3 presents the formulation and solution method of the design optimization problem using a two-stage hybrid optimization scheme. In Section 5.4, 5.5 and 5.6, advantages over a traditional best performance design method are shown; a cross platform comparison is made among several representative e-CVT powertrain designs, using calibrated results from several case studies; and design improvements are suggested. At the end, the new method and its applications are summarized in Section 5.7.

5.2 Formulation of the Optimization Problem

Powertrain performance can be evaluated using the powertrain system model assembled using the introduced component models under selected powertrain architecture. However, identifying the peak powertrain performance remains a challenging task, due to the numerous possible component parameter and control strategy combinations. Instead of

testing various control strategy using a trial and error approach, or lengthy exhaustive search, an optimization based approach is applied to identify the ideal combination quickly and effectively. In this formulation, the transmission output torque is to be maximized. Based on Equations (7), the transmission output can be derived as a function of three sub-functions: torque of the ICE and the two electric machines, as represented by the objective in Equation (9) and constraints in Equations (10). The three dependent torque sub-functions are further constrained by three additional speed variables. Depending upon different clutch engagements in each e-CVT transmission, up to five of the six variables are independent. The optimization problem is formulated as

$$\underset{All\_Veh\_Speed}{\text{Maxmize}} \; T_{output} = f(T_{ICE}, T_{MGA}, T_{MGB}) \tag{9}$$

subject to:

$$\begin{cases} f_1(\omega_{ICE}) \le T_{ICE} \le f_2(\omega_{ICE}) \\ f_3(\omega_{MGA}) \le T_{MGA} \le f_4(\omega_{MGA}) \\ f_5(\omega_{MGB}) \le T_{MGB} \le f_6(\omega_{MGB}) \end{cases} \tag{10}$$

Since the design interest is on the peak output torque curve vs. vehicle speed rather than the peak torque point at any speed, the vehicle speed is further treated as a constraint which is mapped linearly to the output speed from the transmission. This vehicle speed constraint further reduces one variable. The updated objective function is Equation (11) and the constraints are shown in Equation (12), where i is a finite number representing vehicle speed.

$$\underset{(i=n_0 \ldots n)}{\text{Maxmize}} \; T_{output}(i) = f(T_{ICE}, T_{MGA}, T_{MGB}, V_{ICE}) \tag{11}$$

subject to:

$$\begin{cases} \omega_{ICE\_\min} \le \omega_{ICE} \le \omega_{ICE\_\max} \\ \omega_{MGA\_\min} \le \omega_{MGA} \le \omega_{MGA\_\max} \\ \omega_{MGB\_\min} \le \omega_{MGB} \le \omega_{MGB\_\max} \\ V_{veh} = i \times V_{vehcile\_speed\_\text{int}erval} \end{cases} \tag{12}$$

The objective function needs to be solved at different vehicle speed. At each speed, the objective function is nonlinear with multiple variables.

5.3 A Two-Stage Hybrid Optimization Solution Scheme

Without having a thorough understanding on the shape of this complex objective function of Equations (11) and (12), solution of such an optimization problem usually requires global optimization (GO) search methods, such as *generic algorithm* (GA), p*article swarm optimization* (PSO), or *meta-modal based* GO methods [83]. The needed computation is heavy and accurate result is not assured. In this work, an innovative two-stage hybrid optimization method is applied to solve this unique optimization problem.

5.3.1 Separation of the LP and NLP Problems

As the objective function is solved at different vehicle speed, solution at each vehicle speed is defined as a sub-problem (SP) solution of the original objective function. The objective function of each SP consists of a linear component and a nonlinear component. The linear component is solved using the efficient linear programming (LP) search method [84], while the nonlinear component is solved using the pattern search based nonlinear programming (NLP) method. The two-stage hybrid search method takes advantage of the high search efficiency of LP algorithm, and reduces the number of design variables in the solution of the nonlinear optimization search, to allow the solution of the optimization to be identified efficiently.

The first step is to separate the nonlinear component from the linear component in each SP. According to constraints defined in Equation(10), the speeds of M/G A and B are fully determined by given vehicle speed and assigned ICE speed. Consequently, the torque range is determined and the nonlinear components in the constraints are removed. Applying this strategy, the continuously changing ICE speed is converted to a group of finite, discrete values using a fixed step size. About 600-800 sub-sub-problems (SSP) are generated for each SP, where each SSP is solved using LP, based on a step size of 10 RPM. With the optimal value evaluated at each function, nonlinear optimization is used to identify the maximum among all SSPs. The identified result at the end consequently becomes the optimum of each SP, subject to the given step size.

5.3.2 Solution of the LP Problem

As for the system with the 2MT70 transaxle, the objective function of a SSP is defined in Equation (13). The constraints of the variables are known when the ICE speed and the

M/G B speed are determined. The solution of this linear problem is obtained using linear programming [84]. Following the same approach, the optimization problems for other hybrid powertrains in this study are solved.

$$T_{out} = (1+k_2)\times T_{MGB} + \frac{k_1(1+k_2)}{1+k_1}\times T_{ICE} \tag{13}$$

subject to,

$$\begin{cases} \omega_{ICE\_\min} \le \omega_{ICE} \le \omega_{ICE\_\max} \\ \omega_{MGB\_\min} \le \omega_{MGB} \le \omega_{MGB\_\max} \end{cases} \tag{14}$$

5.3.3 Solution of the NLP Problem

Solving the SSP using LP can assure an optimal solution. The next step is to identify the optimum from all calculated SSPs' optima - the optimum of the SP. As there are only 600-800 SSP in each SP, an exhaustive searching approach which computes the function value at every point is feasible in principle. However, since the number of SSPs grows exponentially with the growing number of SPs, the computation load quickly increases and becomes very time consuming. To improve searching efficiency, a direct search optimization strategy, generalized pattern search (GPS), is used. The algorithm is selected due to its robustness and no need of gradient information of the objective function. The process for setting up the searching consists of the following steps.

- Pattern Vector Selection

The first step for carrying out the GPS method is to define the pattern type. There are two commonly used pattern types: maximum basis pattern with *2n* variables and minimum basis pattern is with *n+1* variables, where *n* is the number of variables in the objective function. Applying the first pattern type, the pattern vector defined in this problem is v_1 and v_2, where v_1 =[1], and v_2 =[-1].

- Meshes

GPS searches a set of points, called a mesh. The mesh size, represented by Δ^m, is a scalar which is multiplied with the pattern vectors. For this problem, at a point with value a, we assume:

The current point is *[a]*,
The pattern search vectors are v_1 = [1] and v_2 = [-1].

The current mesh size is 4

The algorithm generates the following mesh:

$$[a]+4\times[1]=[a+4]$$
$$[a]-4\times[1]=[a-4]$$

- Polling and Expending Strategy

GPS either completely polls every meshed points (complete polling) or stop polling points as soon as it finds a better point which reduces the objective function (partial polling). The complete polling strategy can find an equal or better point than the partial polling strategy in each iteration, resulting in a higher computation load. Using either strategy, the polling is called a successful poll if a better point is found with reduced value of the objective function. Since the two polling strategies make little or no difference for a single variable problem, the partial polling strategy is used in solving the problem. Within each iteration, the GPS algorithm changes the value of the step size Δ^m to improve the searching efficiency. Δ^m is multiplied by 2 after a successful polling or by 0.5 after an unsuccessful polling.

- Starting Point

In this work, the shape of the objective functions is revealed using many sample points. The model is of uni-modal shape with the minimum close to the center. Therefore, a simple strategy of using the center point as the starting point of the search is applied. The GPS method can usually identify the optimal solution after 20 to 40 iterations when the design space has 600-800 values. Therefore, the GPS can considerably improve the searching efficiency by 20-30 times, when compared with an exhaustive searching method. To ensure the searching quality of the local optimal based GPS method, exhaustive search is also conducted at selected points to crosscheck the results from the GPS based method.

5.4 Model Validations

The newly introduced method was applied to study the four selected e-CVT powertrains. The obtained results are verified using known solutions. The solutions used for comparison are from the Powertrain System Analysis Toolkit (PSAT), developed at the Argonne National Lab [43]. The Prius platform was selected for benchmarking, due to

the existence of a high fidelity powertrain model which has been validated within 5% error on different driving cycles with different battery state of charge (SOC) against experimental data [42]. The Toyota Prius model in PSAT is based on the 2004 Prius with the powertrain configuration discussed previously.

The PSAT vehicle controller model for the Prius has been developed based upon extensive modeling, analysis and testing to reach peak powertrain and vehicle performance. However, the controller does not necessarily achieve the maximum performance and full potential of the powertrain through the trial and error design-improvement approach. The optimization based method, on the other hand, can quickly identify the maximum performance possible from the powertrain architecture, without the need to develop a vehicle controller model. The quality of the vehicle performance prediction and the optimization results, however, is still subject to the accuracy of the powertrain performance model and simulation. In the comparison, a standard 0-100 *km/h* acceleration drive cycle was applied to simulate the near-peak torque delivery for the specified speed range. Comparisons are made on the speed and torque of the ICE and electric motors. The engine torque and speed during the 0-100 *km/h* acceleration simulation using PSAT and optimization based method are shown in Figure 27.

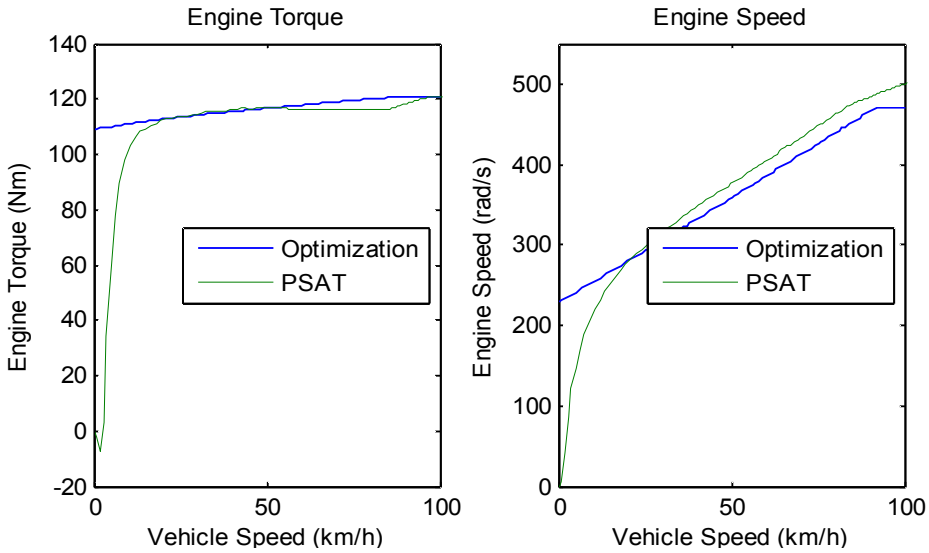

Figure 27 Engine Performance Comparison between Using the Optimization-based Method and PSAT Simulation for the Toyota Prius Powertrain

There is a close match between the two results when the vehicle speed is greater than 20 *km/h*. At lower vehicle speed, the PSAT model simulates the engine starting transient from zero rpm more accurately; at present the optimization based powertrain model assumes the engine is kept on at all time. The optimization based results show that additional powertrain output propulsion is possible if the engine is operated at slightly lowered speed, as shown in the plot on the right of Figure 27. Figure 28 illustrates motor/generator performance comparison between the results from PSAT and the optimization based approach. The plot on the left is engine torque vs. vehicle speed; and the plot on the right is the engine speed vs. vehicle speed.

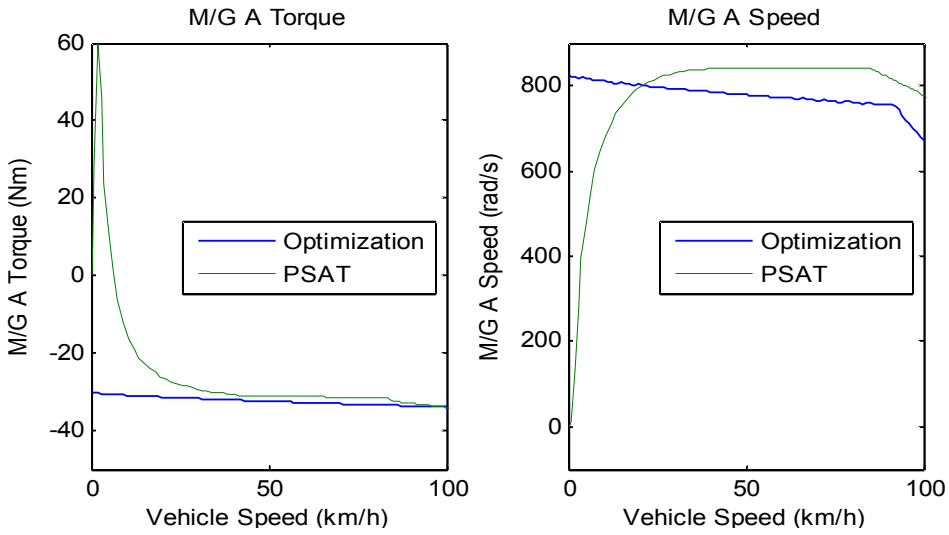

Figure 28 M/G-A Performance Comparison between Using the Optimization-based Method and PSAT Simulation for the Toyota Prius Powertrain

Here M/G A acts as an engine starter as well as an electric generator. Similar to the engine simulation, these results present very good match for vehicle speed greater than 20 km/h. The speed difference of M/G A is caused by the difference of engine speed. Figure 29 presents M/G B performance comparison between the two approaches. The plot on the left is M/G B torque vs. vehicle speed; and the plot on the right is the M/G B speed vs. vehicle speed.

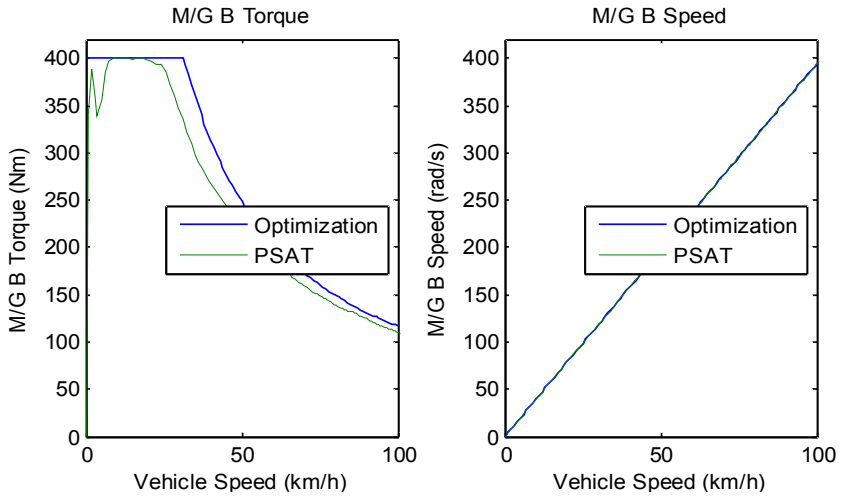

Figure 29 M/G B Performance Comparison between Using the Optimization-based Method and PSAT Simulation for the Toyota Prius Powertrain

M/G B is the primary electric motor for propulsion. The PSAT model contains more transient details. The control algorithm in PSAT did not fully utilize the available torque from M/G B. A clear boundary of available torque from M/G B is shown by the optimization based method, as shown in Figure 29.

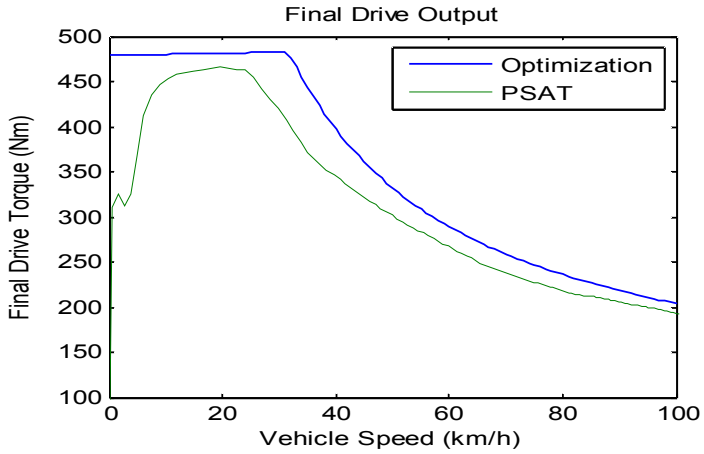

Figure 30 Final Drive Input Torque Comparison between Using the Optimization-based Method and PSAT Simulation for the Toyota Prius Powertrain

Finally, the combined powertrain torque output vs. speed is compared, as shown in Figure 30. The optimization based solution successfully identified peak torque from the powertrain, despite of the missing details for engine staring. The PSAT powertrain model and its controller achieve a near-peak performance close to the maximum

performance from the powertrain. The PSAT model also provides better transient details during the engine starting. It should be noted that the discussed peak performance is in fact in continuous state rather than in transient state, since the maximum continuous operation data is used to model the electric motor and engine. Alternatively, the transient peak performance can be computed with the transient continuous data included in the component modeling.

5.5 Traditional Best Performing e-CVT Design Method

In the traditional e-CVT design approach, search for the best design solution is carried out by performing powertrain performance simulations repeatedly through a time consuming, trial and error process. To illustrate the benefit of the automated, optimization based, systematic best performing e-CVT design approach method, a simple case study is conducted to find the peak output torque of the 2 mode e-CVT system at a speed below 50 km/h, using the same powertrain components discussed previously. A four-step process is needed for every design iteration, and three design iterations are performed in this study.

- The first step is to derive the function that represents the performance target. The output torque of the final drive can be derived from Equation(7), as shown in Equation(15). The output torque is a function of engine torque T_{ICE} and motor/generator B torque T_{MGB}, where k_1 and k_2 are predetermined.

$$T_{Out} = (k_2 + 1) \times T_{M/G\ B} + \frac{(k_2 + 1) \times k_1}{1 + k_1} \times T_{ICE} \tag{15}$$

- The second step is to analyze the problem and generate test result guided rule-based strategy. In this problem, the performance target function is determined by two variables T_{ICE}, T_{MGB}, the range of which is subjective to the current operating point of the complete powertrain system. In order to perform dynamic simulations and calculate the final outputs, the control variable of engine speed needs to be pre-assigned. In this example, a simple strategy of using constant engine speed is used.
- The first attempted strategy is to limit the engine speed at 2,000 rpm based upon the knowledge acquired from previous tests, and assign maximum available torques to both of the engine and M/G B.

- The last step for this design iteration is to compute the final output.

Generating and adding this control strategy as well as all other needed adjustments to modeling demand deep knowledge on the powertrain system and considerable human intervention. The present trial and error approach requires this process to be carried out repeatedly, not only leading to a labour intensive, time consuming and lengthy process, the process also cannot guarantee the identification of the best potential of the given e-CVT based hybrid powertrain. This adds considerable difficulty to the next level of design activity – comparing different e-CVT based powertrain designs and identifying the optimal design solution. Using this trial and error approach, three design iterations are performed. Results of these design iterations are compared with the results generated using the new optimization based method, as shown in Figure 31. The knowledge-driven trial and error approach with 2,000 rpm constant engine speed present the closest solution to the he ultimate best performance profile of the e-CVT. It is however a real challenge to obtain the knowledge to produce this best guess and to know that the guess is very close to the best performance result and it is time to stop the trial. In addition to the time consuming and labour intensive trial and error process, the manual approach is also unable to identify the best potential of the e-CVT as the optimization based method.

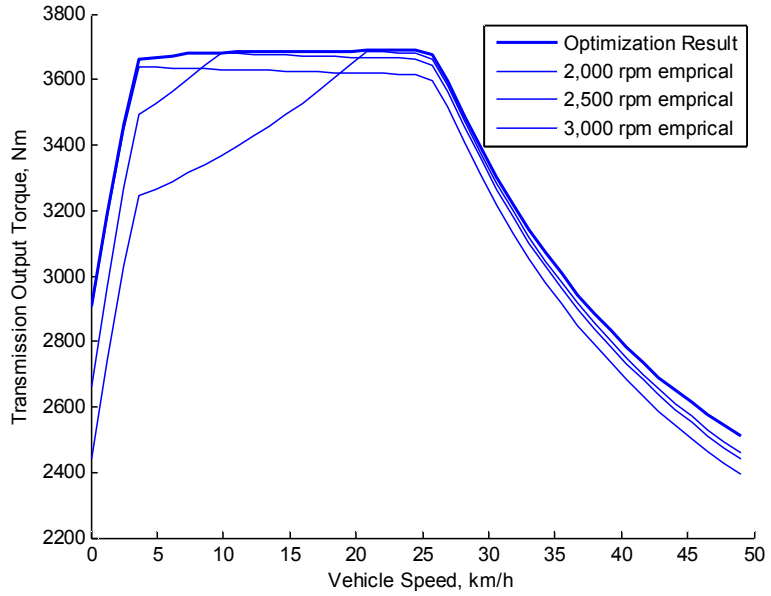

Figure 31 Comparison of Results Generated from Optimization and Empirical based Methods

5.6 Results on Case Studies

5.6.1 Cross Platforms Peak Performance Comparison

In addition to running the benchmark problem on the Prius powertrain, the proposed method is applied to obtain the maximum torque outputs of the four representative e-CVT hybrid powertrains. Since the 4ET50 powertrain of Chevrolet Volt has four different modes, its powertrain capability is discussed separately and plotted in a separated chart. The first comparison is made among three of the four e-CVT systems, including the powertrain of Lexus RX450h, GM 2MT70 system with a 2.4L engine, and Toyota Prius. A powertrain with the 2MT70 transaxle and a 3.6 L engine, which is the engine selection for the stock GM 2-mode vehicle, is also added to the comparison. The model for this added 3.6L engine is however simplified and generated by scaling up the peak torque of the 2.4L engine by 50%, due to in adequate data available for this particular engine. The GM 2MT70 system with a 2.4L engine is used in a research vehicle of the authors' research group with an added 2 mode plus rear wheel drive which is beyond the scope of this paper.

The first comparison is made with engines kept on. According to results shown in Figure 32, the maximum torque and power output at the final drive to wheels are compared. The 2MT70 transaxle with the 3.6L engine has highest available torque at vehicle speed up to 30 km/h. This advantage is overtaken by the RX450h at higher vehicle speed, due to the advantage of its larger electric motors and more powerful 3.5 L engine. The 2MT70 with the 2.4 L engine has comparable peak torque to the RX450h at low vehicle speed in mode 1; and the peak available torque is lower and at a steady value in mode 2. Prius produces lowest torque and power among the four in comparison. The patterns of power and torque output curves are very similar to the RX450h, due to the similarity of powertrain configurations.

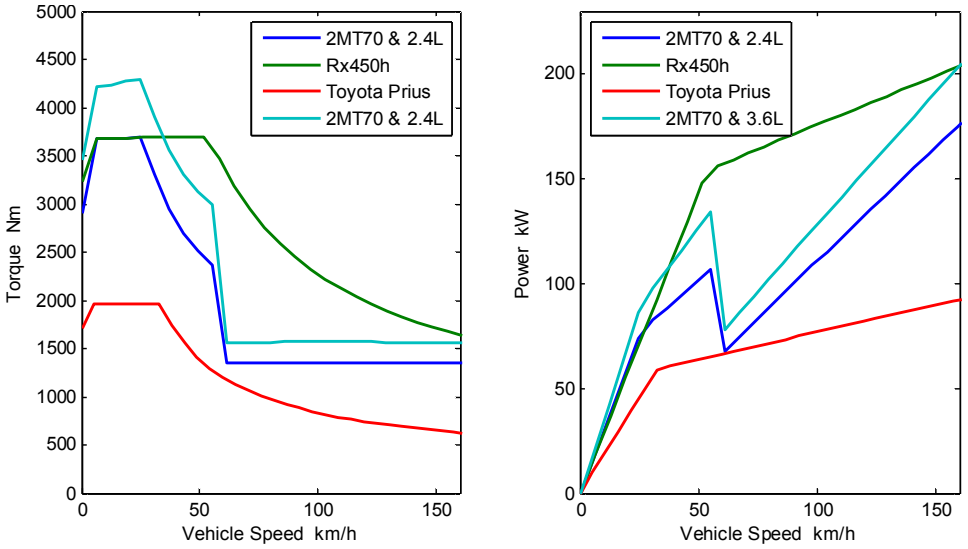

Figure 32 Comparison of Maximum Torque and Power Output from the Final Drive to the Wheels in Normal Mode with Engine on

By turning the optimization problem from maximization to minimization, the optimization based method is used to identify the peak regenerative torque and power during vehicle deceleration. There is no difference of the 2MT70 regenerative braking with different engines. As shown in the results in Figure 33, the RX450h powertrain once again has highest potential for energy regeneration, taking advantage of the two powerful electric motors rated over 100 kW. The 2MT70 and the Prius powertrain have comparable but lower potential for energy recovery.

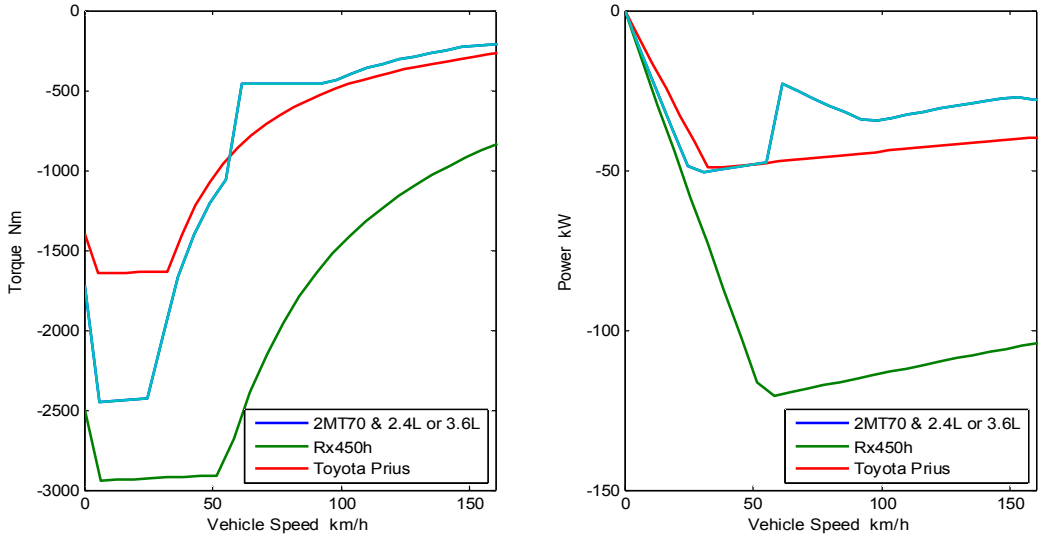

Figure 33 Comparison of Maximum Regenerative Torque and Power Output from the Final Drive to the Wheels in Normal Mode with Engine on

The hybrid powertrain on a Chevrolet Volt uses the 4ET50 transaxle with a 1.4L engine. With different combinations of clutch engagement, the 4ET50 has four operation modes, including one motor EV, two motor EV, one motor Range Extended (RE), and two motors RE. The one motor EV and RE mode has the same output, since only the drive motor provides propulsion. The simulation results for the maximum torque and power is shown in Figure 34. As the result shows, it is more preferable to run the vehicle in one motor EV or RE mode at vehicle speed up to 100 km/h, as considerably higher torque is available in these two modes with one motor operating. At higher vehicle speed, using the two motor EV and RE modes becomes more preferable as more power is available, and the one motor EV or RE mode cannot be used at vehicle speed higher than approximately 150 km/h, due to the motor's top speed limit.

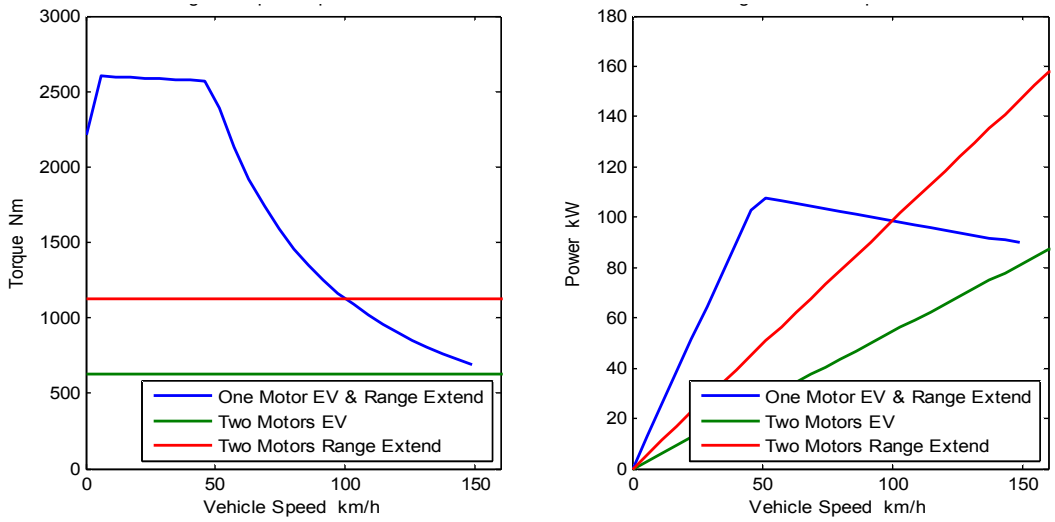

Figure 34 Comparisons of Maximum Torque and Power Output from the Final Drive to the Wheels in Different Operating Modes of the 4ET50 System on Chevrolet Volt

The one motor mode also has significantly higher capacity for generative braking compared with the two motors modes, as shown by the simulation results in Figure 35.

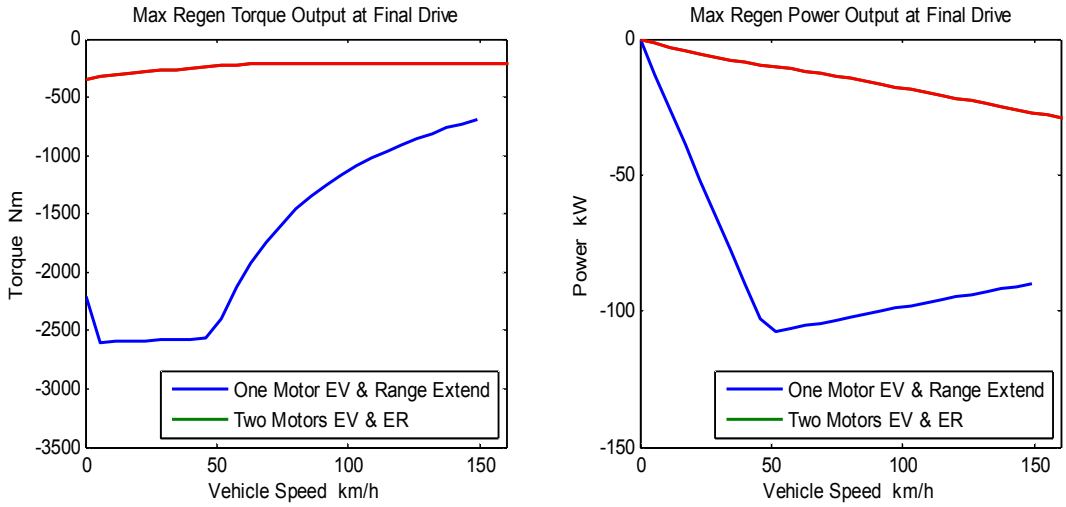

Figure 35 Comparison of Maximum Regenerative Torque and Power Output from the Final Drive to the Wheels in Different Operating Modes of the 4ET50 System on Chevrolet Volt

5.6.2 Performance in EV Mode

The powertrain performance in EV mode is determined by three major components: electric motor(s), batteries, and transmission. The IC engine can be either turned off or kept spinning without injecting fuel. In this analysis, the limit on maximum electric current drawn from the battery is not considered. Not all of the four vehicles have full EV capability. Two of the four selected powertrains, Lexus RX450h and Chevy Volt, can provide satisfying EV performance at vehicle speed up to 160 km/h. The powertrain of a Prius or a 2MT70 may operate in EV mode at high vehicle speed; however, the performance is very limited due to the low peak EV power around 50 kW. The control system thus limits the EV operation to lower vehicle speed. The EV performance of the three vehicle powertrains is summarized in Table 13.

Table 13 Peak EV Performance, Capability and Limiting Factors

	Peak EV Speed	Speed Limiting Factor	Peak EV Power	Power Limiting Factor
2-mode 2MT70	134 *km/h*	MGA speed	51 *kW*	MGB power
Prius	164 *km/h*	MGA speed	49 *kW*	MGB power
RX450h	160 *km/h*	MGB speed	122 *kW*	MGB power

The peak torque and power in the EV mode is compared and shown in Figure 17. The Lexus RX450h powertrain has higher torque and power than the other two compared powertrains. It has more than 80% of its peak torque in normal mode remains in EV mode. The performance of the Chevy Volt powertain is unaffected in the EV mode, due to its series hybrid operation mode. The 2MT70 2-mode powertrain can be operated in EV mode in both Mode 1 and Mode 2, but mode transisent requires turning on the IC engine to synchronize speed for clutch engagement. The available torque in EV only mode is very limited due to the size of the electric motor.

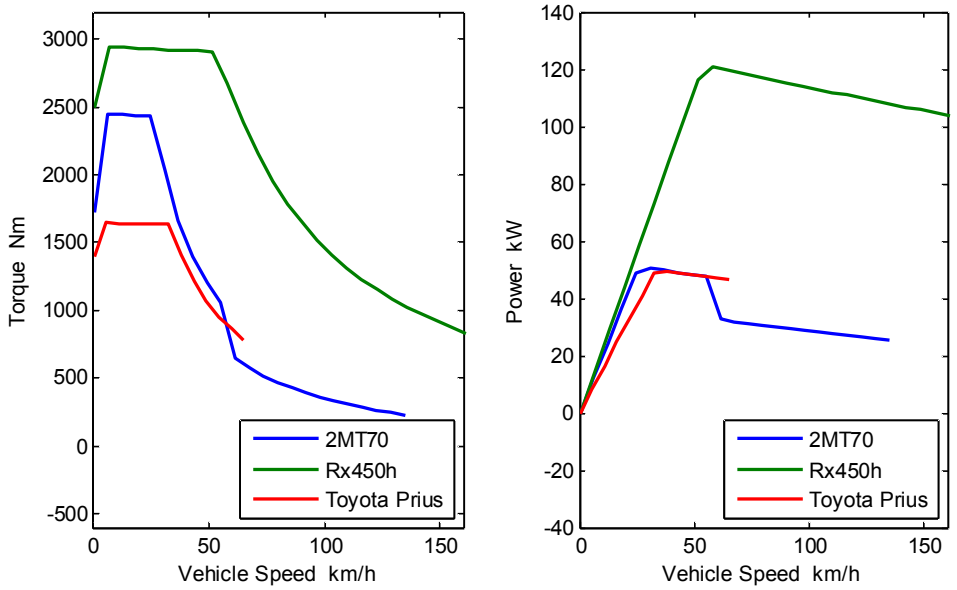

Figure 36 Comparison of Maximum Torque and Power Output from the Final Drive to the Wheels in EV Mode with Engine off

The capacity for regenerative braking in EV mode is also subject to limits on vehicle speed. The torque and power range as shown in Figure 37 follows the similar pattern as the motoring capacity, but with opposite values.

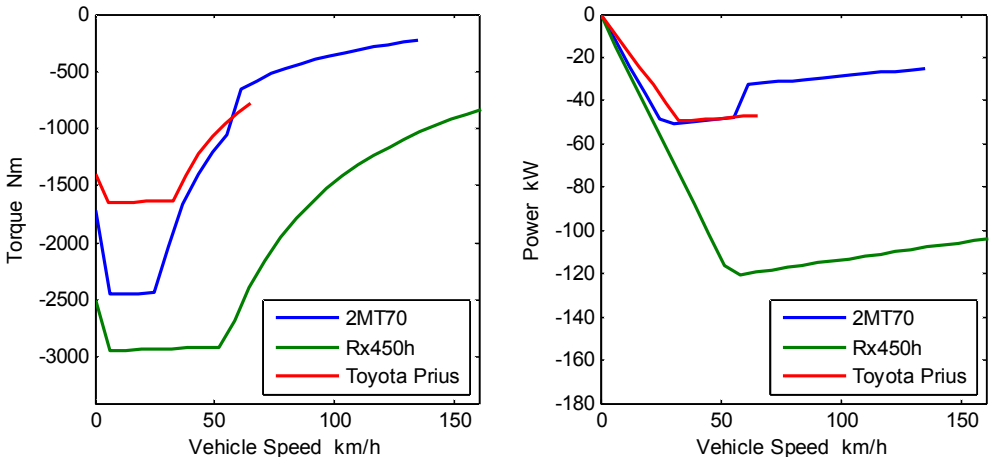

Figure 37 Comparison of Maximum Torque and Power Output from the Final Drive to the Wheels in EV Mode with Engine off

5.6.3 Enhanced Performance in EV Mode with Design Modification

Applying e-CVT based powertrain to PHEV requires enhanced electric drive capability. To explore potential EV drive capability improvement without significantly changing the existing powertrain design, an attempt was made to add different constraints to two of the four studied powertrains and use the optimization based method to evaluate performance improvements of the e-CVT. This research found that to lock the input shaft between the engine and the transmission will enable much improved EV performance. As the results in Figure 38 indicate, the drivetrain performance in EV mode is much improved. With the input shaft locked, the 2MT70 can provide more than doubled torque, with the M/G 1 now providing power. The peak speed range is, however, unchanged. The RX450h can also have much improve EV performance with both electric motors now provides power. It should be noted that shifting from mode 1 to mode 2 on the 2MT70 transaxle still requires starting the engine in order to have synchronized speed during clutch engagement [85]. The top vehicle speed for the 2MT70 system in EV mode is still limited to approximately 140 km/h, and this constraint is imposed by the peak speed of the electric motors.

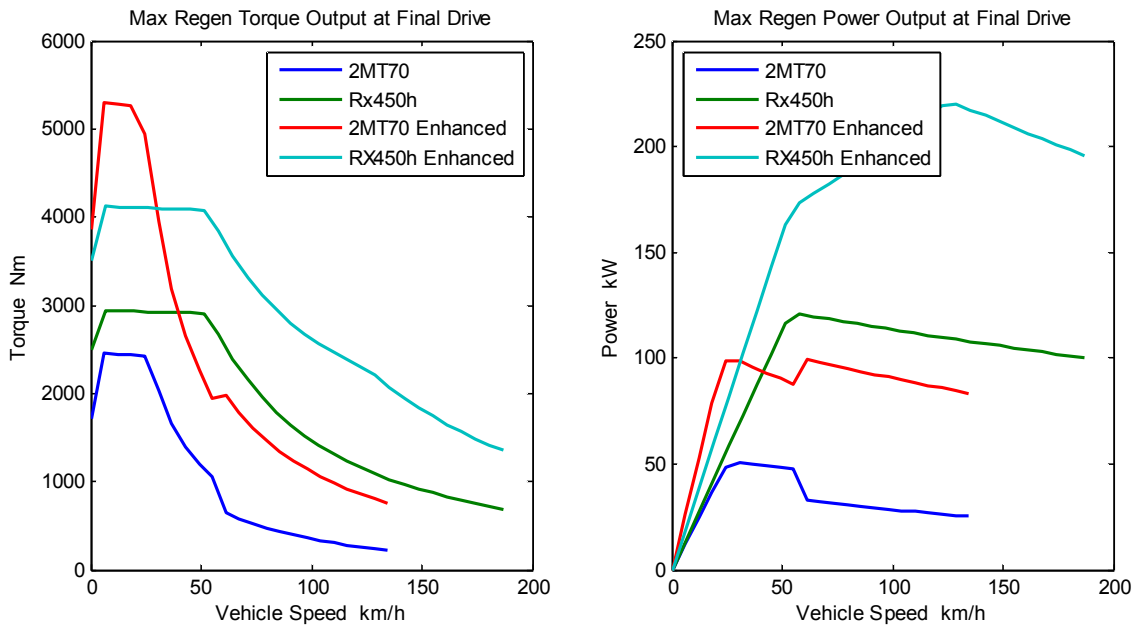

Figure 38 EV Performance Gain with Modified Transaxle by Locking up the Transmission Input

5.6.4 Powertrain Design Optimization Demonstration

Applying this method with the previously introduced automated design approach, design optimization can be carried out on an e-CVT based powertrain. A wide range of design variables, including parameters of the transmission, electric motors, and internal combustion engines, can be selected in the design optimization. A single iteration of design evaluation takes as short as 3-4 minutes using a regular PC. In this section, a simple design optimization example with one design variable is shown, even though the benefit of computational efficiency is more significant in a multi-variables problem. The selected problem for design optimization is the Toyota's THS hybrid powertrain and the gear ratio of the planetary-gear set is treated as the design variable. A number of gear ratios from 1.6 to 3.6 were scanned through, and the peak synergetic performance of the hybrid powertrain was calculated. The peak power output is shown in Figure 39 and summarized in Table 14. With different gear ratios, the difference of combined output power is within 20%.

Table 14 Peak Power Output of the THS Powertrain with Different Gear Ratios

Gear Ratios	1.6	1.8	2	2.2	2.4	2.6
Max Trq. (Nm)	62.7	66.5	69.1	70.1	71.7	73.0
Gear Ratios (Continue)		2.8	3	3.2	3.6	3.8
Max Trq. (Nm) (Continue)		73.5	74.5	75.2	75.9	76.4

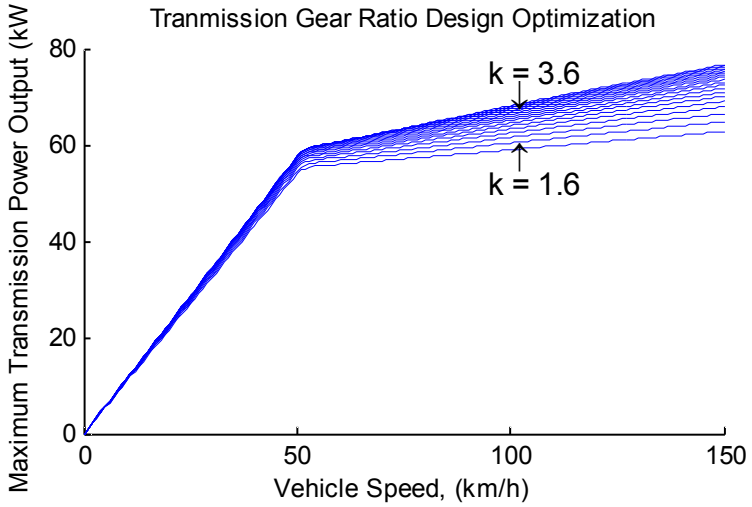

Figure 39 THS Transmission Gear Ratio Design Optimization - Maximum Transmission Power

The output power is generated through two paths: direct power of M/G B and split power of the ICE. It is the difference of the latter power path drives the difference in peak powertrain output. According to Figure 40, less power is split from the ICE to M/G A as the ratio increases. The ICE output power increases linearly as the vehicle speed increases. When gear ratio is higher, the ICE starts at a lower power and its speed increases at a faster rate. Therefore, a higher gear ratio is more favourable for a PHEV application operating in the charge depleting (CD) mode, due to the following three reasons: the higher peak transmission power output is available; less power is withdrawn from the ICE (battery provides more energy); less electric generation losses occur at the M/G A. On the other hand, a medium or lower gear ratio is more preferred for a HEV application which continuously operates in the charge sustaining (CS) mode. The higher ICE power and higher generated power from M/G A allow higher battery charging at vehicle speed 50 *km/h* or lower.

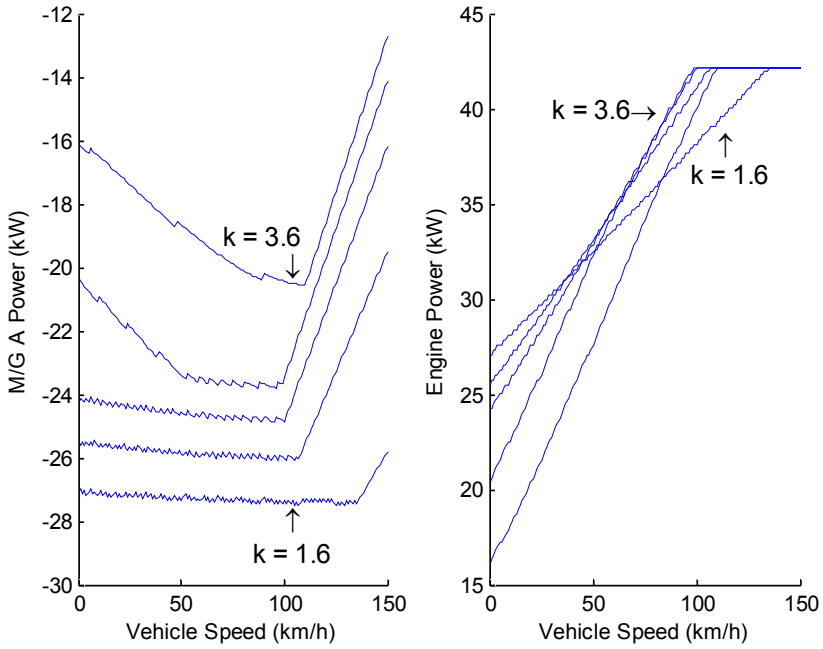

Figure 40 THS Transmission Gear Ratio Design Optimization - Power of MGA and ICE

5.7 Summary

In this chapter, an attempt to combine model-based design and optimization search is made to identify the best performance capability of e-CVT based HEV/PHEV powertrain quickly and effectively. The synergetic peak performance of an e-CVT based powertrain can be automatically calculated, using high fidelity powertrain performance model and optimization search. Formulation of the optimization problem, as well as efficient and effective solution method of the optimization problem is introduced. Comparisons and advantages over the traditional trial and error design approach are made.

With the capability to quickly and systematically identify the best performance potential of an e-CVT based powertrain design, the new optimization search based powertrain design method makes it possible to carry out top level design optimization of complex e-CVT based HEV/PHEV/E-REV powertrains, avoiding the labour intensive and time consuming trial and error process used in present practice.

The proposed method is applied to four representative e-CVT based hybrid vehicle powertrains. The performance characteristics of these powertrains are fully analyzed and the results are compared with results from PSAT simulations. The new powertrain design

optimization method is also demonstrated through the EV performance enhancement and transmission gear ratio selection. The research can form a new foundation for hybrid vehicle powertrain design optimization.

Chapter 6 Model-based Optimization for HEV Control System Design

6.1 Technical Challenges of e-CVT Hybrid Powertrain Design

6.1.1 e-CVT Powertrain for Advanced Hybrid Vehicle

A HEV or PHEV draws propulsion energy from two types of onboard stored energy: (a) a consumable fuel, and (b) a rechargeable energy storage system (RESS) [86]. Two main considerations for the optimal design of such a hybrid powertrain are electric drive capability and system energy efficiency. An e-CVT architecture can satisfy both of the design needs which can optimally draw and blend power from the two energy sources using an internal combustion engine (ICE) and multiple electric motor/generators (M/G) [87]. The extra available control degrees of freedom can potentially increase powertrain efficiency by improving ICE and M/G efficiency, and reducing losses. In comparison, the parallel hybrid architecture suffers from low engine efficiency with engine speed bonded to output speed and gear ratios; the series hybrid is subject to high energy loss during the electric-mechanical energy conversions. As a result, the e-CVT is a preferred powertrain selection for advanced HEV/PHEVs.

6.1.2 Challenges in e-CVT Control Design

Regardless of powertrain configurations, optimal design of control strategy is needed to fully utilize available propulsion and minimize the energy consumption. The strategy for optimal energy management is mainly based on selection of control inputs with each state of three system outputs, including: (a) torque and (b) speed at final drive, and (c) electric power charged to or discharged from the ESS. For a parallel or series configuration, the optimal control selection is much more straightforward as the input variables can be empirically determined when all three outputs are fixed [88].

For an e-CVT powertrain, however, the design space for selecting input variables is much more open as a result of increased control degree of freedoms (DOF). The DOFs of an e-CVT using planetary gears can be calculated according to Eq.(16), where n is number of independently rotated members along the central axis, m is the total

number of planet teeth in contact with other gears, and p is the number of planet gears [89]. Calculations of DOFs are performed on four representative e-CVT related hybrid powertrains, including the Toyota THS 1st generation [3, 71, 72], the Toyota THS 2nd generation [74], GM FWD 2-mode[77], and the GM Volt [69]. According to results shown in Table 15, most e-CVT based hybrid transmissions have two DOFs, shared among six input variables. Identifying the system optimal control inputs with the two DOFs problem is difficult due to the system complexity.

$$DOF = n - m + p \tag{16}$$

Table 15 Number of D.O.F in Representative e-CVT and Hybrid Vehicle Powertrains

	DOF	n	m	p
THS	2	3	2	1
2-mode mode 1	2	4	4	2
2-mdoe mode 2	2	4	4	2
Volt	2	4	4	2
THS 3	2	4	4	2

One commonly applied strategy which can achieve quasi-optimal is the rule-based engine optimal strategy. This approach limits the engine operation near its peak efficiency region and consequently reduces the design space from two dimensions to one dimension. Then the one remaining control variable can be determined when the electric power demand is specified. This rule-based based control strategy narrowly focuses on engine efficiency and ignores the remaining loss of the powertrain. Therefore, achievement of the system optimal energy efficiency is not assured.

To identify the optimum of system efficiency, optimization methods are applied to develop the control strategy, either online in real-time, or offline using extensive simulation data. One approach is to run optimization in real-time to determine control commands. This method is essentially based on minimization of instant fuel consumption and electricity demand with a weighting factor, derived from the Energy Equivalent Consumption Measurement (EECM) method. The objective function is however compromised, since the exact balancing of fuel and electricity cannot be explicitly assigned and can only be tuned by changing the weighting factor. In addition, the real-time control optimization requires extensive computation, presenting considerable

challenges for its implementation using low-cost ECU. The robustness of optimization is of not assured.

This research presents a different new control design method which aims at achieving the optimal control of e-CVT powertrain system by applying optimal control logics obtained through extensive offline optimizations. This offline optimization based method aims at achieving optimal system efficiency with high robustness and low real-time computation need. Using the powertrain model and simulation under various conditions, the optimum of input combinations are identified for different system outputs. The obtained data of optimal inputs and outputs are used to generate a optimal control model by training an Artificial Neural Network (ANN). The developed ANN controller is later used in real-time for vehicle control. A case study has been performed to compare powertrain performance using the developed optimal system control and the conventional rule-based engine optimal control methods.

Table 16 Comparison of Rule and Optimization Based Control Strategy for e-CVT Optimal Energy Management

	Rule-based	Optimization Based	
	Engine Priority	Online Optimization	Offline Optimization
Efficiency Improvement	Low	Medium (Performance is affected by real-time optimization quality)	High (Assured result is obtained from offline optimization)
Control Integration	Medium (Electric power changes in a near-linear pattern with engine power increased)	Difficult (Electric power is only adjustable by tuning weight factor for optimization)	Easy (Electric power is explicitly determined from offline optimization data)
Computational Demand (in vehicle)	Low (Rule-based calculation)	Very high (Online optimization)	Medium (The NNT controller require medium level computation power)
Robustness	High (simple and robust control)	Low (Optimization quality and searching time is subject to change in real-time)	High (The NNT controller can be comprehensively verified before implementation)

6.2 Optimization Objective Formulation

The objective in the e-CVT control problem is to maximize system energy efficiency considering loss at both the engine and electric drive system. In other words, the consumption of fuel and electricity is to be minimized. Instead of applying a weighting factor and minimizing the electricity and fuel consumption at the same time, the electricity consumption is used as a design constraint. Therefore, the optimal system efficiency is achieved when the engine fuel consumption is minimized. The formulated problem bypasses the need for the weighting factor and considerably reduces the difficulty for control implementation at the later stage.

The objective function is formulated in Eq.(17), where the instant fuel consumption (*Inst. Fuel*) is a function of engine speed (ω_{ICE}) and torque (T_{ICE}). The first two constraints in Eq. (18) define the feasible region of the two design variables, within the engine's capability and the boundary conditions of the two electric motors, where T_{ICE_min}, T_{ICE_max}, ω_{ICE_min}, and ω_{ICE_max}, are the minimal and maximum of engine torque and speed, T_{MGA_limit}, T_{MGB_limit}, ω_{MGA_limit}, and ω_{MGB_limit}, are the limits of torque and speed for Motor/Generator A and B. Satisfaction of these two design constraints are enforced by the generated powertrain model. The three system outputs including output torque (T_{Output}), speed (ω_{Output}), and instant power (P_{ESS}) are also applied as constraints to define initial conditions for each optimization run. These initial conditions in continuous space are discretized into finite states by applying fixed step sizes (ss_{torque}, ss_{speed}, ss_{power}). Since electric power consumption cannot be directly used as an initial condition in the powertrain model, an inequality constraint is applied to the charged/discharged electric power to accept electric power to be within the tolerance of σ. With different sets of these three initial conditions, the objective function is to be solved repeatedly with different constraints and the entire solution set will formulate the results for optimal system input selection.

$$\underset{(i=1:m,\,j=1:n,\,k=1:O)}{Minimize} \qquad Inst.Fuel_{T_{output}(i),\omega_{output}(j),P_{ESS}(k)} = f(T_{ICE}, \omega_{ICE}) \tag{17}$$

subject to,

$$\begin{cases} \max\ (T_{ICE\_\min}, f_1(T_{MGA\_limit}, T_{MGB\_limit})) \le T_{ICE} \le \min\ (T_{ICE\_\max}, f_2(T_{MGA\_limit}, T_{MGB\_limit})) \\ \max\ (\omega_{ICE\_\min}, f_3(\omega_{MGA\_limit}, \omega_{MGB\_limit})) \le \omega_{ICE} \le \min\ (\omega_{ICE\_\max}, f_4(\omega_{MGA\_limit}, \omega_{MGB\_limit})) \\ P_{ESS\_\min} + k \times ss_{power} - \sigma < P_{ESS}(k) < P_{ESS\_\max} + k \times ss_{power} + \sigma, (k = 1, 2, ..O) \\ T_{output}(i) = T_{output\_\min} + i \times ss_{torque}, (i = 1, 2, ..m) \\ \omega_{output}(j) = \omega_{output\_\min} + j \times ss_{speed}, (j = 1, 2, ..n) \end{cases} \quad (18)$$

6.2.1 e-CVT mechanical transmission modeling

Computation of the objective function is performed by simulating the powertrain model. The powertrain model primarily includes three components: an ICE, a mechanical gear train, and electric motor/generators.

The mechanics of an e-CVT consist of planetary gear sets and clutches. The Toyota THS, for instance , has one planetary gear [79], while the UVic Chevy EcoCAR 2-mode e-CVT as a more complex design has two planetary gears and four clutches. Modeling of these hybrid transmissions can be carried out using simple mechanics equations[90]. The angular velocity of the sun (ω_{sun}), ring (ω_{ring}), and carrier gear ($\omega_{Carrier}$) can be expressed together with a constant k, where k is defined as the radius of ring gear divided by the radius of sun gear, as in Eq.(19). The torques is defined in Eq.(20), according to [87, 91].

$$\omega_{Sun} + k\omega_{Ring} = (1+k)\omega_{Carrier} \quad (19)$$

$$\begin{cases} Torque_{Sun} = -\dfrac{1}{k+1} \cdot Torque_{Carrier} \\ Torque_{Ring} = k \cdot Torque_{Sun} \end{cases} \quad (20)$$

6.2.2 ICE and Electric Motor Modeling

The engine model includes two calculation components: torque calculation and fuel calculation. The torque component generates engine torque within the feasible region. According to Eq.(21), engine torque T_{ICE} is determined by two constants T_{CTT} (the closed-throttle torque), T_{WOT} (wide-open-throttle torque), and one control command T_{ICE_cmd} (engine torque command between 0~1). Due to the gradient in-continuity of the peak torque at the node points when experimental tests are performed, a 4th order or high polynomials is used to fit peak torque vs. speed curve to support the search in optimizing powertrain performance. The instantaneous engine fuel-rate is a function of engine speed and torque, as represented by Eq.(22).

$$T_{ICE} = T_{CTT} + (T_{WOT} - T_{CTT}) \cdot T_{ICE\_cmd} \tag{21}$$

$$Ins\tan\tan eous\_fuel\_rate = function(\omega_{ICE}, T_{ICE}) \tag{22}$$

The electric motor model is created using a similar approach as the engine model which also includes two components: torque and electric calculation. The torque delivery is calculated by interpolations of the maximum and minimal toque rated on continuous operation basis, as represented by Eq.(23). Using MGA for instance, $T_{MGA\_Prop\_max}$ is the maximum propulsion power, $T_{MGA\_egen\_max}$ is the maximum regenerative power, and T_{MGA_cmd} is the motor control command between -1~1. The instant energy efficiency η_{MGA} is a function of motor speed and torque.

$$T_{MGA} = \begin{cases} T_{MGA\_Prop\_max} \cdot T_{MGA\_cmd}, (T_{MGA\_cmd} > 0) \\ -T_{MGA\_Regen\_max} \cdot T_{MGA\_cmd}, (T_{MGA\_cmd} \le 0) \end{cases} \tag{23}$$

$$\eta_{MGA} = function(\omega_{MGA}, T_{MGA}) \tag{24}$$

6.3 An Optimization Based Approach and Real-time Vehicle Applications

6.3.1 A Forward-backward Hybrid Simulation Approach

Evaluation of the formulated objective function is carried out using modeling and simulations. The engine speed and torque requests are used as independent control variables during simulations and the remaining dependent control variables include torque and speed request from MGA and MGB. The input and output variables for the model are shown in Table 17.

Table 17 Inputs and Outputs Variables for the Powertrain System Model

Input Variables		**Output Variables**
Independent	Engine Speed, Torque	Final Drive Speed
Dependent	Motor/Generator 1 Speed, Torque	Final Drive Torque
	Motor/Generator 2 Speed, Torque	ESS Electric Power

Two commonly applied approaches for vehicle powertrain modeling and simulations are Forward Modeling & Simulation (FMS) [42] and Backward Modeling &

Simulation (BMS) [92], based on the direction of control information flow between the traction at wheels and outputs at power actuators. The FMS performs consistently with vehicle operation and generates more accurate results, but it requires higher computation load due to needed internal control loops. An example of a powertrain simulation tool using the FMS is PSAT (Powertrain SimulAtion Toolkit), the models of which go through a comprehensive validation process[42]. The BMS, on the other hand, propagates vehicle traction to corresponding actuator outputs with minimal feedback loops thus substantially reduce the computation load. The BMS however compromises on result accuracy and misses transient responses. An example of a powertrain simulation tool using BMS is ADVISOR (ADvanced VehIcle SimulatOR) developed at NREL (Nation Renewable Energy Laboratory)[92]. When solving the studied problem with high requirement on results accuracy, the FMS is preferred but the introduced loops considerably increase the computation load. The computational quickly load becomes unacceptable as the number of objective functions to be repeatedly solved grow exponentially with different initial conditions defined in a three-dimensional space. On the other hand, the BMS cannot independently solve the problem because the output variable of electric discharging power can only be computed as a simulation result. Solving the problem using a BMS method requires an additional loop outside the simulation, as shown on the left of Figure 41. The computation load significantly increases. Comparison of result quality and computation load is compared in the following discussion.

A novel hybrid simulation method comprising both FMS and BMS was applied in this work to ensure result accuracy and to reduce computation load. The simulation is performed in two steps. In the first step, two system output requests of final drive torque and speed are applied as initial conditions, as in the BMS method. Then the engine speed and torque are independently assigned and simulations are performed to evaluate the instant fuel rate and electric power, as in the FMS method. A large database is generated in this step with different output torque and speed as initial conditions. In the second step, the third constraint of electric power is applied by filtering the results from the generated database. Then the optimal engine torque and speed combination is identified which

minimize the instant fuel consumption. This two-step solving process is illustrated in Figure 41.

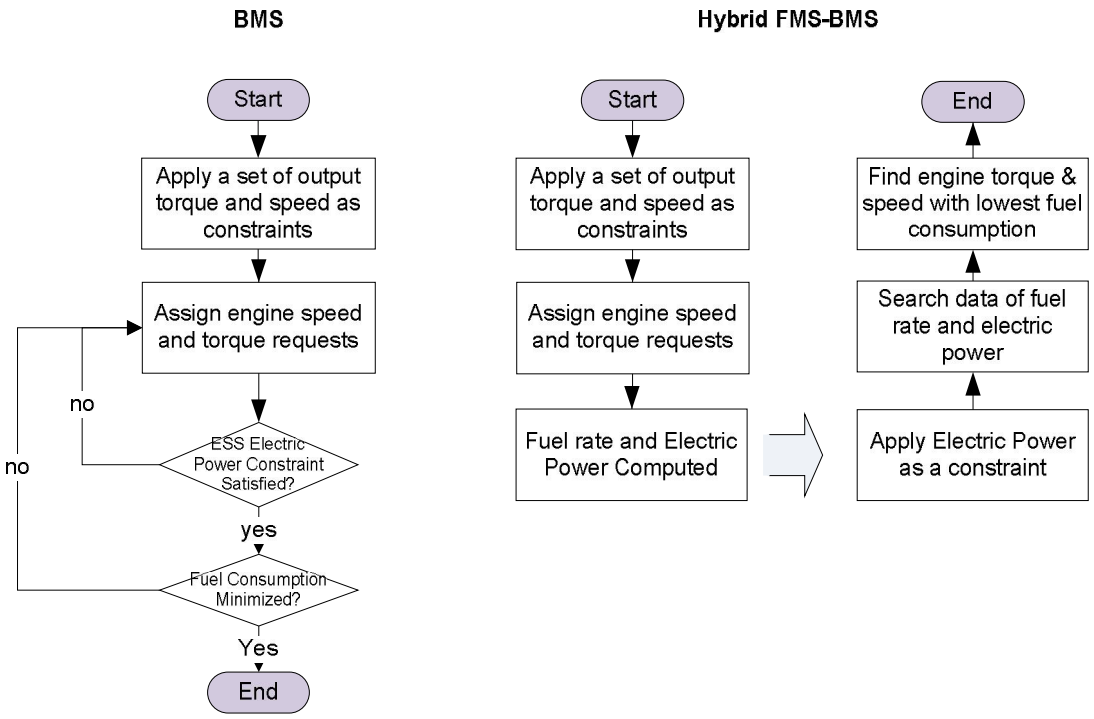

Figure 41 Control Flow Comparison of the Hybrid FMS-BMS Methods

Compared with the BMS based approach, the hybrid FMS-BMS approach can significantly reduce the computation load and ensure result quality. Using a hypothetical problem as defined in Table 18 and Table 19, the hybrid FMS-BMS can solve the problem within much reduced time and the result quality is assured subject to the step of engine speed and torque. The compared computation time is a rough estimate of simulation time using high performance PC and a single function evaluation takes hundreds of millisecond.

Table 18 Defined Data Points of the Optimization Problem

	Range	**Step Size**	**No. of points**
Vehicle Speed (km/h)	0~180	1	180
Torque Output (Nm)	-500~500	10	100
Charge/Discharge (kW)	-30~30	0.2	300
Engine Speed (RPM)	600~8000	10	740
Engine Torque (Nm)	0~300	5	60

Table 19 Comparison of the Hybrid Method and Modified BMS Method

	Modified BMS Mothod	**Hybrid FMS-BMS Method**
No of Sub-problems (SP)	180×100×300=5,400,000	180×100=18,000
Function Evaluations at Each SP	44,400 (exhaustive searching) Thousands(opt. searching)	Upto 740*60=44,400
Total Model Evaluations	2400×10^9 (exhaustive searching) $10\text{-}20\times10^9$ (Opt. searching)	Up to 8×10^9
Computational Time	Months-Years	Days - Week
Result Quality	Un-assured(subject to opt. algorithm)	Assured

6.3.2 Develop a Meta-model Using the Artificial Neural Network

With objective functions minimized at different powertrain output states, a large number of data points are generated when the system optimal is achieved. With these statistical data, a meta-model is needed which should interpret system input and generator optimal control commands for in vehicle implementation. Attempts were made using conventional data fitting approaches, based on linear and nonlinear polynomials. However, the result is unsatisfying due to the data non-linearity and multiple dimensions. The generated file also takes large storage space and slows down computation during simulation. Therefore, the data fitting method is unsuitable to be directly implemented in the storage and computational sensitive vehicle ECU.

Instead, this work applies the artificial neural network (ANN) based approach on the data obtained from optimization solution, and a meta-model is generator to be used in vehicle controller. There are three input variables to be fed into the ANN controller, including vehicle speed, torque output of the ring gear, and power demand at the energy storage system. Two output variables from the controller are desired engine torque and engine speed. In general speaking, a multilayer feed-forward ANN, trained using the back propagation algorithm, is an effective tool for modeling nonlinear relations among massive inputs and outputs, when the mathematical relations among these inputs and outputs cannot be easily formulated [93]. The multiple-layer feed-forward ANN is used to for find the ICE operation that can yield optimal powertrain efficiency. The neural network consists of three layers: an input layer, a hidden layer, and an output layer, with the relation shown in Figure 42. The nodes at between two adjacent layers are joined by

weights matrix *w_1* and *w_2*, as well as bias matrix *b_1* and *b_2*. The network is trained using known data to obtain the optimal weight and bias. The training process consists of the following four steps:

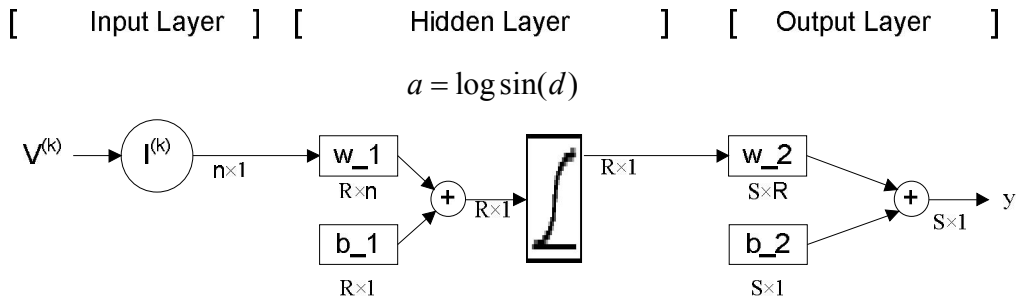

Figure 42 A three-layer feed-forward neural network with n input elements, R neurons in the hidden layer and S output elements

a) It is a standard practice to normalize the inputs before applying them to the network. The raw input-output data is preprocessed into normalized values from -1 to 1 by applying Eq.(25), where $I^k(i)$ is the *k-th* sample of the *i-th* element of the *n* element problem. There are three elements in this problem (*n=3*); each element has approximately 200,000 samples.

a. $$I^{(k)}(i) = \frac{V^{(k)}(i) - V^{(\min)}(i)}{V^{(\max)}(i) - V^{(\min)}(i)} \times 2 - 1, \quad i = 1, 2..n \tag{25}$$

b) The preprocessed data points are divided into three groups: training, testing, and validation. Two commonly used data separation methods are interleaved method and random method. The interleaved method was applied in this work to get an evenly distributed sample points at each group that covers the full range of transmission torque, speed, and electric charges.

c) Using data from the training group, the Levenberg-Marquardt method which is a gradient based searching method is applied to train the networks. This method was designed to approach the second-order speed without having to compute the Hessian matrix [94]. The weights and bias are only updated after all samples have been computed. The process of training a neural network tunes the values of weights and bias so that the mean square error is reduced. One iteration of this algorithm can be written as Eq.(26), where x_k is a vector of current biases, g_k is the current gradient, and α_k is the learning rate.

a. $$x_{k+1} = x_k - \alpha_k g_k \tag{26}$$

d) The training is completed when the magnitude of the gradient is less than 1e-5. The newly trained network is validated using data from the testing and validation group.

6.3.3 Control System Implementation & Performance Evaluation

To implement the ANN controller in vehicle, new control logic is developed to interface with the remaining system. A comparison of simplified control flows is made between the traditional optimal engine efficiency strategy and the optimal system efficiency strategy, as shown in Figure 43 and Figure 44. The optimal engine efficiency based control strategy essentially requires two inputs, ESS power demand and propulsion power demand. The preferred engine speed and torque is determined based on the engine efficiency characteristics. On the other hand, the developed system optimal based strategy requires an additional input of vehicle speed. The preferred engine speed and torque is therefore determined by three instant inputs and the ANN based controller. This control flow remains consistent in model simulation, hardware in-loop simulation, and vehicle testing.

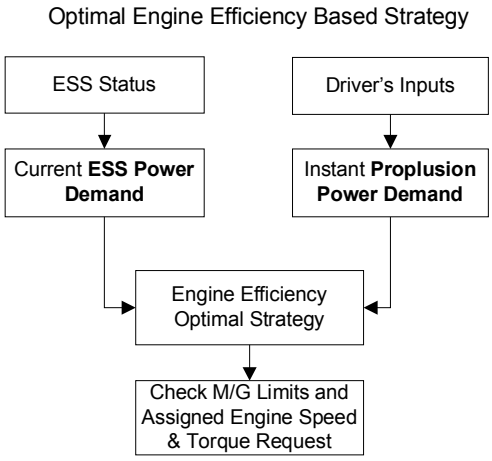

Figure 43 Control Implementation of Optimal Engine Efficiency Based Strategy

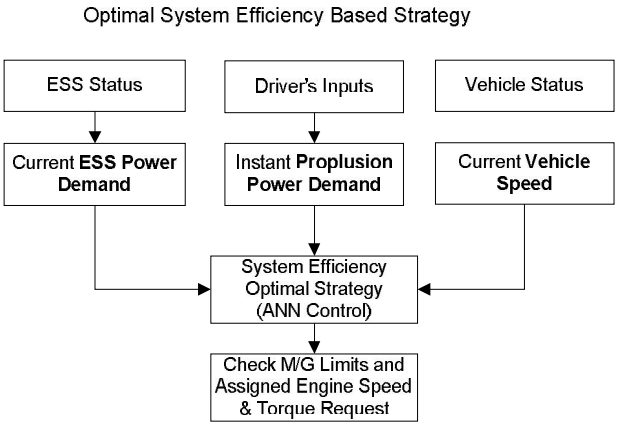

Figure 44 Control Implementation of Developed ANN based Control

6.4 Preliminary Results

6.4.1 Powertrain Case Study

The proposed system optimal based control approach can be applied to a wide range of e-CVT powertrains. To demonstrate performance improvement of an e-CVT powertrain using this method, a case study is performed on the Toyota Prius powertrain platform. Using simulations, comparisons are performed between the rule-based engine optimal based controller and the proposed system optimal based controller. Selected drive cycles include simplified cycles of steady state vehicle speed and certification cycles representing city and highway driving conditions. The simulated Toyota Prius model using Powertrain System Analysis Toolkit (PSAT) is developed at Argonne National Lab (ANL) [43]. The model based on 2004 Prius is a high fidelity powertrain model validated within 5% on different cycles with different SOC against experimental data [42]. The simplified powertrain configuration, including mechanical transmission, electric drives, and ICE, is shown in Figure 45. In the following context, the legend of "engine optimal" refers to simulation results using the traditional engine optimal based control strategy built within the PSAT model; the legend of "system optimal" refers to simulation results using the proposed optimization and ANN based controller which aim to achieve system efficiency.

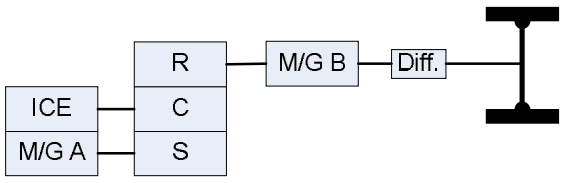

Figure 45 A Simplified Powertrain Configuration of the Toyota Prius

6.4.2 Simplified Drive Cycles

Simulations are first carried out using simplified drive cycles, featuring steady state vehicle speed after an initial starting and acceleration period. These drive cycles with long steady state vehicle speed period can help isolate powertrain loss in steady states from powertrain loss in transient states. Four selected steady vehicle speed are 30 mph, 40 mph, 50 mph, and 70 mph, representing most frequently operated vehicle speed. An extended duration of 10,000 seconds is simulated for each cycle so that the net electric

energy consumption is minimized under the charge sustaining control strategy. With two implemented controllers and four drive cycles, there are eight sets of simulations results. For comparisons of the powertrain's energy efficiency, both fuel consumption and electric energy consumption are considered. The results in

Table 20 show total fuel consumption, final battery SOC, electric loss, engine on/off time, and computed efficiencies. The unit of watt-hour is used for consistent measurement of both fuel and electricity. The initial battery SOC for all simulations is 70%. The electric loss is the sum of loss from two electric motor/generator, DC/DC power converter, and batteries. The Fuel-to-Wheel efficiency is calculated as the output energy to the wheels divided by the input energy from fuel and electricity, where the majority of the energy is from fuel due to the long simulation duration and charge sustaining control strategy. The efficiency gain shows changes of Fuel-to-Wheel efficiency using different control strategies.

Table 20 Simulation Results of Steady Vehicle Speed Drive Cycles

		Fuel Consumption	Battery SOC Final	Electric Loss	Fuel-to-Wheel Efficiency	Engine Switch Times	Engine Off Time	Efficiency Gain
30 mph	Eng. Opt.	33269 Wh	69.7%	1242 Wh	17.6%	1	2.8%	12.8%
	Sys. Opt.	29135 Wh	71.4%	1923 Wh	20.2%	9	41.4%	
40 mph	Eng. Opt.	49777 Wh	68.9%	3762 Wh	20.8%	1	1.3%	4.3%
	Sys. Opt.	47713 Wh	69.4%	1761 Wh	21.7%	1	1.3%	
50 mph	Eng. Opt.	72646 Wh	68.3%	6315 Wh	23.4%	1	1.1%	2.9%
	Sys. Opt.	69843 Wh	68.9%	3440 Wh	24.3%	1	1.1%	
70 mph	Eng. Opt.	140990 Wh	67.6%	9084 Wh	27.7%	1	0.8%	3.4%
	Sys. Opt.	136215 Wh	68.1%	6417 Wh	28.7%	1	0.8%	

Interpreted from simulation results, the overall efficiency improvement is between 2.5% and 12.8%, using the system optimal control strategy. The most significant improvement is at vehicle speed of 30 mph. At this speed, the fuel consumption is very low under the engine optimal control strategy because the engine continuously operates at low power output and low efficiency. The system optimal strategy, on the other hand, operates the engine at higher power band and switched it on and off to leverage the net power output. At vehicle speed 40 mph and above, both strategies keep the engine on for the majority of time; the system optimal strategy can achieve improved overall efficiency

between 3-4%. The efficiency improvement mostly comes from the considerably reduced electric loss up to 50%; the engine efficiency alone is slightly reduced by 1-2% from drive cycle to cycle.

6.4.3 Certification Drive Cycles

The simplified drive cycles can test powertrain's performance in steady states; however, they don't truly represent the dynamic speed patterns in real world driving conditions. The certification drive cycles are formulated by government agencies and organizations to measure the fuel efficiency and GHG emissions of new and existing road vehicles when operated in real world conditions. Two representative certification drive cycles selected are highway fuel economy driving schedule (HWFET) and urban dynamometer driving schedule (UDDS), both created by the U.S. Environmental Protection Agency (EPA).

- HWFET Drive Cycle

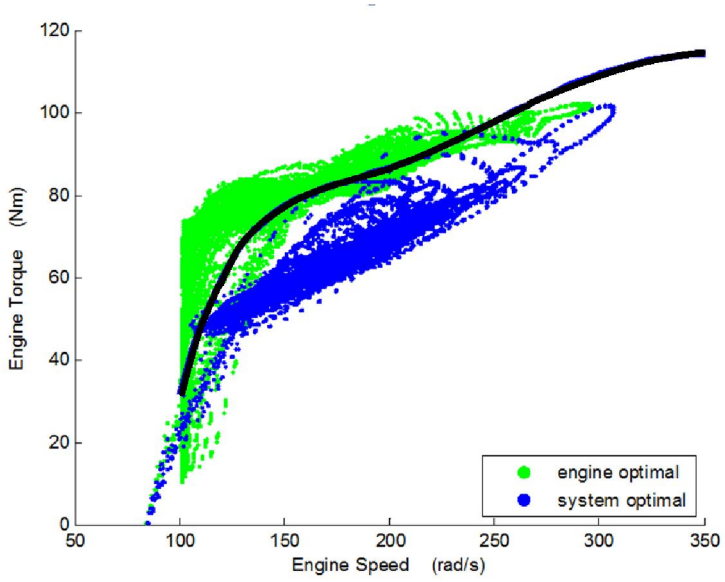

Figure 46 Simulation Results Running ten repeated HWFET Cycles

For the HWFET cycle, comparison of outputs from the engine and two electric motor/generators are made. Simulation results show that the engine optimal strategy operates the engine more closely to the optimal engine efficiency curve; the system optimal strategy operates the engine at a region of slightly lower torque and increased

speed, as shown in Figure 46. The solid line is the ideal best engine efficiency curve. As a result of further away from the optimal engine curve, the engine efficiency is slightly reduced from an average of 34.8% using the engine optimal strategy to 33.6% using the system optimal strategy.

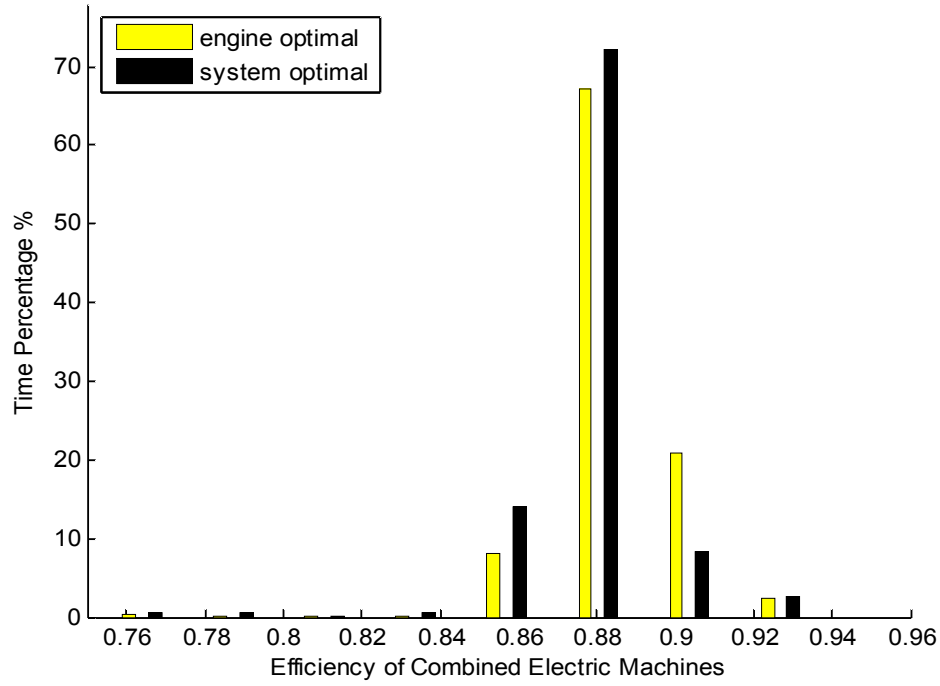

Figure 47 Efficeincy of the combined electric machines running HWFET Cycles

The efficiency of combined two electric machines is defined as the total energy output divided by the total energy input. In the motoring mode, the input is as the electricity consumption and the output is the mechanical power. In the generating mode, the input is the mechanical power and the output is electricity generation. The histogram of calculated efficiency is shown in Figure 47. According to more detailed results in

Table 21, the electric motor efficiency is very close between the two control strategies. Therefore, the improvement of energy efficiency is not coming from the increased motor operation efficiency. To further explore the reason for of fuel consumption reduction, energy balancing charts are drawn as shown in Figure 48 and Figure 49**Error! Reference source not found.**. One noticeable energy loss comes from the split power from the engine blended with regenerative braking energy. This power flow circulates through MG1 and MG2, and creates considerable electric loss by having the mechanical and electric energy conversions two times. In Comparison, the system optimal strategy

significantly reduces the input of the power circulation from 15,099 Wh to 7,802 Wh. Consequently, the electric loss during the energy conversion is much lower. More detailed results in

Table 21 show that the total electric loss including accessory load is reduced by 28.6% from 4580 Wh to 3269 Wh. As a result of reduced electric loss, less energy input is required from the engine side. The engine fuel consumption is 2.8% less despite of slightly compromised engine efficiency. Overall, the powertrain efficiency is improved using the system optimal based control when simulating over the HWFET drive cycle; the fuel consumption is reduced by 2.8% and the final SOC is at 70.7% which is 0.7% higher than the simulation using the engine optimal strategy. The gearbox loss remains largely unchanged.

Table 21 Detailed Results of Ten HWFET Simulations

		Engine Optimal	System Optimal	Comparison/ Improvement
Engine	Fuel Consumption	52662.5 Wh	50803.6 Wh	2.8%
	Net Output	18327.3 Wh	17022.6 Wh	
	Average Efficiency	34.80%	33.51%	
	On/Off Counts	160	153	
	On Time/Total Time	79.0%	76.7%	
M/G1	Average Prop. Efficiency	88.25%	88.5%	
	Average Regen. Efficiency	90.58%	88.9%	
	Electric Loss	1675.3 Wh	1216.6 Wh	27.4%
M/G2	Average Prop. Efficiency	86.71%	86.31%	
	Average Regen. Efficiency	86.69%	86.61%	
	Electric Loss	1861.2 Wh	1004.3 Wh	46.0%
ESS& Accessory Load	Final SOC	70.0%	70.7%	
	Electric Total	1044 Wh	1048 Wh	
Gearbox	Loss	344 Wh	340 Wh	
Total Electric Loss		4580 Wh	3269 Wh	28.6%

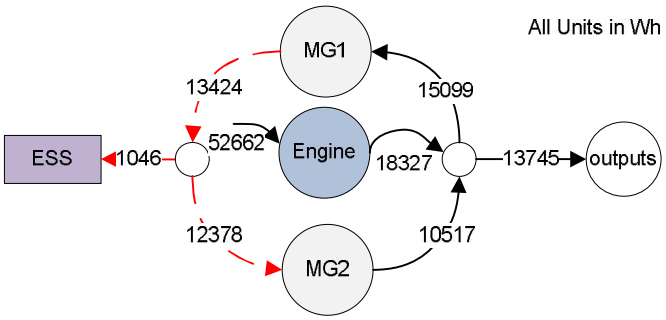

Figure 48 Energy Balancing Running Ten HWFET Cycles (engine optimal strategy)

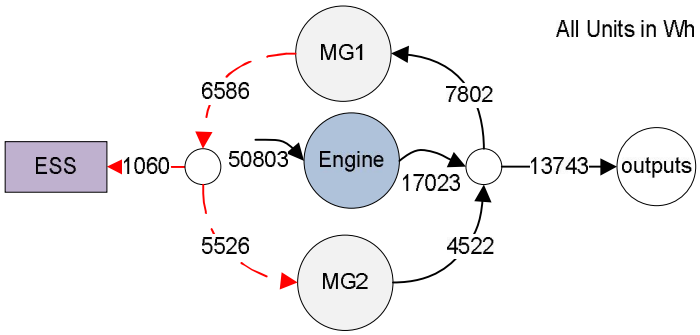

Figure 49 Energy Balancing Running Ten HWFET Cycles (system optimal strategy)

- UDDS Drive Cycle

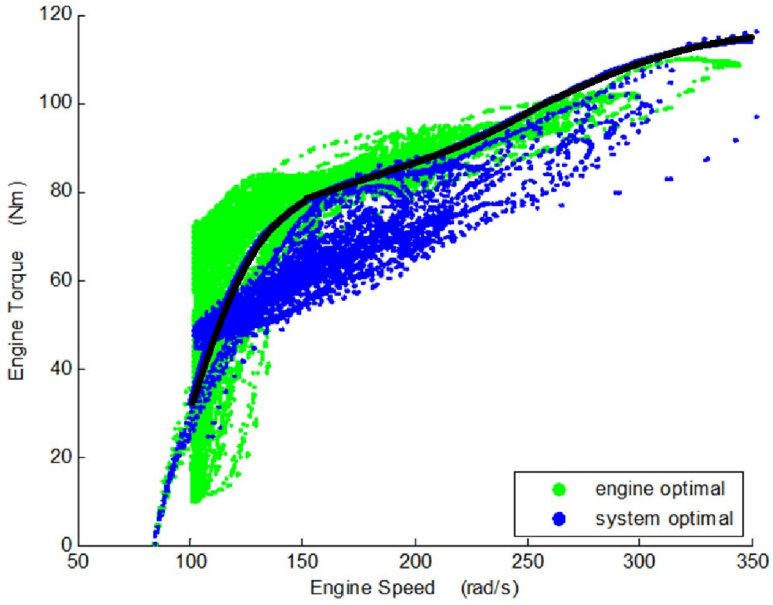

Figure 50 Simulation Results Running Ten repeated UDDS Cycles

The UDDS is a more dynamic drive cycle than the HWFET with many rapid accelerations, decelerations, and stop-starts. The braking energy that can be potentially recovered is higher than that of highway drive cycles. Simulation results of the UDDS cycle show similar trend of engine operation region compared with the HWFET cycle. The engine optimal strategy operates the engine more closely to the optimal efficiency curve and the system optimal strategy operates the engine operated at a region of slightly lower torque and increased speed, as shown in Figure 50, where the solid line is the ideal best engine efficiency curve. Similarly, the average engine operating efficiency is reduced from 34% using the engine optimal strategy to 32.8% using the system optimal strategy.

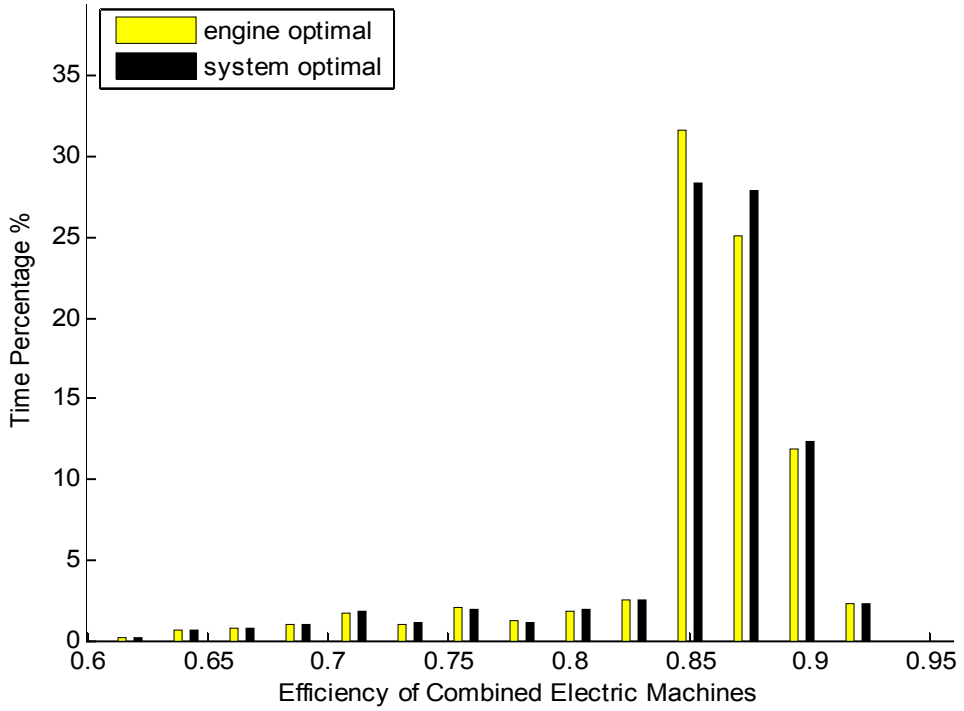

Figure 51 Efficeincy of the combined electric machines running UDDS Cycles

The efficiency of combined electric machines is also calculated and the results are shown in Figure 51. According to results in

Table 21, the average efficiency of the electric motors using the two control strategies is very close. The energy balancing charts are drawn as shown in Figure 52 and Figure 53. Different from the powertrain energy balancing in the HWFET simulation, both electric motor/generators have a net positive electricity generation. The increase of generated

power is because of the high regenerative energy coming from the final drive. The final battery SOC is however not increased with the positive energy input, due to significant electric loss at the battery and power converters. The total electric loss including the accessory load is reduced from 5115 Wh using engine optimal strategy to 4488 Wh using system optimal strategy. The input demand from the engine is also reduced as a result of reduced electric loss. The fuel consumption is reduced by 1.8% and the average engine operating efficiency is slightly lower.

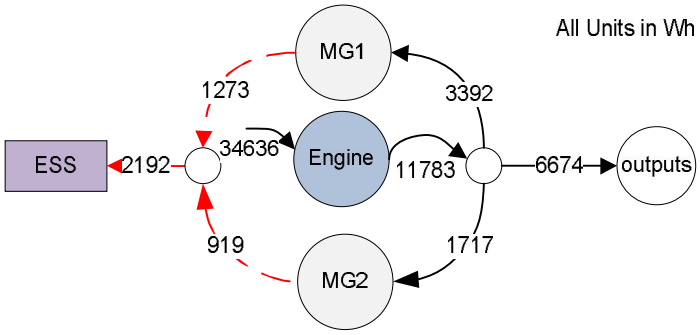

Figure 52 Energy Balancing Running Ten UDDS Cycles (engine optimal strategy)

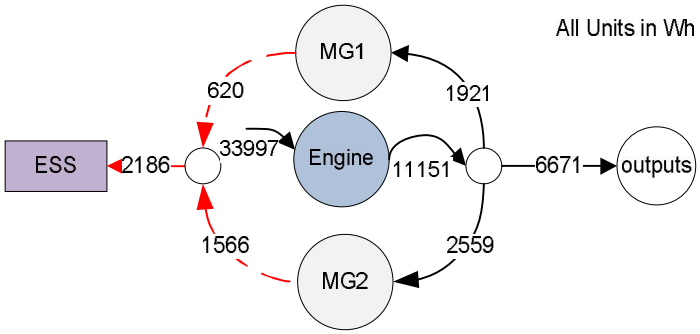

Figure 53 Energy Balancing Running Ten UDDS Cycles (system optimal strategy)

Table 22 Detailed Results of Ten UDDS Simulations

		Engine Optimal	System Optimal	Comparison
Engine	Fuel Consumption	34636 Wh	33997 Wh	1.8%
	Net Output	11783 Wh	11151 Wh	
	Average Efficiency	34.0%	32.8%	
	On/Off Counts	358	330	
	On Time/Total Time	32.1%	30.6%	
M/G1	Average Prop. Efficiency	85.30%	85.54%	
	Average Regen. Efficiency	87.78%	87.72%	
	Electric Loss	2118.5 Wh	1301.3 Wh	38.6%
M/G2	Average Prop. Efficiency	86.23%	86.00%	
	Average Regen. Efficiency	86.56%	86.59%	
	Electric Loss	797.87 Wh	993 Wh	24.4%
ESS & Accessory Load	Final SOC	69.48%	69.36%	
	Electric Total	2199 Wh	2194 Wh	
Gearbox	Loss	373.9 Wh	370.5 Wh	
Total Electric Loss		5115 Wh	4488 Wh	12.3%

6.5 Summary

In this work, a modeling and optimization based approach is applied to develop optimal system efficiency based control for e-CVT hybrid powertrains. This offline optimization based approach first identifies the optimal control inputs in the powertrain simulation environment. Then the artificial neural network method is applied to train a vehicle controller for real-time implementation. In addition to presenting the problem

formulation and methodology, a case study is carried out on a representative e-CVT hybrid powertrain with a high fidelity model. The performance of developed controller is compared with a controller using the conventional rule-based strategy. The system optimal control strategy can effectively improve the overall efficiency by significantly reducing the electric loss in the internal electric power circulation. Results show fuel efficiency gain between 3 and 13 percent on simplified drive cycles of steady vehicle speed, and 2 to 3 percent on certification cycles of the HWFET and UDDS. This approach is also suitable for implementing on mass produced vehicles with low on-board computation power, since the intensive computation is carried out offline and no significant computation load and storage space is needed from the vehicle controller.

Even though considerable fuel efficiency gain is achieved using the proposed method, further improvement of energy efficiency is still feasible. One important assumption while the optimization problem is formulated is the minimization of energy consumption in steady state. This is likely to cause the less significant efficiency gain in the dynamic certification drive cycles, compared with the steady speed drive cycles. The minor inconsistency between the powertrain model for controller development and powertrain model for vehicle simulation can also affect the final gain. Because the data fitting method was applied to models in controller development in order to better support optimization searching.

Chapter 7 Case Study – Design and Development of a Next Generation Extended Range Electric Vehicle

Advances in battery and hybrid powertrain technology have significantly expanded the automotive design space. In this chapter, the design process of a new extended range electric vehicle (E-REV) is presented, following the industry standard model-base design process. The UVic EcoCAR development is aimed at retrofitting a 2009 Saturn VUE SUV with advanced hybrid powertrain. The new powertrain design incorporates a GM 2-Mode transmission, a GM E85 flex-fuel engine, a rear traction-motor and a high-capacity battery system from A123 System. The design attempts to achieve zero fuel consumption in charge depleting mode under normal operating conditions, while maintaining the highly efficient 2-Mode hybrid functionality in charge-sustaining mode. By integrating an additional traction motor with the 2-Mode transmission, the new design overcomes the constraints imposed by the size of the electric motors and gearing configuration in the 2-Mode transmission, to allow the vehicle to be operated at higher speeds and loads without turning on the IC engine. To effectively achieve the design targets, this EcoCAR development followed the MBD process, and the development is a result of the collective efforts of the UVic EcoCAR team in the EcoCAR – Next Challenge collegiate advanced vehicle technology engineering competition.

7.1 Vehicle Introduction

The developed vehicle participated in the EcoCAR competition, which aim at building a hybrid vehicle which could reduce fossil fuel dependence and carbon dioxide footprint. To achieve the target, the UVic team applied the industrial standard vehicle development process (VDP) which is implemented though out the project from architecture selection to final calibration. The timeline of the three-year project is shown in Table 23. Based on the design needs as well as components availability, the UVic team designed a 2-Mode plus, AWD, E-REV using a 2009 Saturn VUE as a baseline platform, the vehicle powertrain integrates a 2-Mode [95] system, a GM ICE, a 125 kW electric motor from UQM, and a high capacity battery system from A123 System.

Table 23 EcoCAR 3 Years Vehicle Development Process

	MECHANICAL	ELECTRICAL	CONTROLS
Y1 Design June 2009	Life Cycle Analysis, Vehicle Architecture Selection, and Performance Modeling		
	CAD - Component	Define Electrical Requirements	Control System Design
	CAD - Routing and Integration	HIL Design/Setup	Simple Control and SIL/HIL
	Finalize Component Selection and Acquisition		
Y2 Mule Vehicle June 2010	Vehicle Modification	Vehicle Harness/ System Design	HIL Finalization and Communication Setup
	Component Integration	Vehicle Harness Setup	HIL Testing - Safety and Fault Mitigation implementation
	Control Integration and Vehicle Testing		
Y3 Optimization and Refinement June 2011	Aero, Light weighting, Ride and Handling and Noise, Vibration and Harshness	Refinement and optimization	Refinement and Optimization
	99% Buy off - Vehicle Ready for Production		

7.2 Powertrain Design

7.2.1 Literature Review

Progressing through the VDP process, a literature search was performed to identify the vehicle architecture and component selections that best match the desired vehicle performance, as required by vehicle technical specifications (VTS) from the competition organizer. The power-split architecture is identified as the most appropriate architecture for this application. This architecture allows the ICE power to be delivered through either a mechanical path or an electro-mechanical path [12] to the wheels. The fuel efficiency can be improved and good EV capability is ensured.

7.2.2 Vehicle Technical Specifications

While re-engineering the powertrain of a stock Saturn VUE, all competing vehicles should to achieve better energy efficiency without compromising vehicle performance.

The baseline target of vehicle performance is defined by a competition required VTS. The UVic team decided to pursue a higher vehicle performance than the minimum VTS, as shown in the comparison in Table 23. This UVic target VTS reflects team goals, which include the minimization of fuel consumption, reduction of GHG emissions, optimization of overall system efficiency, good drivability, and performance.

Table 24 Competition Requirement and Team VTS

Specification	Competition Requirement	UVic Target
Accel 0-60 mph	≤14 s	7.5 s
Accel 50-70 mph	≤10 s	5 s
UF Weighted FE	7.4L/100 km	2.5L/100km
Towing Capacity	≥680 kg @ 3.5%, 20 min @ 72 km/h	680 kg
Cargo Capacity	H/D/W: 457 mm / 686 mm / 762 mm	0.70 m3
Passenger Cap.	≥4	4
Braking 60 – 0 mph	< 51.8 m	45 m- 50 m
Mass	≤ 2268 kg	2145 kg
Starting Time	≤ 15 s	≤ 2 s
Ground Clearance	≥178 mm	178 mm
Range	≥ 320 km	≥ 320 km

7.2.3 Power Simulation

To determine the propulsion and braking power requirements of a vehicle with the UVic target VTS, a representative vehicle slider was modeled and simulated to compute the vehicle power requirements on different drivecycles. According to the results shown in Table 24, the vehicle power requirements have a high peak to average ratio. Aggressive driving patterns such as US06 could demand over 118 kW peak power while the average power demand for city driving and highway (UDDS/HWFET) is in 10-20 kW range. The peak power demand was used to size the drivetrain components while the average power demand could be used to size battery and fuel tank capacity.

Table 25 Drive Cycle Power Requirements

	Average / Peak Propulsion Power	Average / Peak braking Power

City (UDDS)	10.02 kW / 45.2 kW	8.1 kW / 28.5 kW
Highway (HWFET)	19.1 kW / 38.3 kW	9.9 kW / 38.6 kW
Aggressive (US06)	33.3 kW / 118.2 kW	19.6 kW / 67.1 kW
LA92	16.1 kW / 63.2 kW	12.2 kW / 119.2 kW

7.2.4 Battery Sizing

Lithium-ion batteries have the advantage of high power/energy volumetric and mass densities relative to batteries of other chemistries. A123 Systems, a US battery manufacturer, provided several Li-ion battery options to the competition participants. However, design the cooling system for the batteries is each university team's responsibility. General battery design considerations include power, energy, packaging, weight, and system voltage. Capacity is a critical parameter that determines vehicle range, fuel economy, and petroleum usage. As battery capacity increases, more electric energy could be stored onboard and more electric energy is available for vehicle propulsion. In the meantime, vehicle weight increases. Detailed calculations are performed to evaluate the trade-off between battery size and vehicle efficiency. Vehicle range in CD mode defines the utility factor, which is used in the calculation of proposed J1711 fuel consumption. Figure 52 plots this fuel economy versus battery mass; the utility factor for each point was calculated based on the estimated vehicle range and fuel economy.

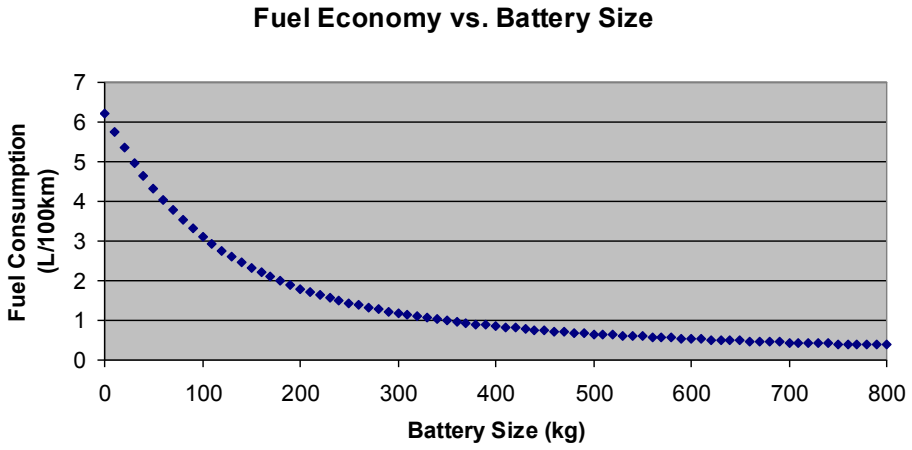

Figure 54: Fuel Economy vs. Battery Capacity

According to the results, increase of battery mass and thus utility factor, results in lower fuel consumption. However, the marginal decrease in fuel consumption is

increasingly outweighed by the increase in battery size and weight. A battery size of approximately 300 kg represents the most feasible solution when fuel efficiency, packaging, weight constraints and cost are taken into considerations.

7.2.5 Fuel Selection

The four major contributing factors regarding fuel selection are fuel economy, GHG emissions, CAC emissions and petroleum use. The fuel selection also indirectly affects the vehicle performance characteristics, since provided ICEs are fuel dependant.

The properties of four liquid consumable fuels are listed in Table 25. The properties were obtained from GHGenius [96], a model for lifecycle assessment of transportation fuels. Levels of CO_2 per kWh of energy are determined by the percentage of carbon in a unit of fuel, the volumetric density and mass energy density.

Table 26 Properties of Various Fuels

Fuel Property	Gasoline	Diesel	Biodiesel	Ethanol
g / L	739.2	843.2	884	789.3
% C	86.2%	85.8%	77.0%	52.2%
mJ/L	34.686	38.653	36.936	23.579
g CO_2 / MJ	67.4	68.6	67.6	64.1
g CO_2 / kWh	242.5	247.1	243.3	230.7

The competition values for upstream GHG emissions and petroleum use were incorporated into the data, and values for each fuel with one kWh of energy content were established. Appropriate adjustments were made to biofuel blend to account for the energy density difference in comparison to their petroleum counterparts as shown in Table 26. Using E85 can yield lowest GHG emissions and using electricity consumes least petroleum. Among liquid fuels, E85 has approximately three times less petroleum use compared to B20. NOx emissions are difficult to model due to the transient conditions exhibited by the engine. In addition, differences in control strategies can drastically affect the emissions profile of a particular architecture, due to variations of cold starting frequencies, engine-on durations, and steady state or varying state operating time. Overall, E85 and electricity are the final fuel choices due to their low petroleum energy use and low GHG emissions. The increased use of electricity as a source of

propulsion energy has a positive impact on petroleum use and fuel efficiency. The degree to which electricity use impacts the total petroleum use, fuel efficiency, and GHG emissions is dependent on the vehicle range in charge depleting mode and the resulting utility factor; this utility factor is used to calculate the SAE J1711 fuel economy.

Table 27 Petroleum Use and GHGs for Competition Fuels

	E10	E85	B20	Electricity
Upstream g CO_2/kWh	63.3	1.57	1.99	699.18
Upstream petroleum kWh/kWh consumed	0.0931	0.0832	0.0642	0.0785
% petroleum	90%	15%	80%	0%
% petroleum (energy basis)	92.98%	20.61%	80.72%	0%
Fuel g CO_2/kWh	241.7	233.1	246.3	0.0
Total petroleum Energy kWh/kWh consumed	99.31%	23.32%	86.42%	7.85%
Total GHG g CO_2/kWh	304.96	234.66	248.32	699.18

7.2.6 Internal Combustion Engine Selection

A number of IC engines of different sizes are provided to the competition. Considering compatibility with E85 fuel, comparisons are made among three engines. The 1.6L LDE, 1.8L LWE, and 2.4L Ecotec LE9 can either directly or modified to run E85. The native fuel compatibility, power output, and speed of the three engines are shown in Table 28. Effects on powertrain mass were taken into considerations.

Table 28 Internal Combustion Engine Options

	2.4L LE9	1.8L LWE	1.6L LDE
Native Fuel Compatibility	E85	E10	E10
Peak Propulsion Power (kW)	123	105	88
Range of Peak Efficiencies (%)	34 - 36 - 34	32.5 - 34.5 - 32.3	32 - 34.7 - 32
Power Range (kW)	13 - 60 - 72	12 - 27 - 52	10 - 33 - 56
Engine Speed (rad/s)	104 - 335 - 377	131 - 209 - 330	125 - 293 - 461

The 2.4 Ecotec engine was selected as the power plant of choice because of the fuel compatibility and power rating. The high power rating of this engine will lead to better vehicle performance during acceleration and towing. The high peak efficiency and broad

efficiency range of the 2.4L engine were also deciding factors in the selection. Examinations of the fuel maps show that the smaller 1.8L and 1.6L engines have lower efficiency than the 2.4 L engine at power demand over 7kW.

7.2.7 Motor Selection and Sizing

Electric motor and controller sizing was determined by examining the trade-offs between vehicle acceleration performance, efficiency, and size. Physical packaging constraints also limit motor choice to permanent magnet motor motors instead of the larger and heavier induction motors. Four electric motors between 50kW to 145 kW are modeled and the vehicle performance is simulated. The UQM Powerphase 145 motor is selected for higher propulsion power and good energy efficiency. The specification of this motor is shown in Table 29.

Table 29 Electric Motor Specifications

Parameter	Value
Peak/Continuous Power	145/85 kW
Peak/Continuous Torque	400/180 Nm
Maximum Speed	8000 RPM
Maximum Efficiency	94%
Operating Voltage Input Range	300 – 420 V
Maximum Current Rating	600 A

7.3 A 2-Mode Plus Extended Range Electric Vehicle

Based on the previous analysis, as well as component availabilities, three hybrid architectures were considered in the final selection stage: an E-REV 2-mode with RTM, a series hybrid E-REV, and a BAS+/Parallel E-REV. Models of the three hybrid architectures are generated and simulations were run to determine adherence to the competition and Team VTS. All designs include high-capacity battery packs to enable good all-electric propulsion functionality. The 2-Mode plus architecture excelled as the final selection. This architecture consists of an ICE and a 2-mode transmission coupled to the front wheels and an additional rear traction motor (RTM) coupled to the rear wheels.

7.3.1 Description of the 2-mode Plus Hybrid Powertrain

The 2-Mode Plus powertrain design convert the 2009 GM Saturn VUE stock compact SUV into an E-REV. Major powertrain components are listed in Figure 55. The GM Ecotech ICE can operate either gasoline or E85 blended fuel. The GM 2-Mode hybrid transmission is a strong hybrid transmission [97, 98] with two planetary gearsets and two 55 kW permanent magnet electric motors. The engine and the 2-Mode system are packed in the front engine compartment and connected to the front wheels. The 145kW UQM Powerphase 145 permanent magnet electric motor is connected to the rear wheels through a Borg-Warner transaxle. The 21 kW-hr A123 battery pack provides power to both the 2-Mode transmission and UQM motor.

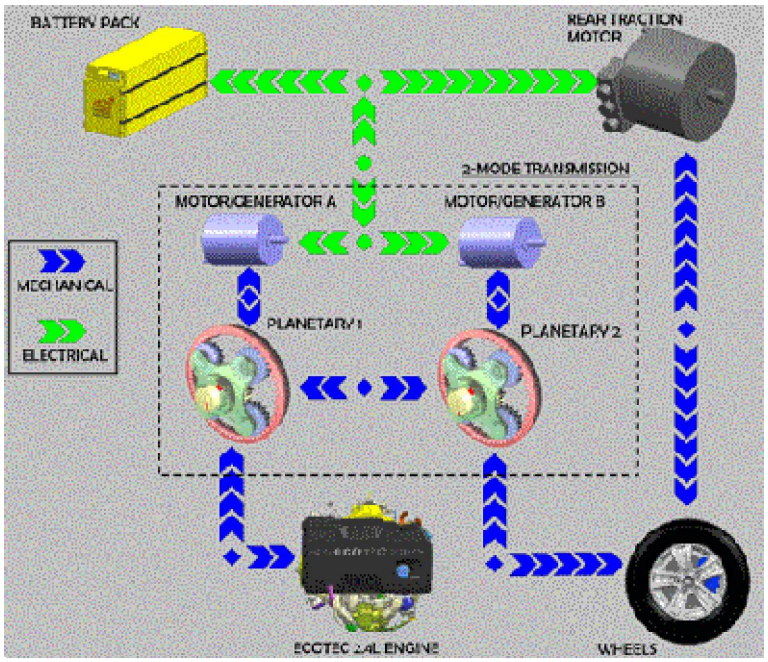

Figure 55 2-Mode plus Hybrid Powertrain

Table 30 2-Mode plus Powertrain Components

Components	Description

ICE	2.4L Ecotec flexfuel
Fuel	E85
Transmission	GM 2-mode 2MT70
RTM Size	UQM Powerphase 145
Battery Capacity	Li-ion by A123 System
Battery Power	21.1 kWh 65 kW continuous /200 kW peak

7.3.2 Electric Propulsion Strategy

The RTM connects to a rear differential, the ratio of which is selected to match with top vehicle speed and optimal motor efficiency. With fixed differential ratio, the RTM operates at a low speed range when the vehicle speed is low. At vehicle speed 60 km/h or lower, the RTM can only delivery 40% or less of its peak power. The limited available power at low vehicle speed results in limited propulsion power from the rear axle. To enhance the vehicle performance at lower vehicle speed, MGB in the 2-Mode transmission provides additional propulsion. The motor/generator B (MGB) in the 2-Mode transmission is geared to the front wheels through the second compound planetary gear set and the front differential gear (FDG). At vehicle speed between zero and seventy kilometre per hour, MGB operates between zero and the maximum speed range, while the transmission is in Mode 1 and the ICE is off. At vehicle speed of 70 km/hr or higher, the RTM independently provides electric propulsion.

In addition to the added propulsion power, using both of the MGB and RTM in EV mode has the potential to achieve higher overall electrical efficiency, compared to using either motor independently. As the RTM and MGB are geared at different ratios to the wheels, the performance and efficiency characteristics versus vehicle speed are different between the two motors. Actively splitting power between the two motors at different vehicle load and speed can improve energy efficiency. The MGB enters high RPM range earlier as vehicle speed increases and reaches high efficiency zone at 30-50 km/h. The RTM will reach its high efficiency zone at higher vehicle speed.

Based on vehicle dynamic analysis, the weight distribution varies between the front and rear wheels as vehicle acceleration changes. When the vehicle decelerates, the available traction on the front wheels is considerably higher than the tractions on the rear wheels. Therefore, having the MGB enabled at EV mode can more effectively recover brake energy during regenerative braking.

7.4 Model Development and Simulation

Upon completion of conceptual powertrain design, computer models of every powertrain components are generated and powertrain system simulations are carried out, using state-of-the-art model-based design tools. These tools provide an interactive modeling environment for multi-physics systems, e.g. mechanical, electrical and control design interfaces. In addition to the multi-physics modeling environment, other tools are available for tuning design parameters using optimization based approaches. Taking advantage of the recent developments in model-based design tools, the development time is significantly shortened.

A dynamic vehicle model named 2MPSIM (2-Mode plus vehicle SIMulation) was developed in MATLAB, dSpace software environments. Models for powertrain components are mostly driven by experimental data provided by the original equipment manufacturers (OEMS), e.g. General Motors, A123 batteries, UQM motors. The model simulations can be performed at three phases: model in-the-loop (MIL), software in-the-loop (SIL) and hardware in-the-loop (HIL). Using these high fidelity vehicle models, not only the vehicle performance can be simulated, but also the ECU hardware can be programmed using HIL simulation.

7.4.1 Mechanical System Modeling

The mechanical system modeling of the designed vehicle includes an ICE, 2-Mode transmission, drive shafts, and vehicle dynamics. Models of these components are built in a multi-physics programming environment supported by the Simulink/SimDriveline toolbox.

ICE - The engine is modeled to simulate torque generation, fuel consumption, and tailpipe emissions. The thermal effects, combustion process and exhaust system lack sufficient data and are not included at the current stage. The torque command between zero and one is sent to the engine model. This command is multiplied by the maximum engine torque at the current engine speed to determine the engine torque at the next integration step. Based on engine speed and torque, transient fuel rate and emissions flow is calculated at each integration step. Modeling of the engine ECU which manages engine idling as well as interfacing with supervisory controllers is described in the control

system modeling section. An alternative approach to model an ICE is to use commerciality available engine models, such as the dSpace ASM engine model [99]. This model is a semi-empirical model combining first principle and data driven models to simulate a fuel system, an engine combustion system, an air path, and engine coolant system, and an exhaust system. This more complex ASM engine model however requires extensive calibration to fully represent the selected engine. This model is therefore not chosen for system simulation due to insufficient data available.

2-Mode Transmission – The 2-Mode transmission, a hybrid propulsion system developed by GM, applies a multiple geared hybrid scheme to improve fuel efficiency and provide partially EV capability. The selected 2MT70 2-Mode transmission integrates electro-mechanical power-split operating modes with four fixed gear ratios [97]. All components including the two planetary-gear sets, two permanent synchronous electric motors and four clutches are packaged in the same transmission case. The gearing configuration can be viewed in Figure 56. Labels R, C, S represents the ring, carrier and sun gears of the two planetary-gear sets. CL1 to CL4 represents four synchronized clutches, and motor A and B represents the two electric motors. The mechanical system modeling of the 2-Mode transmission system includes the planetary gears, clutches and the differential. Using the SimDriveline environment, gears and clutches can be built from corresponding libraries and configured for the 2-Mode design.

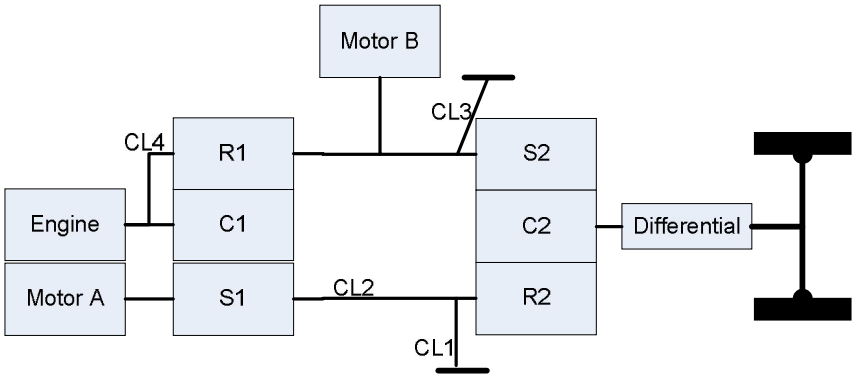

Figure 56 FWD 2-Mode Transmission

Vehicle Dynamics Modeling - A vehicle dynamic model simulates vehicle behaviors in the longitudinal, lateral, and vertical directions. Modeling of the longitudinal dynamics has been the primary focus in the current model. In the longitudinal direction,

the vehicle resistances include three main components, aerodynamics resistance, rolling resistance, and drag by gravity forces caused by slope of the road surface. In addition to the three resistances, there is also the force caused by the moment of inertia during vehicle speed change.

7.4.2 Electrical System Modeling

The electrical system modeling in the design vehicle includes the high voltage electric drives, power electronics, and energy storage system. Two different modeling approach, first principle modeling and data driven modeling are applied for different components.

The first principle modeling was attempted to model the electric drives and power electronics. This approach models a complex electric system from basic elements, such as transformers and resisters. Modeled using fundamental physical equations, the transient phenomena of the complex electric system can be well represented. This approach is however not appropriate for modeling of the existing system, due to the needed data for calibration and computational expensive calculations.

The data-driven modeling approach is applied to model the electric system. For electric motors, torque and speed capabilities as well as energy efficiency from experimental testing are applied to modeling. Experimental data for the electric driven is provided by the UQM and by A123 system for the battery system.

7.4.3 Control System Design

The scope of the control system design for the developed hybrid vehicle is mainly high level supervisory control. Two main controllers are modeled, including a 2-Mode system controller (named as 2-Mode TPIM) and a supervisory controller (named as UVic1 controller).

- 2-Mode TPIM Controller

The 2-Mode TPIM manages power flow among the ICE, two electric motors, and transmission outputs. The TPIM receives inputs of torque commands from the UVic 2 controller and controls corresponding torque required from the motors and the engine.

- Supervisory Controller (UVic 1)

The UVic 1 supervisory controller is at the highest control level. It interfaces with driver's commands and controls the 2-Mode system, rear traction motor, brake system,

and energy storage system. To finely use the available propulsion combinations of the powertrain, five operating modes are defined, including electric only drive at low vehicle speed (EV_LS), electric only drive at high vehicle speed (EV_HS), engine and electric motors drive in at Mode1 (HEV_M1), engine and electric motors drive in at Mode2 (HEV_M2), engine and motor at fixed gears (HEV_FGs). The shifting sequence among the five modes is shown in the diagram in Figure 57. Among the five modes, the EV_LS and EV_HS are limited power output modes (LPMs) with peak power rating of 150 kW; the HEV_M1, HEV_M2 and HEV_FGs are full power output modes (FPMs) with peak power rating of 250 kW. It should be noted that both LPMs and FPMs are capable of propelling the vehicle up to the full speed range (0-180 km/h).

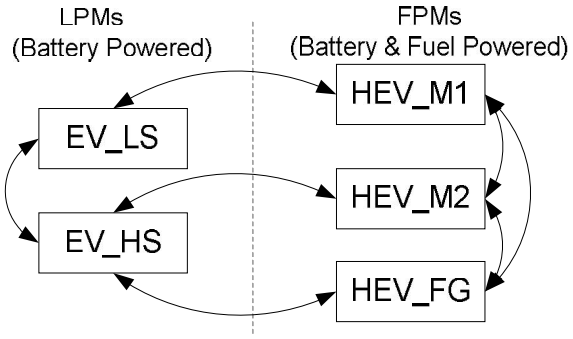

Figure 57 Limited power and full power operation modes

On daily commuting basis, the design intends to reduce fuel consumption and replace the energy demand by electricity. With the battery fully charged, the vehicle operates in LPMs until the battery is depleted to a predetermined low battery SOC; then the vehicle switches to FPMs using ICE to maintain the battery SOC. In the LPM, traction split between front and rear wheels can affect the overall efficiency. The control strategy should ensure the vehicle drivability and maximize the vehicle efficiency[100]. To model different operation modes and the transitions in between, an interactive control development tool named Stateflow was used. Stateflow is suitable of modeling event-driven systems traction from one operating mode to another in response of event and conditions.

7.5 Optimal Control for High Efficiency EV Mode Operation

In EV mode, the powertrain allows propulsion power to be withdrawn from three electric motors. The EV traction control strategy is developed to control power split among the electric drives in order to achieve optimal electrical efficiency.

7.5.1 Vehicle Traction System Modeling

The first step to develop the optimal power split strategy is to generate the vehicle dynamic model and computes traction limits between wheels are the road surface. Figure 58 displays a car travelling on an inclined road surface with an angle of θ, the parameters are described in Table 31.

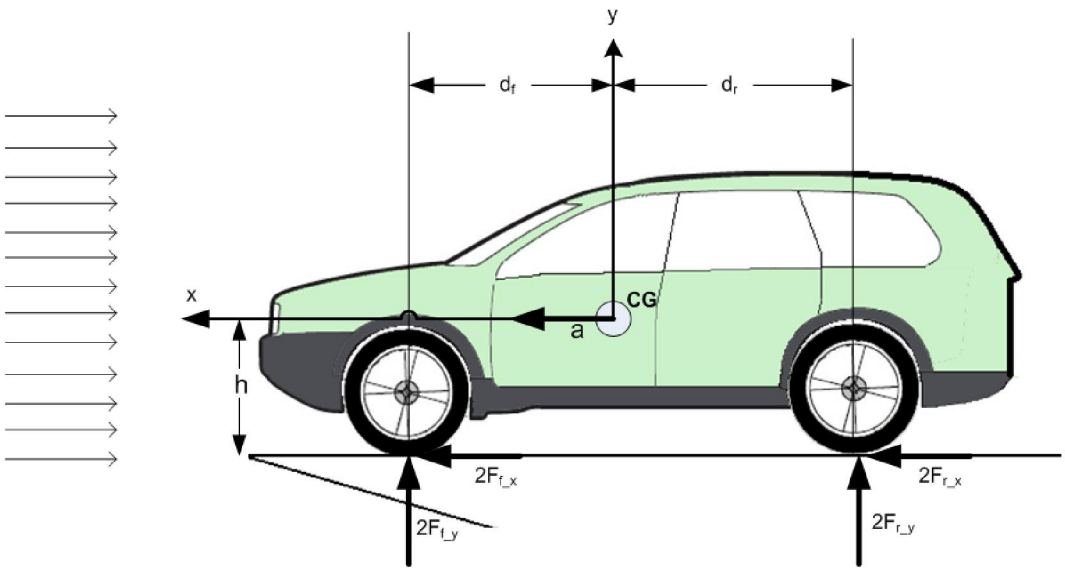

Figure 58 a SUV dynamics Model on an inclined surface

Table 31 Vehicle Dynamics Model Parameters

Symbol	Description	Unit
x, y	coordinate axis	
Ff_x, r_x	Traction force on front and rear tire in x direction	N
Ff_y, r_y	Traction force on front and rear tire in y direction	N
a	acceleration	m_2
CG	Center of gravity	
h	Height of CG to road surface	m
d	wheel base	m
df (dr)	distance from front (rear) axle to CG	m
θ	Incline angle	o

The normal force Ff_y, Fr_y on each of the front and rear wheels satisfy relations expressed by Eq. (27):

$$\begin{aligned} F_{f\_y} &= \frac{1}{2}mg(\frac{d_r}{d}\cos\theta - \frac{h}{d}\sin\theta) - \frac{1}{2}ma\frac{h}{d} \\ F_{r\_y} &= \frac{1}{2}mg(\frac{d_f}{d}\cos\theta + \frac{h}{d}\sin\theta) + \frac{1}{2}ma\frac{h}{d} \\ d &= d_f + d_r \end{aligned} \tag{27}$$

Therefore, the maximum traction force in the x direction on the front and rear wheels is given by Eq. (28), where μ_tire is the frictional coefficient between the tire and the road surface. The only dynamic term in equation (28) is $\pm\frac{1}{2}ma\frac{h}{d}\mu_{tire}$. According to this term, a positive "a" leads to decreased maximum traction force on the front axle and increased maximum traction force on the rear axle. When the maximum traction forces on both axles are equal, the breakeven acceleration a_e is represented by Eq. (29).

$$\begin{aligned} F_{f\_x} &= F_{f\_y} \times \mu_{tire} = \frac{1}{2}mg\mu_{tire}(\frac{d_r}{d}\cos\theta - \frac{h}{d}\sin\theta) - \frac{1}{2}ma\frac{h}{d}\mu_{tire} \\ F_{r\_x} &= F_{r\_y} \times \mu_{tire} = \frac{1}{2}mg\mu_{tire}(\frac{d_f}{d}\cos\theta + \frac{h}{d}\sin\theta) + \frac{1}{2}ma\frac{h}{d}\mu_{tire} \end{aligned} \tag{28}$$

$$a_e = \frac{g(d_r - d_f)\cos\theta}{2h} - g\sin\theta \tag{29}$$

Applying the 50/50 front/rear weight distribution of the UVic EcoCAR, the breakeven acceleration a_e is further simplified as:

$$a_e = -g\sin\theta \tag{30}$$

where a_e is non-positive value varying upon the incline angle of the road surface. Therefore, the maximum traction forces on front wheels during acceleration on a level road surface are always less than that on the rear wheels. When travelling on a positively inclined road (travelling uphill), the maximum traction on front wheels is further reduced. When travelling on a negative inclined road (doing downhill), the front wheels gain more available tractions than the rear wheels do.

Based on the vehicle traction model, the maximum allowable traction force on both front and rear wheels is calculated and represented in Figure 59 and Figure 60.

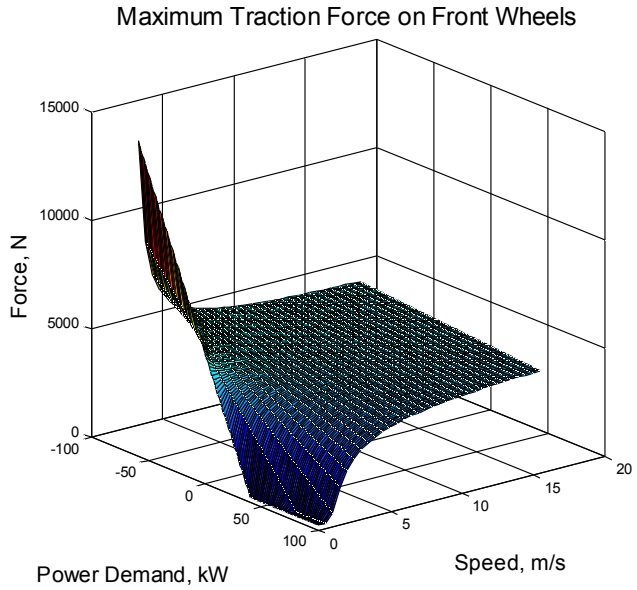

Figure 59 Maximum Allowable Traction Force on the Front Wheels

According to results shown in Figure 59, when vehicle speed is fixed, the maximum traction force (MTF) on front wheels increases as vehicle power demand decreases. When power demand is fixed, the MTF on front wheels increase when the vehicle speed increases. Similarly, conclusion could be drawn from Figure 60 for MTFs on the rear wheels. In summary, the maximum allowable traction on front wheels is low during a fast acceleration at low speed and extremely high when decelerating at low speeds.

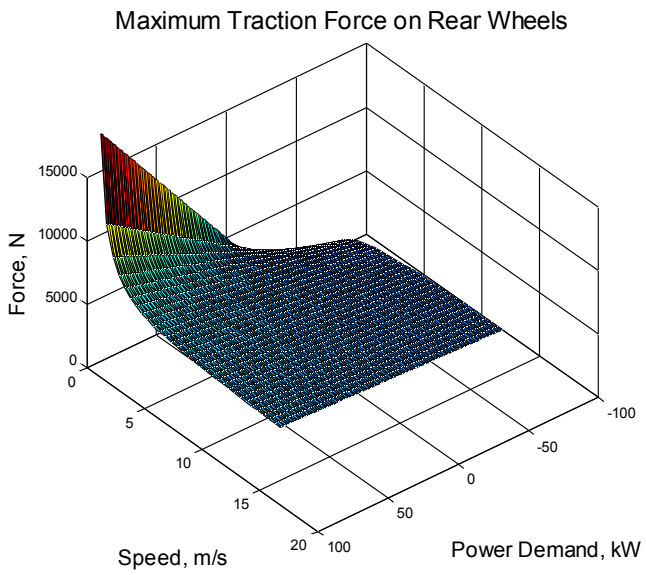

Figure 60 Maximum Allowable Traction Force on Rear Wheels

7.5.2 Problem Formulation

The searching for optimal power split ratios is formulated as an optimization problem. The objective function is defined by Eq. (31).

$$\eta = f(v, T, p_{MGB}) \tag{31}$$

The electrical efficiency η defines the electrical/mechanical energy conversion efficiency of the electric drives. When motors are propelling the vehicle, η is the mechanical power output divided by the electrical power input. When motors are generating electricity, η is the generated electrical power divided by the mechanical power input. The power flow when batteries are discharging is defined as positive. Likewise, the power flow when batteries are charging is defined as negative. The vehicle speed v is in meter per second. T is the overall vehicle torque demand at the wheels in Newton meter and P_{MGB} is the commanded power output at MGB in kilo watt.

To derive the optimal control rules for MGB and RTM under varying vehicle load conditions, a grid is generated to represent different combinations of v and T. The problem is then transferred into solving P_{MGB} at each grid point $g_{(v,T)}$. A negative sign is applied in front of η to convert the maximization problem into a minimization problem. Then modified objective function and constraints are defined by Eq. (32):

$$\eta = f(v, T, p_{MGB}) \tag{32}$$

subject to

$$\begin{cases} 0 \le v \le 60; \\ -0.8 \times P_{battery\_charging} \le v \times T \le 0.8 \times P_{battery\_discharging}; \\ -P_{regen}(n_{MGB}) \le P_{MGB} \le P_{prop}(n_{MGB}); \\ -P_{regen}(n_{MGB}) \le P_{MGB} \le P_{prop}(n_{MGB}); \end{cases}$$

The four constraints reflect the following relations of the system. The EV speed range with two motors driving is 0-60 km/h. The vehicle power demand defined by V×T is within 80% of the battery charging and discharging capability. Power output at MGB and RTM has to be within the power limits based on the characteristics of each motor.

7.5.3 Optimization Algorithms and Results

Several local and global optimization techniques were applied to solve the optimization problem. The first attempt was to use local optimization algorithms due to their low computation load. The sequential quadratic programming (SQP) method was applied, which solves a quadratic programming sub-problem at each iteration. This algorism quickly converged to a solution but trapped to local minima. Then three global optimization algorithms were applied to solve the problem, including particle swarm optimization (PSO), Genetic Algorithm (GA), and Hybrid Adaptive Meta-modeling Method (HAM). Three sets of results were obtained with function evaluated at each of the 120 points. From these three solution sets, a new quasi-optima solution set is created, by using the minimal solutions among the three solution sets. A comparison of Solutions computational time and result quality is shown in Table 32. Results solved by PSO are closest to the quasi-optima solution; HAM has the quickly converge speed but the solution accuracy is less than ideal. Result generated using GA is less accuracy than PSO, the computational time is also significantly longer.

Table 32 Statistical Results Compared with the Quasi-optimal Results

	Max		Mean	N(>1e-4)	N(>1e-3)	N(>1e-2)	Time(s)
	values	%					
PSO	0.0029	0.3	3.6E-05	4	1	0	32940
GA	0.0330	3.6	0.0016	20	15	8	>10 hr
HAM	0.0347	3.8	0.0030	52	34	11	864

The solved solutions are applied to develop the control strategy for power split between the front and rear wheels. The power split ratios are determined as a function of vehicle speed and power demand. As shown in Figure 61, the direct fit solutions in which the surface go through each solution point can better represent the original optimization solutions; the quadratic interpolated surface shown in Figure 62 is smoother and ensures smooth power delivery.

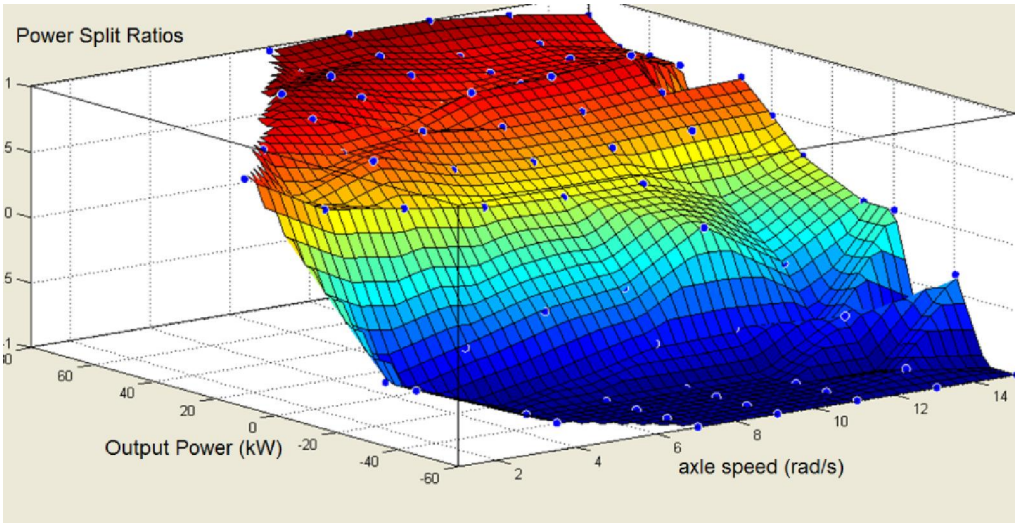

Figure 61 Optimal Efficiency Control Map Developed Using Direct Fit of the Optimization Solutions

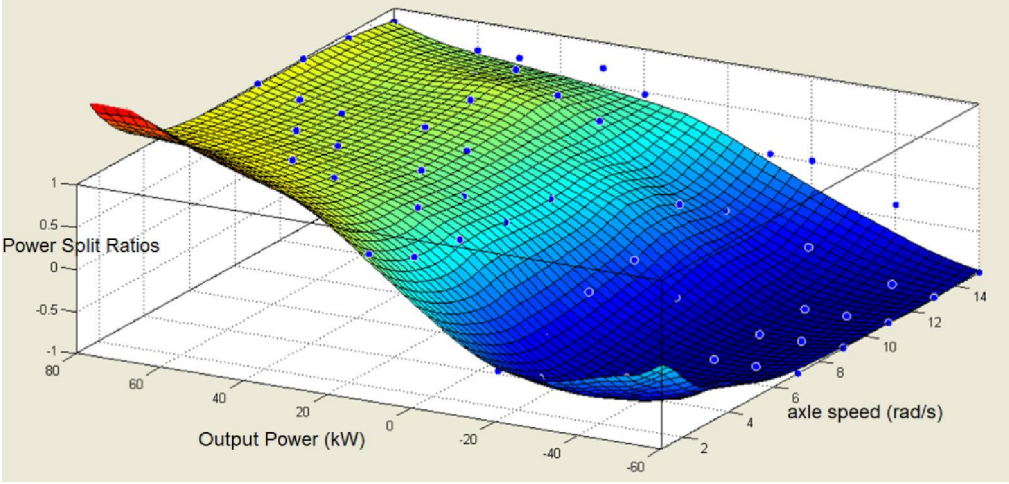

Figure 62 Optimal Efficiency Control Map Developed Using Quadratic Fit of the Optimization Solutions

7.6 Control Development

7.6.1 Controller Hardware Selection

According to the functions and I/O requirements, a dSpace controller/ECU was selected as the supervisory controller. The dSpace MABX (DS1401/1505/1507) offers four CAN 2.0 bus channels and sixteen 12-bit analog input channels, providing the capacity to handle large volumes of sensor and CAN traffic. Two of the CAN channels connect to the GM CAN bus and the other two connect to non-GM CAN bus. The 800MHz CPU makes it a high performance controller ideal for high-volume signal processing and possible to implement real-time computational demanding controls.

7.6.2 Simulations Setup

After fine-tuning the model and parameter settings, hardware readable codes are generated using the Real-time Workshop. System validation and calibration testing are performed in the hardware-in-the-loop (HIL) environment. The simulation configuration diagram is shown in Figure 63.

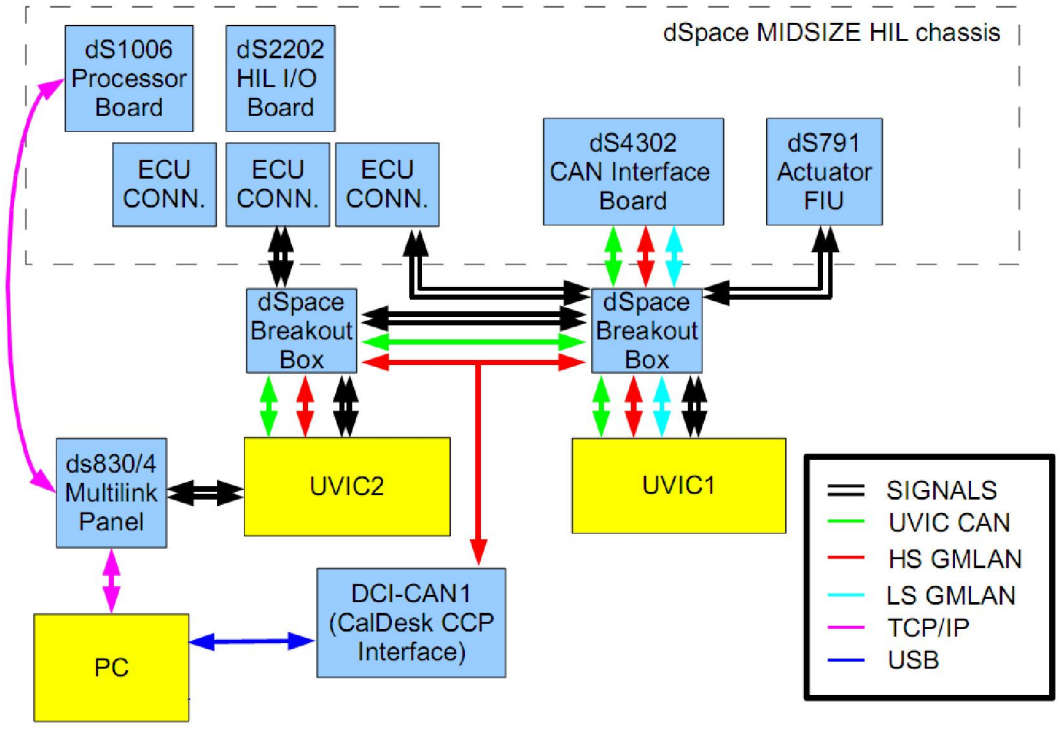

Figure 63 HIL Setup

The control strategy compiled code was loaded to the MABX and the powertrain plant model was load to the HIL simulator. The wiring harness between the MABX and the HIL simulator is consistent with the connection in the vehicle. Through observing the vehicle's performance in real-time using the MABX, complications caused by signal latency, discretization, and signal noise can be more easily recognized and addressed. dSPACE's ControlDesk was used to perform data analysis which proved beneficial for data logging and visualization of system parameters. In addition, to better conceptualize the physical representations of the results, a 3D vehicle visualization was created in dSpace's MotionDesk and interfaced with the driver's control. The HIL was also used to test fault and failure mitigation routines of the vehicle's supervisory controller, including emergency disconnect switch (EDS). This was achieved through utilization of a relay board in the HIL which allows for electrical signals to be set to open circuit, shorted to ground or battery.

7.6.3 Vehicle Control Setup

The vehicle control system setup merges the stock vehicle control with the added powertrain modules, such as the ESS and RTM. The control system topology is similar to the simulations in HIL and the configuration is shown in Figure 64.

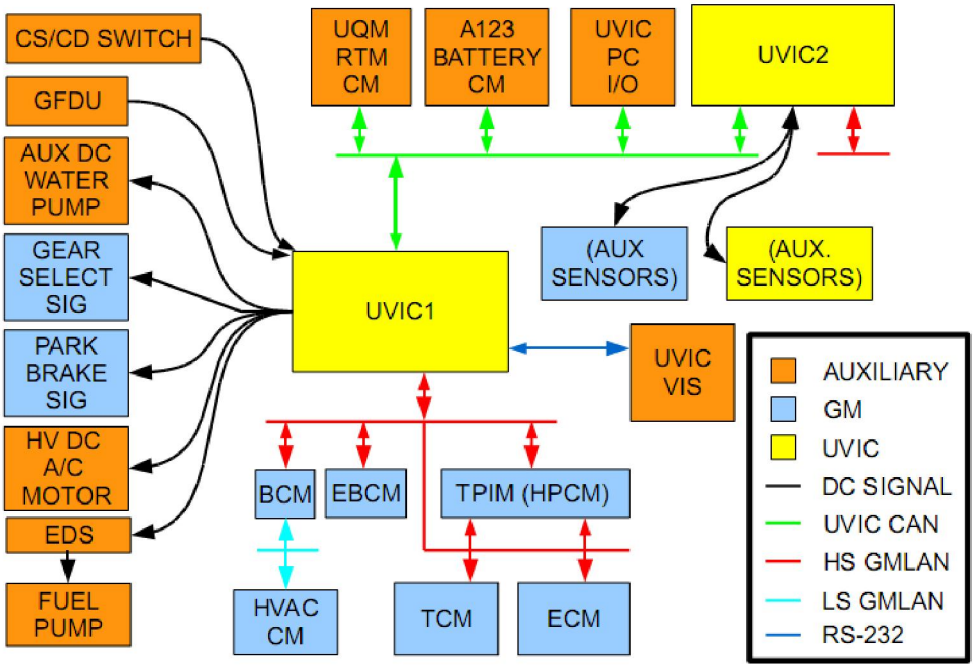

Figure 64 In Vehicle Control System Setup

UVIC1 is the main vehicle supervisory controller using the dSpace MABX. UVIC2 is an additional controller which performs on-board diagnostics and vehicle data acquisition. UVIC1 interfaces with a number of GM stock modules, the UQM RTM control module, and the battery control module (BCM). The UVIC PC I/O block represents an interface between UVIC1 and a laptop PC. Stock GM CMs are show in blue. The body CM relays data regarding the chassis, and acts as a gateway to other control modules on the GMLAN low speed (LS) CAN bus. The electronic brake control module (EBCM) sends data regarding the braking system which are used by UVIC1 to calculate regenerative breaking. The 2-mode transmission is controlled by the transmission/powertrain interface module (TPIM).

Control commands from the UVIC1 controller include desired engine torque, fuel cutoff, desired mode/gear, optimal input speed in mode 1 and 2, and desired engine state (on/off). This set of commands impact the control strategy of the vehicle, as is discussed in the following section. An in-vehicle display and data acquisition system is implemented. This is a PC-based system with a dash-mounted LCD screen.

7.7 Vehicle Testing and Competition Performance

The research carried out in this dissertation work was motivated by the UVic EcoCAR development and the research used UVic EcoCAR as the model, prototype and test vehicle. Between 2008 and 2011, the UVic EcoCAR went through a three-year development process from conceptual design to road test. The developed vehicle successfully demonstrated new powertrain technology and fulfilled original design goals, achieving good EV capacity, high fuel efficiency, and improved vehicle performance. The designed vehicle was transported to several competition locations and vigorous testing is performed, including hot weather testing at the GM's desert proving ground in Yuma, Arizona; performance testing at the Milford proving ground in Milford, Michigan; and tailpipe emission testing at the US EPA research center at Ann Arbour, Michigan. The vehicle successfully completed most of the challenging tests; in the meantime, a number of the problems were encountered and resolved. Throughout the three years process, the UVic EcoCAR team won a number of awards, including best acceleration award, MathWorks modeling award, dSpace control awards, etc. The UVic's success in

the EcoCAR competition also provides the university a strong push in research drive to the university's hybrid vehicle and clean energy transportation research.

Figure 65 Front View of the UVic EcoCAR Participating 2011 Competition in Washington DC

Figure 66 Close View of the Engine Bay Where the ICE, and 2-mode Transmission is located

Figure 67 Close View of the Rear Cargo Area and Installation of the High Capacity Li-ion Batteries

7.8 Summary

The EcoCAR: The NeXt Challenge competition offers a unique platform for testing the hybrid powertrain studies and validates computer models. The advanced model-based design technique not only accelerates the powertrain design process, but also provides an open environment for design improvement and optimization. This validated powertrain software environment allows scientific research to be carried out with minimum expensive hardware prototyping. The prototype vehicle forms ideal platform for the verification of newly introduced designs and design methods. The proposed design and control optimization method are partially applied to developing of the competition vehicle. Full vehicle test is underway in early 2012 with the installation of the new testing facility.

Chapter 8 Summary and Research Contributions

8.1 Summary of this Work

This research applies model-based design method and optimization to the design and development of advanced powertrain system for next generation hybrid electric vehicles. The work consists of four major components: fuel selection study, powertrain design optimization, vehicle control development, and a case study. These researches cover a wide range of activities in vehicle development process, from conceptual design to vehicle testing. The four components in the research form a complete design cycle in developing the future hybrid powertrains.

The integrated fuel and powertrain selection method provides guidance in the strategic selection of vehicle powertrain technologies. Various perspectives of each technology including energy efficiency, emissions, economic costs, and level of technical challenges are discussed.

The proposed design optimization and control optimization methods form new extensions to the model-based powertrain design process. The design optimization based powertrain design method presents a new approach for exploring the best performance potential of a given e-CVT powertrain architecture. Identification of the best hybrid architectures can thus be carried out through an additional layer of design optimization on top of this new e-CVT powertrain design optimization method. The proposed control optimization method is an efficient approach to identify the true energy efficiency potential of a hybrid vehicle powertrain for given instant vehicle torque and speed demands. This instant vehicle control method can be further extended by combining it with driving pattern recognition schemes to form adaptive vehicle control strategy.

The EcoCAR competition and vehicle platform provides important resources and a unique platform for this work. The proposed methods are applied to the development of the competition vehicle and vehicle tests are partially performed to verify the computational results.

8.2 Research Contributions

In this work, a systematic approach for designing and developing advance hybrid vehicle powertrain is presented. This approach applies optimization tools to automate the time-consuming vehicle design process and uses global optimization search schemes to identify the powertrain performance potential. The model-based design methods are effectively integrated into the design process and a real world vehicle development project is used to test and verify the presented approach. This systematic approach includes four important components, each of which have unique impact to the hybrid powertrain design process.

The work on powertrain and fuel selection formed the foundation for advanced hybrid powertrain development, showing a clear pathway that leads to a low environmental impact solution for future transportation.

The application of optimization technique to the design of powertrain and control system has transformed the present model-based powertrain design method from an analysis guided trial and error process to systematic search. This change can significantly improve design efficiency by avoiding time consuming design iterations and unnecessary human intervention in searching through various design combinations. The method can also considerably improve the quality of the resulting hybrid powertrain design by identifying a better or close-to-optimal solution.

The newly introduced design method is tested in the development of an Extended Range Electric Vehicle, UVic EcoCAR, with advanced 2-mode plus hybrid powertrain for verification and validation. The research and its application provided invaluable real world HEV development experience that bridges the gap between university education and industrial practise.

8.3 Future Work

The model-based design and optimization approach introduced in this work supports the design optimization of the e-CVT based hybrid electric powertrain, its control system and the optimal control for given instant power demand of the hybrid vehicle. To improve fuel economy and reduce GHG emissions, an important area of future research is the optimal power management considering real time vehicle operation demands, the state of

the vehicle, and the SOC of the ESS. This high level, strategic control task requires additional knowledge on the power demand of coming driving rather than the instant speed and torque demands to achieve optimal energy management. This intelligent energy management task can be potentially accomplished using future driving pattern prediction and real-time vehicle control based on the powertrain and ESS models. Both techniques rely on optimization and the multiphysics simulation models similar to those used in this research.

Bibliography

1. *Oil: Crude and Petroleum Products Explained*. 2011 [cited 2011 Auguest 10]; Available from: http://www.eia.gov/energyexplained/index.cfm?page=oil_home#tab2.
2. NHTSA, U.S.E.a., *Standard for model year 2012 through 2016 light-duty vehicles to educed GHG emissions and improve fuel economy*, 2010.
3. Sasaki, S. *Toyota's newly developed hybrid powertrain*. in *Proceedings of International Symposium on Power Semiconductor Devices and IC's, 3-6 June 1998*. 1998. Kyoto, Japan: Inst. Electr. Eng. Japan.
4. Lipman, T.E. and M.A. Delucchi, *A retail and lifecycle cost analysis of hybrid electric vehicles*. Transportation Research Part D: Transport and Environment, 2006. 11(2): p. 115-132.
5. Brooke, L., *Chevy Volt Developnment Story of the Pioneering Electrified Vehicle*. Electrification Series2011: SAE International.
6. Wishart, J.D., L.Y. Zhou, and Z. Dong, *Review of multi-regime hybrid vehicle powertrain architecture*. International Journal of Electric and Hybrid Vehicles, 2008.
7. Wishart, J., L. Zhou, and Z. Dong, *Hybrid Vehicle Technical Review*, 2006, University of Victoria, Azure Dynamics: Victoria.
8. Zhou, L., *Modeling and Simulation of Hybrid Electric Vehicle*, in *Department of Mechanical Engineering* 2007, University of Victoria: Victoria, BC.
9. Emadi, A., et al., *Topological overview of hybrid electric and fuel cell vehicular power system architectures and configurations*. IEEE Transactions on Vehicular Technology, 2005. 54(3): p. 763-770.
10. Westbrook, M., *The Electric Car:Development and future of battery, hybrid and fuel-cell cars*. IEE Power and Energy Series 38, ed. A. Johns and D. Warne2001, London, United Kingdom: Institution of Electrical Engineers.
11. Wouk, V., *Hybrids: then and now*. IEEE Spectrum, 1995. 32(Compendex): p. 16-21.
12. Miller, J. *Comparative Assessment of Hybrid Vehicle Power Split Transmissions*. in *Proceedings of the 2005 Fourth Vectronics Institute Winter Workshop Series*. 2005. Warren, MI.
13. Rahman, K.M., et al., *Application of direct-drive wheel motor for fuel cell electric and hybrid electric vehicle propulsion system*. IEEE Transactions on Industry Applications, 2006. 42(5): p. 1185-1192.
14. Zeraoulia, M., M.E.H. Benbouzid, and D. Diallo, *Electric motor drive selection issues for HEV propulsion systems: a comparative study*. IEEE Transactions on Vehicular Technology, 2006. 55(6): p. 1756-64.
15. Sato, E., *Permanent magnet synchronous motor drives for hybrid electric vehicles*. IEEJ Transactions on Electrical and Electronic Engineering, 2007. 2(2): p. 162-8.
16. Okuno, K., et al., *High-rate discharge properties of Ni-MH battery using new substrates for HEV applications*. SEI Technical Review, 2006(62): p. 29-33.
17. Karden, E., et al., *Energy storage devices for future hybrid electric vehicles*. Journal of Power Sources, 2007. 168(1): p. 2-11.

18. Garrett, J., *Hybrid Sells, but lack battery technology upgrade*, in *The Boston Globe*2007, Copley News Service: Boston.
19. Cunningham, W., *Mercedes-Benz S400 BlueHybrid: First Planned HEV With Li-Ion Battery*, in *Mercedes-Benz claims battery breakthrough*2008.
20. Hunber, P. and M. Mills, *Electron Cache.* The Digital Power Report, 2001. March 2001/Vol.2 I(3).
21. Auer, J., G. Sartorelli, and J. Miller. *A gatekeeper energy management strategy for eCVT hybrid vehicle propulsion utilising ultracapacitors*. 2006. Coventry, UK: Inst. of Eng. and Technol.
22. Burke, A.F., *Batteries and ultracapacitors for electric, hybrid, and fuel cell vehicles.* Proceedings of the IEEE, 2007. 95(4): p. 806-20.
23. Pesaran, A., et al., *Ultracapacitors and Batteries in Hybrid Vehicles*, 2005: United States. p. 38p.
24. Yoo, H., et al., *System integration and power-flow management for a series hybrid electric vehicle using supercapacitors and batteries.* IEEE Transactions on Industry Applications, 2008. 44(1): p. 108-114.
25. Morrison, D., *Ultracapacitor options (and ways to charge them) grow.* Power Electronics Technology, 2007. 33(6): p. 54-5.
26. Reedy, J. and S. Lunzman, *Model Based Design Accelerates the Development of Mechanical Locomotive Control*, in *SAE 2010 Commercial Vehicle Engineering Congress*2010, SAE International: Chicago.
27. Jalil, N., N.A. Kheir, and M. Salman. *A rule-based energy management strategy for a series hybrid vehicle*. 1997. Albuquerque, NM, USA: American Autom. Control Council.
28. Hofman, T., et al. *Rule-based energy management strategies for hybrid vehicle drivetrains: a fundamental approach in reducing computation time*. 2006. Heidelberg, Germany: VDI/VDE-Gesellschaft Mess- und Automatisierungstechnik.
29. Chan-Chiao, L., et al., *Power management strategy for a parallel hybrid electric truck.* IEEE Transactions on Control Systems Technology, 2003. 11(6): p. 839-49.
30. Perez, L.V., et al., *Optimization of power management in an hybrid electric vehicle using dynamic programming.* Mathematics and Computers in Simulation, 2006. 73(1-4 SPEC ISS): p. 244-254.
31. Pu, J. and C. Yin, *Optimal control of fuel economy in parallel hybrid electric vehicles.* Proceedings of the Institution of Mechanical Engineers, Part D: Journal of Automobile Engineering, 2007. 221(9): p. 1097-1106.
32. Kyoungcheol, O., et al., *Optimization of control strategy for a single-shaft parallel hybrid electric vehicle.* Proceedings of the Institution of Mechanical Engineers, Part D (Journal of Automobile Engineering), 2007. 221(5): p. 555-65.
33. Eslinger, R.G.C.J.M.G.C.T.K.O.J., *Algorithm for noisy problems in gas transmission pipeline optimization.* Optimization and Engineering, 2002. 2:139-157.
34. Montazeri-Gh, M., A. Poursamad, and B. Ghalichi, *Application of genetic algorithm for optimization of control strategy in parallel hybrid electric vehicles.* Journal of the Franklin Institute, 2006. 343(4-5): p. 420-35.

35. Williamson, S.S. and A. Emadi, *Comparative assessment of hybrid electric and fuel cell vehicles based on comprehensive well-to-wheels efficiency analysis.* IEEE Transactions on Vehicular Technology, 2005. 54(Compendex): p. 856-862.
36. Messagie, M., et al. *Life Cycle Assessment of conventional and alternative small passenger vehicles in Belgium*. in *2010 IEEE Vehicle Power and Propulsion Conference (VPPC), 1-3 Sept. 2010*. 2010. Piscataway, NJ, USA: IEEE.
37. Campanari, S., G. Manzolini, and F. Garcia de la Iglesia, *Energy analysis of electric vehicles using batteries or fuel cells through well-to-wheel driving cycle simulations.* Journal of Power Sources, 2009. 186(Compendex): p. 464-477.
38. Van Vliet, O., et al., *Energy use, cost and CO2 emissions of electric cars.* Journal of Power Sources, 2011. 196(Compendex): p. 2298-2310.
39. Elgowainy, A., et al., *Well-to-wheels energy use and greenhouse gas emissions of plug-in hybrid electric vehicles.* SAE International Journal of Fuels and Lubricants, 2009. 2(Compendex): p. 627-644.
40. Wang, M.Q., *Development and Use of the GREET Model to Estimate Fuel-Cycle Energy Use and Emissions of Various Transportation Technologies and Fuels*, 1996, Center for Transportation Research, Argonnoe National Laboratory.
41. Wang, M., *Fuel choices for fuel-cell vehicles: well-to-wheels energy and emission impacts.* Journal of Power Sources, 2002. 112(Copyright 2003, IEE): p. 307-21.
42. Rousseau, A., P. Sharer, and M. Pasquier, *Validation Process of a HEV System Analysis Model: PSAT*, 2010, Argonne National Laboratory: Chicago.
43. ANL. *PSAT (Powertrain System Analysis Toolkit)*. 2010; Available from: http://www.transportation.anl.gov/modeling_simulation/PSAT/index.html.
44. EPA, *Regulatory Announcement: EPA Issues New Test Methods for Fuel Economy Window Stickers*, 2006.
45. *What's Moving: U.S. Auto Sales.* The Wall Street Journal, 2011.
46. Taylor, A.M.K.P., *Science review of internal combustion engines.* Energy Policy, 2008. 36(Copyright 2008, The Institution of Engineering and Technology): p. 4657-67.
47. Foundation, E.P.R., *Implementation Issues for the Renewable Fuel Standard - Part I -- Rising Corn Costs Limit Ethanol's Growth in the Gasoline Pool*, 2011.
48. Radich, A., *Biodiesel Performance, Cost, and Use*, 2010, U.S. Energy Information Administration.
49. Blencoe, G. *Cost of Hydrogen from Different Sources*. Hydrogen Car Revolution 2009 Nov 9, 2009; Available from: http://www.h2carblog.com/?p=461.
50. Sun, J., et al. *Control of DISI engines: analytical and experimental investigations*. in *Proceedings of Workshop on Advances in Automotive Control, 28-30 March 2001*. 2001. Kidlington, UK: Elsevier Science.
51. Budik, G., *Conversion of internal combustion engine from gasoline to E85 fuel.* Periodica Polytechnica Transportation Engineering, 2010. 38(Compendex): p. 19-23.
52. Niven, R.K., *Ethanol in gasoline: Environmental impacts and sustainability review article.* Renewable and Sustainable Energy Reviews, 2005. 9(Compendex): p. 535-555.
53. Argonne_National_Lab, *First images made of hydrogen burning in working internal combustion engine*, in *Argonne National Lab Newsroom 2006*2006.

54. Shudo, T., *Improving thermal efficiency by reducing cooling losses in hydrogen combustion engines.* International Journal of Hydrogen Energy, 2007. 32(Copyright 2007, The Institution of Engineering and Technology): p. 4285-93.
55. Escalante Soberanis, M.A. and A.M. Fernandez, *A review on the technical adaptations for internal combustion engines to operate with gas/hydrogen mixtures.* International Journal of Hydrogen Energy, 2010. 35(Copyright 2011, The Institution of Engineering and Technology): p. 12134-40.
56. Association, T.N.H., *Hydrogen Workshop For Fleet Operators*, 2010.
57. Semin and R.A. Bakar, *A Technical Review of Compressed Natural Gas as an Alternative Fuel for Internal Combustion Engines.* American Journal of Engineering and Applied Sciences, 2008. 1(Copyright 2010, The Institution of Engineering and Technology): p. 302-11.
58. Mohamed Amine Fakhfakh, M.H.K., *Thermal Analysis of a Permanent Magnet Synchronous Motor for Electric Vehicle.* Journal of Asian Electric Vehicles, 2008. 6(December).
59. Frenette, G. and D. Forthoffer, *Economic commercial viability of hydrogen fuel cell vehicles from an automotive manufacturer perspective.* International Journal of Hydrogen Energy, 2009. 34(Copyright 2009, The Institution of Engineering and Technology): p. 3578-88.
60. *Ethanil is the perfect fuel for fuel cells*. [cited 2011 July 29]; Available from: http://running_on_alcohol.tripod.com/id30.html.
61. Hinds, G., *Performance and Durability of PEM Fuel Cells: A Review*, 2004, Japan Atomic Energy Res. Inst., Naka, Ibaraki, Japan: Japan. p. 42.
62. Flanz, S., *Three years of practical tests of Ford fuel cell vehicles*
Drei Jahre Praxiserprobung von Ford Brennstoffzellenfahrzeugen. VDI Berichte, 2008(Compendex): p. 233-245.
63. Jinfeng, W., et al., *A review of PEM fuel cell durability: degradation mechanisms and mitigation strategies.* Journal of Power Sources, 2008. 184(Copyright 2008, The Institution of Engineering and Technology): p. 104-19.
64. Wall, G., et al., *Cleaner vehicle buses in Winchester.* Transport Policy, 2008. 15(1): p. 55-68.
65. U.S. DOE, E.E.R.E., *Fuel Cell System Cost for Transportation - 2008 Cost Estimate.* 2009.
66. Guerrero, C.P.A., et al. *Hybrid/Electric Vehicle Battery Manufacturing: The State-of-the-Art*. in *2010 IEEE International Conference on Automation Science and Engineering (CASE 2010), 21-24 Aug. 2010*. 2010. Piscataway, NJ, USA: IEEE.
67. *The End of the Oil Age, 2011 and Beyond*, in *Global Market Research*2010, Deutsche Bank.
68. Hu, M., *Power flow and efficiency of planetary gear transmission.* Chinese Journal of Mechanical Transmission, 1998(2): p. 13-16.
69. Morris, R., *Chevrolet Volt - GM's concept electric vehicle - Could nearly eliminate trips to the gas station.* Automotive Industries AI, 2007. 187(2).
70. Miller, M.A., et al., *The GM "Voltec" 4ET50 Multi-Mode Electric Transaxle*, in *2011 SAE World Congress*2011: Detroit, MI. p. 2011-01-0887.

71. Staunton, R.H., et al., *Evaluation of 2004 Toyota Prius Hybrid Electric Drive System*, 2006, U.S. Department of Energy, FreedomCAR and Vehicle Technologies, EE-2G: Washinton, D.C.
72. Stewart, B. *2010 Toyota Prius Plug-in Hybrid Prototype: Next-Gen Test Drive*. 2007 [cited 2009 October 7]; Available from: http://www.popularmechanics.com/automotive/new_cars/4227944.html.
73. Kawahashi, A. *A new-generation hybrid electric vehicle and its supporting power semiconductor devices*. in *Proceedings of the 16th International Symposium on Power Semiconductor Devices & IC's, 24-27 May 2004*. 2004. Kitakyushu, Japan: Inst. of Elec. Eng. of Japan.
74. Crosse, J., *Lexus RX 450h.* Automotive Engineer, 2009. 34(6): p. 12.
75. Abe, S. and G. Killmann, *Hybrid technology in the Lexus RX400h.* AutoTechnology, 2006. 6(FEB.): p. 44-47.
76. Yamaguchi, J., *Lexus hybridizes sports sedan [ICE-electric hybrid system].* Automotive Engineering International, 2006. 114(10): p. 74-80.
77. Grewe, T.M., B.M. Conlon, and H.A. G, *Defining the General Motors 2-Mode Hybrid Transmission*, in *2007 SAE World Congress*2007, SAE.
78. Team, U.E., *EcoCAR Design Report 3*, 2009, University of Victoria: Victoria.
79. Yamamoto, M., *Development of a Toyota Plug-in Hybrid Vehicle.* SAE Publication, 2010. 2010-01-0839.
80. Oyobe, H., et al. *Development of ultra low-cost, high-capacity power generation system using drive motor and inverter for hybrid vehicle*. in *2005 IEEE Industry Applications Conference, 40th IAS Annual Meeting, Oct 2-6 2005*. 2005. Kowloon, Hong Kong, China: Institute of Electrical and Electronics Engineers Inc., Piscataway, NJ 08855-1331, United States.
81. Tim M. Grewe, B.M.C.a.A.G.H., *Defining the General Motors 2-Mode Hybrid Transmission.* SAE Technical Paper Series, 2007. 2007-01-0273.
82. Zhang, Y., et al., *Performance modeling and optimization of a novel multi-mode hybrid powertrain.* Journal of Mechanical Design, 2006. 128(1): p. 79-89.
83. Zhou, L., et al., *Optimization of Control Strategy and Key Components of a Multi-regime Hybrid Vehicle*, in *12th AIAA/ISSMO Multidisciplinary Analysis and Optimization Conference*2008: Victoria, BC.
84. Cooper. Leon, *Method and applications of linear programming*1974: Philadelphia, Saunders.
85. Yang, H., et al., *Development of Two-Mode Hybrid Powertrain with Enhanced EV Capability*, in *2011 SAE World Congress*2011: Detroit, MI. p. 2011-01-0883.
86. Williams, M.C. *Fuel cells and the world energy future*. in *Proceedings of Power Engineering Society Summer Meeting, 15-19 July 2001*. 2001. Piscataway, NJ, USA: IEEE.
87. Miller, J.M., *Hybrid electric vehicle propulsion system architectures of the e-CVT type.* IEEE Transactions on Power Electronics, 2006. 21(3): p. 756-767.
88. Lo, E.W.C. *Review on the configurations of hybrid electric vehicles*. in *2009 3rd International Conference on Power Electronics Systems and Applications (PESA) - Electric Vehicles and Green Energy, 20-22 May 2009*. 2009. Piscataway, NJ, USA: IEEE.

89. Colbourne, J.R., *Simplified kinematic analysis of planetary gear trains.* Mechanism and Machine Theory, 1972. 7(3): p. 307-316.
90. Wishart, J.D., Y. Zhou, and Z. Dong. *Review, Modelling and Simulation of Two-Mode Hybrid Vehicle Architecture*. in *9th International Conference on Advanced Vehicle and Tire Technologies (AVTT)*. 2007. Las Vegas, NV, US.
91. Kukhyun, A., et al., *Performance analysis and parametric design of the dual-mode planetary gear hybrid powertrain.* Proceedings of the Institution of Mechanical Engineers, Part D (Journal of Automobile Engineering), 2006. 220(D11): p. 1601-14.
92. Markel, T. and K. Wipke. *Optimization techniques for hybrid electric vehicle analysis using advisor*. in *2001 ASME International Mechanical Engineering Congress and Exposition, Nov 11-16 2001*. 2001. New York, NY, United States: American Society of Mechanical Engineers, New York, NY 10016-5990, United States.
93. Simpson, P.K., *Artificial neural systems :foundations, paradigms, applications, and implementations*. 1st ed. ed1990, New York: Pergamon Press. xiii, 209 p.
94. Hagan, M.T. and M.B. Menhaj, *Training feedforward networks with the Marquardt algorithm.* Neural Networks, IEEE Transactions on, 1994. 5(6): p. 989-993.
95. Jost, K., *GM's hybrid SUVs: best aei engineered vehicle 2008.* Automotive Engineer, 2008. 33(5): p. 65-70.
96. inc, S.T.C. *GHGenius - A model for life cycle assessment of transportation fuel* 2004.
97. Grewe, T.M., B.M. Conlon, and H.A. G, *Defining the General Motors 2-Mode Hybrid Transmission*, 2007, SAE.
98. Conlon, B., *Comparative Analysis of Single and Combimed Hybrid Electrically Variable Transmission Operating Modes.* SAE Technical Paper Series, 2005. 2005-01-1162.
99. dSpace. *ASM - Gasoline Engine Simulation Package*. 2008; Available from: http://www.dspaceinc.com/ww/en/inc/home/products/sw/automotive_simulation_models/asm_gasoline_engine_simulation.cfm.
100. Zhou, L. and Z. Dong, *Traction Control Optimization of a AWD PHEV*, in *Canadian Society of Mechanical Enginnering Forum 2010*2010: Victoria, BC.